SECURITY CLASSIFI

RI

READ INSTRUCTIONS BEFORE COMPLETING FORM

1. REPORT NUMBER GRL/9401	ON NO. 3. RECIPIENT'S CATALOG NUMBER
4. TITLE (and Subtit BASIC STUDY OF THE PUMPING OF A GAMMA-RAY LASER	5. TYPE OF REPORT & PERIOD COVERED Annual Report 03/15/93 - 03/14/94
	6. PERFORMING ORG. REPORT NUMBER
7. AUTHOR(s) C. B. Collins	8. CONTRACT OR GRANT NUMBER(s) N00014-93-K-2005
9. PERFORMING ORGANIZATION NAME AND ADDRESS University of Texas at Dallas Center for Quantum Electronics P.O. Box 830688 Richardson, TX 75083-0688	10. PROGRAM ELEMENT, PROJECT, TASK AREA & WORK UNIT NUMBERS
11. CONTROLLING OFFICE NAME AND ADDRESS Naval Research Laboratory 4555 Overlook Avenue, S.W. Washington, D.C. 20375-5000	12. REPORT DATE 04/15/94 13. NUMBER OF PAGES 105
14. MONITORING AGENCY NAME & ADDRESS(if different from Controlling Office) Dr. Paul Kepple Naval Research Laboratory 4555 Overlook Avenue, S.W. Washington, D.C. 20375-5000 Attn: Code 6721 Bldg. A50 Rm# 148	15. SECURITY CLASS. (of this report) Unclassified 15a. DECLASSIFICATION/DOWNGRADING SCHEDULE

16. DISTRIBUTION STATEMENT (of this Report)

This document has been approved for public release and sale; its distribution is unlimited.

17. DISTRIBUTION STATEMENT (of the abstract entered in Block 20, if different from Report)

18. SUPPLEMENTARY NOTES

19. KEY WORDS (Continue on reverse side if necessary and identify by block number)

Gamma-ray laser, Ultrashort wavelength laser

20. ABSTRACT (Continue on reverse side if necessary and identify by block number)

The most productive approaches to the problem of the gamma-ray laser have focused upon upconversion techniques in which metastable nuclei are pumped with long wavelength radiation. At the nuclear level the storage of energy can approach tera-Joules (10^{12}J) per liter for thousands of years. However, any plan to use such a resource for a gamma-ray laser poses problems of a broad interdisciplinary nature requiring the fusion of concepts taken from relatively unrelated fields of physics. Our research group has described

(continued on next page)

DD FORM 1 JAN 73 1473 EDITION OF 1 NOV 65 IS OBSOLETE
S/N 0102-LF-014-6601

SECURITY CLASSIFICATION OF THIS PAGE (When Data Entered)

20. Abstract (continued)

several means through which this energy might be coupled to radiation fields with cross sections for stimulated emission that could reach 10^{-17} cm^2. Such a stimulated release could lead to output powers as great as 3 x 10^{21} Watts/liter. Since 1978 we have pursued an approach for the upconversion of longer wavelength radiation incident upon isomeric nuclear populations that can avoid many of the difficulties encountered with traditional concepts of single-photon pumping. Experiments have confirmed the general theory and have indicated that a gamma-ray laser is feasible if the right combination of energy levels and branching ratios exists in some real material. Of the 1,886 distinguishable nuclear materials, the present state-of-the-art has been adequate to identify 29 first-class candidates, but further evaluation cannot proceed without remeasurements of nuclear properties with higher precision. A laser-grade database of nuclear properties does not yet exist, but the techniques for constructing one have been developed and utilized under this contract. Resolution of the question of the feasibility of a gamma-ray laser now rests upon the determination of: 1) the identity of the best candidate, 2) the threshold level of laser output, and 3) the upconversion driver for that material.

Previous work focused upon our approach that is the nuclear analog to the ruby laser. It embodies the simplest concepts for a gamma-ray laser and not surprisingly, the greatest rate of achievement in the quest for a subAngstrom laser was realized in that direction. For ruby the identification and exploitation of a bandwidth funnel were the critical keys in the development of the first laser. There was a broad absorption band linked through efficient cascading to the narrow laser level.

In 1987 we reported a major milestone which showed that comparable structure existed at the nuclear scale in the first of the 29 candidate isomers available for testing, $^{180}Ta^{m}$. Populations of the isomer were successfully pumped down with flashes of x rays absorbed through an astonishingly large cross section of 40,000 on the usual scale (~ 10^{-29} cm^2 keV) where 10 describes a fully-allowed process. This corresponded to a partial width for useful absorption of 0.5 eV, even better than what had been assumed for idealized nuclei. In the course of successive work we discovered that the giant pumping resonances occurred with a gratifying frequency throughout the table of nuclides, reaching optimal size and strength in the mass region where the better candidates lie.

At the conclusion of that work we focused upon the extension of our achievements in pumping nuclei to those having laser-like transitions with microsecond lifetimes. For the test cases of ^{181}Ta and ^{176}Hf giant resonances were found for the pumping of fluorescence with the Texas-X linear accelerator installed in our facility for dedicated use in gamma-ray-laser research. The importance of those first results is that the particular nuclei studied are very close neighbors in the sense of nuclear structure to the still unavailable first-class candidate nuclei for a gamma ray laser. Such favorable results with those close simulations argued strongly for analogous successes with the actual candidate nuclei.

During the most recent reporting period efforts focused upon identification and study of the best of the 29 candidate isomers for a gamma-ray laser, the 31 year isomer of hafnium, $^{178}Hf^{m2}$. It stores the greatest energy density available for release in a gamma-ray laser, 1.3 kilojoules per microgram. Because of the expected difficulty in obtaining samples of this exceedingly rare material, efforts this past year were concentrated upon systematic studies and new technologies that will reduce the amount of isomeric material needed for the critical experiments planned.

TABLE OF CONTENTS

REPRINTS AND PREPRINTS OF MANUSCRIPTS PUBLISHED OR TO BE PUBLISHED UNDER THIS CONTRACT

PREPRINTS OF MANUSCRIPTS TO BE PUBLISHED IN CONFERENCE PROCEEDINGS UNDER THIS CONTRACT

Status and issues in the development of a γ-ray laser III. Preferred nuclides

By C. B. Collins and J. J. Carroll
University of Texas at Dallas,
Center for Quantum Electronics
P.O. Box 830688, Richardson, TX 75083-0688

Abstract

A gamma-ray laser would stimulate the emission of radiation at wavelengths below 1 A from excited states of nuclei. However, the anticipation of a need for very high pump powers tended to discourage early research and the difficulties in demonstrating a device were first assumed to be insurmountable. Over the past decade advances in pulsed power technology have changed these perceptions and studies have built a strong momentum. The concept for a nuclear analog of the ruby laser now appears in the textbooks and many of the component steps for pumping the nuclei have been demonstrated experimentally. A quantitative model based upon the new data and concepts has shown the gamma-ray laser to be feasible if some real isotope has its properties sufficiently close to the ideals modeled. The greatest positive impact upon feasibility has come from the discovery of giant resonances for pumping nuclei that greatly reduce the levels of pump power needed. Most recently attention has been focused upon efforts to demonstrate prelasing levels of fluorescence from nuclides which are actual candidates for use in a gamma-ray laser. Problems being addressed are the acquisition of macroscopic samples for testing and the demonstration of appropriate instrumentation.

1. Introduction

A decade ago the difficulties in realizing a gamma-ray laser were considered almost insurmountable. However, in 1982 we began to emphasize an interdisciplinary concept of upconversion which ultimately launched a renaissance in the field (Collins, et al. 1982). The essential concept was the "optical" pumping of nuclei. In this case optical meant x rays, but the fundamentals were the same. Useful, resonant absorption of pump power would occur over short distances to produce high concentrations of excited nuclei while wasted wavelengths would be degraded to heat in much large volumes. Of all the cases considered, the nuclear analog of the ruby laser embodied the simplest concepts for a gamma-ray laser. Not surprisingly, the greatest rate of achievement has been realized in that direction.

For ruby, the identification and exploitation of a bandwidth funnel were the critical keys in the development of the first laser. There was a broad absorption band linked through efficient cascading to the narrow laser level. Our concept called for a nuclear analogy of this structure which was unknown in 1986 when the first phase of experiments was started. Moreover, we had envisioned pumping not only the ground states of nuclei, but also isomeric levels. Such metastable nuclei store keV and even MeV of energy for years so most of the pump power could be input long before the time of use and triggering requirements would be minimized. The model has been confirmed in principle and now appears in the textbooks (Collins 1991).

The use of intense flashes of x rays to dump the stored energy of an isomer was first shown (Collins, *et al.* 1988) for the rare nuclide $^{180}Ta^{m}$ which exists naturally as 100% inverted. Then experiments with the unique superconducting linac at Darmstadt showed that populations of the isomer $^{180}Ta^{m}$ are pumped down through two isolated resonances of extraordinary strength, about 10^{4} times larger than expected for the excitation of nuclei by x rays (Collins, *et al.* 1990). A quantitative model based upon the new data showed the gamma-ray laser to be feasible if one of the real nuclear isomers has its properties sufficiently close to the ideals modeled (Collins, *et al.* 1992; Collins, *et al.* 1993).

The greatest impediment to research on the feasibility of a gamma-ray laser has come from the lack of suitable materials. There are 1886 distinguishable nuclear isotopes, but most do not occur naturally and there have not been any reasons to produce them artificially. In 1986 a search of all nuclear properties identified 29 isotopes as first-class candidates for a gamma-ray laser and three are shown in Table I as examples. Only the two poorest, $^{180}Ta^{m}$ and ^{123}Te could be acquired for testing. Those are the ones upon which the breakthrough discovery of the giant pumping resonance was made.

The better candidates for a gamma-ray laser have never been available in sufficient quantities for evaluation and research had to focus instead upon 19 simulation materials that served to teach the systematics for using the giant pumping resonances to excite nuclei (Carroll, *et al.* 1991). The results on those simulated candidates were extremely encouraging as the giant resonance for

pumping with bremsstrahlung were found in many of them. Moreover, the results have considerable significance as they served to identify the best candidate material for pumping a gamma-ray laser, the 31-year isomer of ^{178}Hf.

2. Technical Background

2.1 Pump Model

The sequence for triggering the release of the energy stored in an isomeric state (Collins, *et al.* 1982; Collins 1991) is described by an integrated cross section for the pumping of that level with a continuum of x rays. The population is transferred through a gateway state where the selection rules that would otherwise limit the process do not apply. The normal decay from the gateway is accompanied by the emission of immediate fluorescence that leads to the principal laser level from which the sustained output of power will be emitted. Such processes fall into the general category of (γ,γ') reactions shown schematically in Fig. 1. Population can be accumulated in the output level by continuing to run the pump cycle for a time comparable to the lifetime of the output state. In the case of the ^{178}Hf that lifetime is an almost ideal value of about 70 sec.

Whether or not the initial state being pumped in a (γ,γ') reaction is the ground state or a long-lived isomeric level, the principal figure of merit is the integrated cross section for pumping an output transition through such a broad band, $\pi b_a b_o \Gamma \sigma_o/2$. Constituent parameters are identified in Fig. 1 where it can be seen that the branching ratios b_a and b_o specify the probabilities that a population pumped by absorption into the j-th broad level

will decay back into the initial state or by cascade to the output level, respectively.

For a sample which is optically thin at the pump wavelength, a computation of the number of nuclei pumped into a fluorescence level in the scheme of Fig. 1 is straightforward (Collins, *et al.* 1982; Collins 1991). Most intense x-ray sources emit continua, either because bremsstrahlung is initially produced or because spectral lines are degraded by Compton scattering in the immediate environment. The time-integrated yield of final-state nuclei, N_f obtained by irradiating N_i initial targets with an x-ray flux, Φ_0 in photons cm^{-2} delivered in a continuum is,

$$N_f = N_i \Phi_0 \int_0^{E_0} \sigma(E) F(E, E_0)\, dE \quad , \qquad (1)$$

where $F(E,E_0)$ is the distribution of intensities up to an endpoint energy E_0 within the input spectrum normalized so that

$$\int_0^{E_0} F(E, E_0)\, dE = 1 \quad , \qquad (2)$$

and $\sigma(E)$ is the effective cross section for the excitation of the final state from the initial.

All (γ,γ') reactions occurring at energies below the threshold for particle evaporation excite discrete pump bands, or gateways, as shown in Fig. 1. Although only one gateway appears in the figure, there could be more. Each would be excited at a different pump energy but all would branch to some extent into the same

fluorescence level, f. The j-th gateway is shown in Fig. 1 as typical.

Although the width of level j is broad on a nuclear scale, it is narrow in comparison to the scale of energies, E over which $F(E,E_0)$ varies. Then, the final-state yield, expressed as the normalized activation per unit photon flux, $A_f(E_0)$ can be written from Eq. (1) as,

$$A_f(E_0) \equiv \frac{N_f}{N_i \Phi_0} = \sum_j (\sigma\Gamma)_{fj} F(E, E_0) \quad . \quad (3)$$

In this expression $(\sigma\Gamma)_{fj}$ is the integrated cross section for the production of final-state N_f as a result of the excitation of the gateway at E_j , so that

$$(\sigma\Gamma)_{fj} = \int_{E_j-\Delta}^{E_j+\Delta} \sigma(E)\, dE \quad , \quad (4)$$

where Δ is an energy small compared to the spacing between gateways and large in comparison to their widths. Levels of this type are sometimes called intermediate states or doorways.

It is straightforward to show that,

$$(\sigma\Gamma)_{fj} = (\pi b_a b_o \Gamma \sigma_0/2)_{fj} \quad , \quad (5)$$

where $\sigma_0/2$ is the peak of the Breit-Wigner cross section for the absorption step, and

$$\sigma_0 = \frac{\lambda^2}{2\pi} \frac{2I_e+1}{2I_g+1} \frac{1}{\alpha_p+1} \quad , \qquad (6)$$

where λ is the wavelength of the gamma ray at the resonant energy, E_j; I_e and I_g are the nuclear spins of the excited and ground states, respectively; and α_p is the total internal conversion coefficient for the system shown in Fig. 1.

2.2 Experimental Confirmation

In experimental work of the last five years the bremsstrahlung from five accelerators in different experimental environments was used to verify the model of Eqs. (1) - (4) for pumping nuclear fluorescence and to cross-check the accelerator intensities (Carroll, *et al.* 1991). Spectral intensities were calculated with the EGS4 coupled electron/photon transport code (Nelson, *et al.* 1985) adapted for each individual configuration from closely monitored values of accelerator currents. In this way both $F(E,E_0)$ and Φ_0 were obtained. In some cases Φ_0 was verified by in-line dosimetry.

During these experiments samples with typical masses of grams were exposed to the bremsstrahlung from the five accelerators for times ranging from seconds to hours for the continuously operating machines and to single flashes from the pulsed devices. Results were in close agreement (Anderson & Collins 1987; Anderson, *et al.* 1988a; Anderson & Collins, 1988b) with the predictions of Eq. (3) used with literature values of $(\sigma\Gamma)_{rj}$. The most detailed confirmation of theory was obtained with the reaction $^{87}Sr(\gamma,\gamma')^{87}Sr^m$ as shown in Fig. 2. It served to completely confirm the model and

to validate the use of the EGS4 code for calculating bremsstrahlung intensities from measured accelerator parameters.

Many of the 29 candidates belong to the class of nuclei deformed from the normally spherical shape (Collins 1991). For those systems there is a quantum number of dominant importance, K which is the projection of individual nucleonic angular momenta upon the axis of elongation. To this is added the collective rotation of the nucleus to obtain the total angular momentum J. The resulting system of energy levels resembles that of a diatomic molecule.

In most cases an isomeric state has a large lifetime because its value of K differs considerably from those of lower levels to which it would otherwise be radiatively connected. As a consequence, bandwidth funneling processes such as shown in Fig. 1 that start from isomeric levels must span substantial changes in K and component transitions have been expected to have large, and hence unlikely, multipolarities.

From this perspective the third of the isomers listed in Table I, ^{180}Ta was initially unattractive as it had one of the largest changes of angular momentum between isomer and ground state, 8ħ. However, because a macroscopic sample was readily available, ^{180}Ta became the first isomeric material to be optically pumped to a fluorescent level.

This particular isomer, ^{180}Ta^{m} carries a dual distinction. It is the rarest stable isotope occurring in nature and it is the only naturally occurring isomer. The actual ground state of ^{180}Ta is 1^{+} with a halflife of 8.1 hours while the tantalum nucleus of mass 180

occurring with 0.012% natural abundance is the 9^- isomer, $^{180}Ta^m$. It has an adopted excitation energy of 75.3 keV and a halflife in excess of 1.2×10^{15} years.

In an experiment conducted in 1987, 1.2 mg of $^{180}Ta^m$ was exposed to the bremsstrahlung from a 6 MeV linac and a large fluorescence yield was obtained (Collins, *et al.* 1988). This was the first time a (γ,γ') reaction had been excited from an isomeric target as needed for a gamma-ray laser and was the first evidence of the existence of giant pumping resonances. Simply the observation of fluorescence from a milligram sized target proved that an unexpected reaction channel had opened. Usually grams of material have been required in this type of experiment. Analyses (Collins, *et al.* 1988; Collins, *et al.* 1990) of the data indicated that the partial width, $b_a b_o \Gamma$ for the dumping of $^{180}Ta^m$ was around 0.5 eV.

To determine the transition energy, E_j from the $^{180}Ta^m$ isomer to the gateway level, a series of irradiations (Collins, *et al.* 1990) was made at the S-DALINAC facility using fourteen different endpoints in the range from 2.0 to 6.0 MeV. The existence of an activation edge was clearly seen in the data shown in Fig. 3. The fitting of such data to the expression of Eq. (3) by adjusting trial values of $(\sigma\Gamma)_{rj}$ provided the integrated cross sections for the dumping of $^{180}Ta^m$ isomeric populations into freely-radiating states. Reported values (Collins, *et al.* 1990) were 12,000 and 35,000 in the usual units of 10^{-29} cm^2 keV for gateways at 2.8 and 3.6 MeV, respectively. These are enormous values exceeding anything previously reported for transfer through a gateway by two

orders of magnitude. In fact they are 10,000 times larger than the values usually measured for nuclei.

A survey of 19 isotopes (Carroll, *et al.* 1991) conducted with the four U.S. accelerators over a fairly coarse mesh of bremsstrahlung endpoints confirmed the existence of giant resonances for transferring K in the region of masses near 180 as shown in Fig. 4. Activation edges continued to support the identifications of integrated cross sections for pumping and dumping of isomers that were of the order of 10,000 times greater than usual values. The details of these studies of systematics have been reported in recent reviews (Collins, *et al.* 1992; Collins, *et al.* 1993) together with the analyses of the nuclear structures to which these giant pumping resonances may be attributed. The conclusion of these modeling studies is that the best of the 29 candidate materials for a gamma-ray laser is the first listed in Table I. Because it should be the easiest to trigger, the 31-year isomer $^{178}Hf^{m2}$ is the nuclide of choice for the pumping of a gamma-ray laser.

3. Candidate Isomer for a Gamma-Ray Laser

3.1 Candidates and Simulations

While an exact ranking of the 29 candidate isomers for a gamma-ray laser depends upon a complex weighting of combinations of nuclear parameters, the potential importance of several nuclides is magnified by some very pragmatic considerations. These issues are typified by comparisons of the three examples presented in Table I.

From the perspective of shelf life and availability, the third entry in Table I, $^{180}Ta^{m}$ is far superior. It is a naturally

occurring material composing 0.01% of all Ta and can be prepared simply by separating natural Ta by atomic masses. Samples of milligram weight exist and one such specimen was used in the breakthrough experiment proving the use of x rays to dump the energy stored in isomeric populations. In contrast the entire world inventory of the first entry, $^{178}Hf^{m2}$ appears to be about 10^{15} nuclei (Oganessian, *et al.* 1992).

However, from the perspective of triggering, $^{180}Ta^{m}$ appears to be much less practical. Although the energy storage is still impressively high, the isomeric level lies quite low in energy when compared to the value for the K-breaking gateway at 2.8 MeV. For $^{178}Hf^{m2}$ the energy of the isomer at 2.45 MeV is the highest known that still lies below the likely gateway energy between 2.5 - 3.0 MeV. The isomer ^{174}Hf is even higher at 3.312 MeV, but the availability (Walker, *et al.* 1990) of a spontaneous transition down to the K-mixing level at 2.685 MeV reduces the shelf halflife to only 3.7 μsec.

The ideal energy for an isomer to store for ease in triggering would be as much as possible without exceeding the energy of the K-breaking level for that nuclide. As long as the transition energy needed for triggering is positive, the isomer cannot dump spontaneously as happens with $^{174}Hf^{m}$, so the lifetime of the initial population will be as long as possible and problems of storage will be minimized. Guided to $^{178}Hf^{m2}$ by energetics, a reasonable next concern from the pragmatic viewpoint is for the duration of the trigger pulse.

Even in the best cases the requirement for the energy in a trigger pulse is large. The problem is compounded if the fluorescence lifetime of the level into which the isomeric population is to be dumped by the trigger is too short. Large scale pulsed-power devices typically deliver their outputs in pulses with duration of nanoseconds to a few microseconds, so it would be fortunate to find a laser candidate with strong fluorescence lifetimes of comparable magnitudes. In this case as well, the $^{178}Hf^{m2}$ is favorable having transitions with lifetimes of both tens of nsec and tens of μsec, as will be seen in the following section.

Since the experiments needed to confirm our pragmatic scoring of the better of the 29 candidates for a gamma-ray laser have been postponed by the difficulties in obtaining samples, it has seemed useful to identify simulations which can serve as vehicles with which to develop systems and instrumentations for triggering. To be useful a simulation nuclide needs to have a strong output fluorescence transition that can be reached by cascade from a K-breaking level pumped from the ground state by intense x-ray pulses. Moreover the levels radiating such transitions should have lifetimes of tens of nsec to tens of μsec. Four convenient simulation nuclides are shown in Table II.

Recently we have studied the pumping of the 4 simulation nuclides shown in Table II (Hong 1993). Excitation was provided by our 4 MeV linac which produces 150 mA pulses of electrons of 3 μs duration at a repetition rate of 360 Hz. These are routinely converted to bremsstrahlung with a cooled tungsten converter. The

Compton scattering of this bremsstrahlung from a milligram-sized target support usually produces the main background noise tending to obscure gamma fluorescence from the nuclei being irradiated.

Our present system has used a gated detector to reduce the sensitivity during the pump period. A combination of issues limits the recovery of the system to times after a certain minimum product of photon energy and delay time for the fluorescence signal. As currently implemented this limit is 150 keV x 2 μs. Shown in Fig. 5 is data from the delayed fluorescence of ^{181}Ta detected at 482 keV with a recovery time from the end of the x-ray pulse of 7.22 μs. The literature value of the lifetime of the fluorescent state being pumped is 18 μs which agrees well with the decay constant seen. The energetics of the process are summarized in the diagram in Fig. 6. Similar results are shown in Fig. 7 for the nuclide ^{176}Hf for which the relevant energy levels are summarized in Fig. 8. Analyses of the fluorescence data using Eqs. (1) - (4) yielded new values for the integrated cross sections for pumping short-lived fluorescence. Figure 9 shows these results included in the summary plot of Fig. 4. It is encouraging to observe that the systematics for the pumping of these simulated laser levels closely follows the trends already established for the excitation of longer lived levels that were easier to study. As yet the complementary data on the excitation energies needed to reach the pumping gateways has not been measured in these simulations, but they might reasonably be expected to also continue the established systematics.

3.2 First-Ranked Candidate

The first priority candidate for a gamma ray laser is the 31-year isomer of ^{178}Hf shown in the first line of Table I and it is superior to the next possibilities by orders-of-magnitude. The difficulty has been that macroscopic samples have not been available.

The energy level diagram for ^{178}Hf is shown in Fig. 10 with prominent fluorescent transitions indicated. The fundamental question is whether the K-breaking band will be found at the level shown in the figure that is predicted by systematics.

In case of a weak success in which K-breaking is tending to fail we would expect the preferential population of the band to the right of the figure leading to fluorescence at 437 keV with 35% efficiency from the bandhead having 68 μs lifetime. This is well within current capabilities demonstrated by the simulations.

In case of a strong success in which K-breaking is complete we would expect to preferentially populate the left-side band which leads to fluorescence at 922 keV with 65% efficiency and 1247 keV with 30% efficiency from the bandhead having 78 nsec lifetime. In this case demonstrations of dumping the populations would need to use an accelerator with shorter pulses such as APEX-I in our facility which produces 30 kA of electrons in pulses of 30 nsec having endpoint energies variable from 0.7 to 1.2 MeV. Although a single shot device, it served well in our first investigations of gamma fluorescence (Anderson & Collins 1988b). There is a great advantage in the use of this device since it can be configured to pump the left-side band with bremsstrahlung having 0.7 to 0.8 MeV

endpoint that will give signal fluorescence at 1.25 MeV. It should be straightforward to set discrimination levels in the electronics to reject the scattered pump radiation since it consists of such lower energy photons.

Using the model of the preceding section we can calculate the expected number of fluorescent photons with two assumptions about the overall integrated cross section for pumping to fluorescence,

$$(\sigma\Gamma)_{sys} = 5 \times 10^{-25} \text{ cm}^2 \text{ keV} \quad , \text{ and} \qquad (7a)$$

$$(\sigma\Gamma)_{best} = 2.5 \times 10^{-23} \text{ cm}^2 \text{ keV}, \qquad (7b)$$

where the first is a number consistent with the measurements of Fig. 9 and the second is scaled for the dependence on pump energy given by Eq. (6). The range of excitation energies spanned by the measurements of Fig. 9 is insufficient to determine any correlation between ($\sigma\Gamma$) and the energy needed. As can be seen from the results summarized in Table III, there is an ample safety margin for the arrangement of realistic geometries for the collection and detection of the fluorescent photons if samples of the sizes shown can be acquired.

4. Conclusions

In the most recent years a breakthrough in research on the feasibility of a gamma-ray laser has proven the pervasive occurrence of K-breaking levels which can be used to dump the energies stored in isomeric nuclei by pumping them with x rays. Studies of systematics have shown these levels to lie between 2.5 - 3.0 MeV for nuclei lying in the range of masses spanned by ^{167}Er and ^{195}Pt. An extension of those studies being reported here has now shown that the favorable occurrence of such giant resonances for

pumping nuclear fluorescence extends to the excitation of laserlike transitions having lifetimes between ns and μs. These latest results have provided further guidance in the rankings of the 29 candidate isomers for a gamma-ray laser that have served to identify the one most likely to be successfully pumped, the 31-year isomer, $^{178}Hf^{m2}$.

While the paucity of actual samples has inhibited the final demonstration of feasibility, estimates of likely yields from such experiments have shown that strong levels of fluorescence from laserlike levels of the 31-year isomer $^{178}Hf^{m2}$ should be observable when samples become available. These conclusions would seem to provide a strong motivation for the production of this first ranked candidate for use in a gamma-ray laser.

References

Anderson, J. A. & Collins, C. B. 1987 *Rev. Sci. Instrum.* **58**, 2157.

Anderson, J. A. *et al.* 1988a *Phys. Rev. C* **38**, 2833.

Anderson, J. A. & Collins, C. B. 1988b *Rev. Sci. Instr* **59**, 414.

Carroll, J. J. *et al.* 1991 *Phys. Rev. C* **43**

Collins, C. B. *et al.* 1982 *J. Appl. Phys.* **53**, 4645.

Collins, C. B. *et al.* 1988 *Phys. Rev. C* **37**, 2267.

Collins, C. B. *et al.* 1990 *Phys. Rev. C* **42**, R1813.

Collins, C. B. 1991 *Handbook of Laser Science and Technology* (CRC Press, Boca Raton, FL), pp. 561-567.

Collins, C. B. *et al.* 1992 *Laser Interaction and Related Plasma Phenomena*, G. H. Miley and H. Hora, eds. (Plenum, New York) Vol. 10, pp. 151-166.

Collins, C. B. *et al.* 1993 *Laser and Particle Beams* **11**, 43.

Hong, C. Ph.D. Dissertation 1993 University of Texas at Dallas.

Nelson, W. R. *et al.* 1985 The EGS4 Code System, Stanford Linear Accelerator Center Report No. SLAC 265 (Stanford Linear Accelerator Center, Stanford, CA).

Oganessian, Yu. Ts. *et al.* 1992 *J. Phys. G* **18**, 393.

Walker, P. M. *et al.* 1990 *Phys Rev. Lett.* **65**, 416.

Table I: Examples of nuclear properties for three of the 29 candidate isomers for a gamma-ray laser that are of pragmatic importance in estimating the probabilities for the successful use of that material.

ISOMER	ENERGY DENSITY (Joules/μg)	SHELF HALFLIFE	TRIGGER PHOTON (MeV)
$^{178}Hf^{m2}$	1300	31 years	<0.5
$^{179}Hf^{m2}$	600	25 days	~1.5
$^{180}Ta^{m}$	40	10^{15} years	~2.5

Table II: Summary of properties of nuclides useful in simulating the pumping of the better of the 29 candidates for a gamma-ray laser.

Nuclide	Abundance (%)	Output transitions (keV)	Fluorescence lifetime (μs)
^{81}Br	49.31	260 276	37.6
^{176}Hf	5.206	736 1043	9.9, 9.6
^{181}Ta	99.988	346 482	18
^{201}Hg	13.1	521	92

Table III: Summary of expected numbers of excitations from microweight samples of the 31-year isomer of ^{178}Hf pumped with the UTD linac in a 100 % coupling geometry.

Isomeric (^{178}Hf) Nuclei	($\sigma\Gamma$)	Linac (3.3 x 10^{18} photons/cm^2 per hour)
3 x 10^{13}	Systematic	2.3 x 10^{4}
	Best	1.1 x 10^{6}
10^{14}	Systematic	7.6 x 10^{4}
	Best	3.8 x 10^{6}
3 x 10^{14}	Systematic	2.3 x 10^{5}
	Best	1.1 x 10^{7}
10^{15}	Systematic	7.6 x 10^{5}
	Best	3.8 x 10^{7}

Captions

Figure 1: Schematic representation of the decay modes of a gateway state of width Γ sufficiently large to promote bandwidth funneling. The initial state from which population is excited with an absorption cross section σ_0 can be either ground or isomeric.

Figure 2: Activation efficiencies, A_r for the reaction $^{87}Sr(\gamma,\gamma')^{87}Sr^m$ are shown as functions of the endpoint, E_0 of the bremsstrahlung used for excitation. The solid curve plots values computed from Eq. (3) using gateway parameters found in the literature together with calculated photon spectra. The figure compares these A_r values with measurements obtained from four different accelerators.

Figure 3: Activation efficiencies, A_r for the reaction $^{180}Ta^m(\gamma,\gamma')^{180}Ta$ are shown as functions of the endpoint, E_0 of the bremsstrahlung used for excitation. Gateway parameters were found from calculated photon spectra using Eq. (3).

Figure 4: Integrated cross sections for pumping isomeric nuclei obtained in the survey of Carroll *et al.* 1991. The groupings of pumping strengths seen in the figure correspond to mass islands between magic numbers for neutrons and protons. The best candidates for a gamma-ray laser lie within the island containing the largest values of integrated cross sections corresponding to giant pumping resonances. Within each island the integrated cross

sections, and the gateway excitation energies plotted with the right-hand axis, vary only slowly with changing mass number, A.

Figure 5: Fluorescence detected from decay of the 615 keV isomer of ^{181}Ta. The data were obtained using a gated detector system and correspond to nearly 10^6 acquisition cycles. Each cycle began when the detector was gated on 7.22 μs (t = 0 on the horizontal axis) after the end of a 3 μs pulse of x rays from the linac, as illustrated in schematic form. The solid line shows a fit to the data which agrees well with the literature value of 18 μs.

Figure 6: Schematic diagram showing the energy levels important for the excitation of the 615 keV, 18 μs laserlike level in ^{181}Ta. The large upward arrow indicates the absorption transition to a gateway located near 2.8 MeV which populates the laserlike level by a branch of its decay cascade (shown by the downward dashed arrow). Transitions providing photons used to detect the decay of the 18 μs state are indicated with their energies.

Figure 7: Fluorescence detected from decay of the 1333 keV isomer of ^{176}Hf. The data were obtained using a gated detector system and correspond to nearly 10^5 acquisition cycles. Each cycle began when the detector was gated on 7.22 μs (t = 0 on the horizontal axis) after the end of a 3 μs pulse of x rays from the linac. The solid line shows a fit to the data which agrees well with the literature value of 9.6 μs.

Figure 8: Schematic diagram showing the energy levels important for the excitation of the 1333 keV, 9.6 μs laserlike level in ^{176}Hf. The large upward arrow indicates the absorption transition to a gateway located near 2.8 MeV which populates the laserlike levels by branches of its decay cascade (shown by the downward dashed arrows). Transitions providing photons used to detect the decay of the 9.6 μs state are indicated with their energies.

Figure 9: Integrated cross sections for pumping laserlike levels along with those of Fig. 4 for the pumping of long-lived isomers. Again the groupings correspond to mass islands between magic numbers and the best candidates are identified as neighbors of the nuclide ^{180}Ta.

Figure 10: Energy level diagram of ^{178}Hf. The spontaneous decay of the 31-year isomeric state does not excite transitions in the left-side band nor is it able to excite the K = 14 bandhead which cascades through the right-side band during its 68 μs halflife. The K-mixing level inferred from systematics is shown by the wide shaded band near 2.8 MeV and the large upward arrow symbolizes the pumping step from the 31-year isomer. Transitions providing photons useful for detection of the dumping reaction are identified along with their energies.

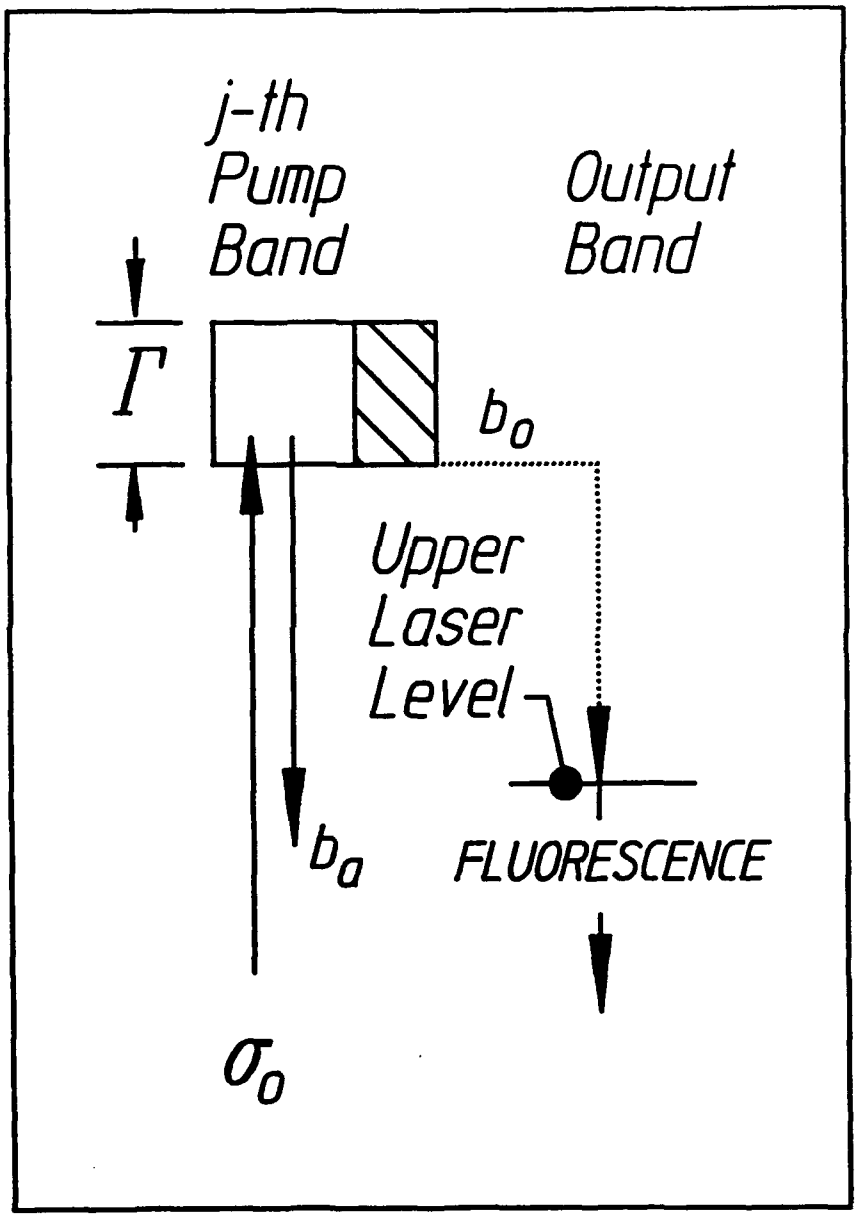
j-th
Pump
Band
Output
Band
Γ
b_o
Upper
Laser
Level
b_a
FLUORESCENCE
σ_o

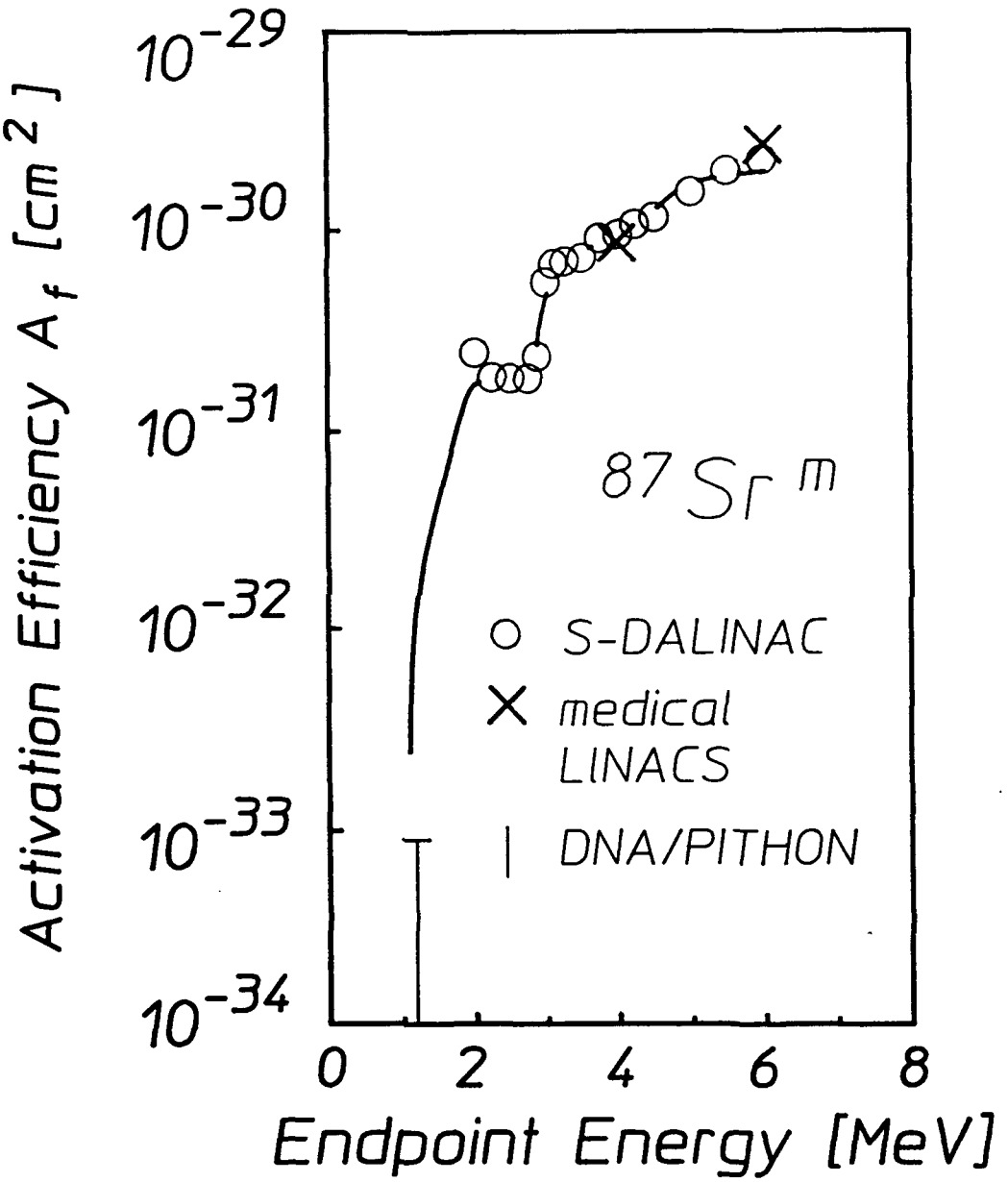
Activation Efficiency A_f [cm^2]
10^{-29}
10^{-30}
10^{-31}
10^{-32}
10^{-33}
10^{-34}
$^{87}Sr^m$
S-DALINAC
medical LINACS
DNA/PITHON
0
2
4
6
8
Endpoint Energy [MeV]

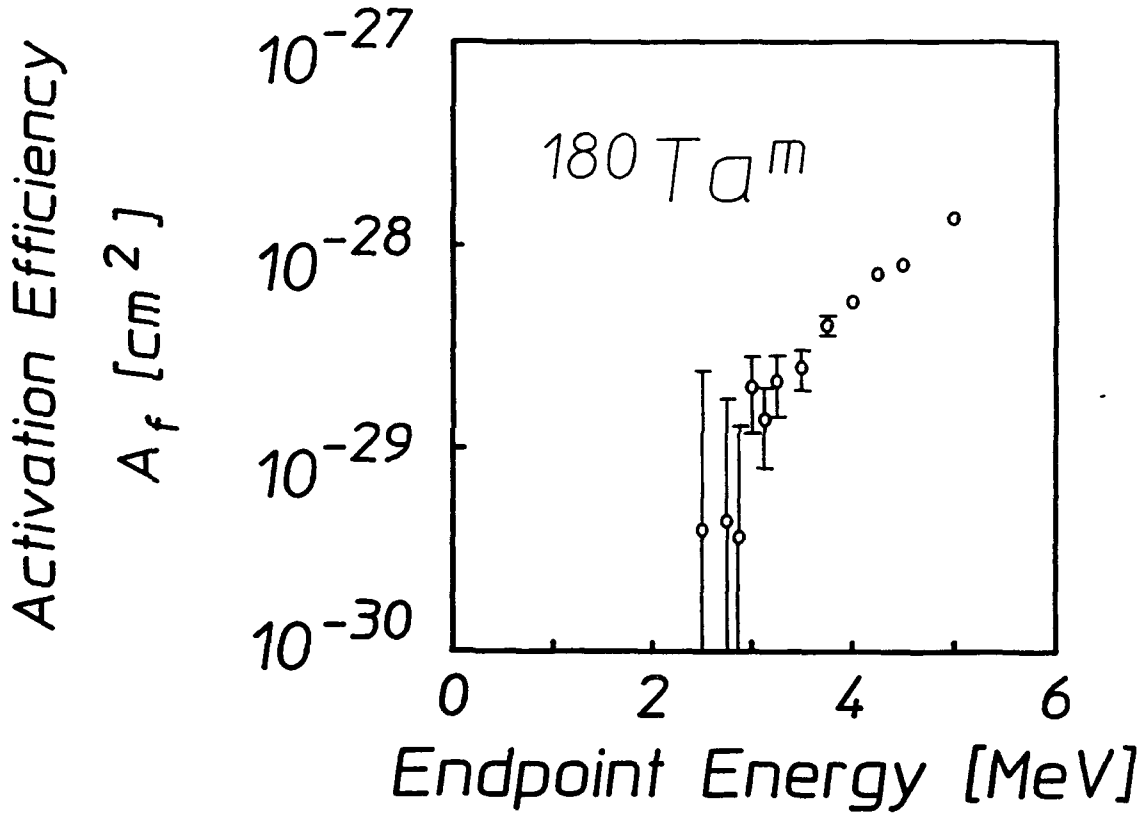
Activation Efficiency
A_f [cm^2]
10^{-27}
10^{-28}
10^{-29}
10^{-30}
$^{180}Ta^m$
0
2
4
6
Endpoint Energy [MeV]

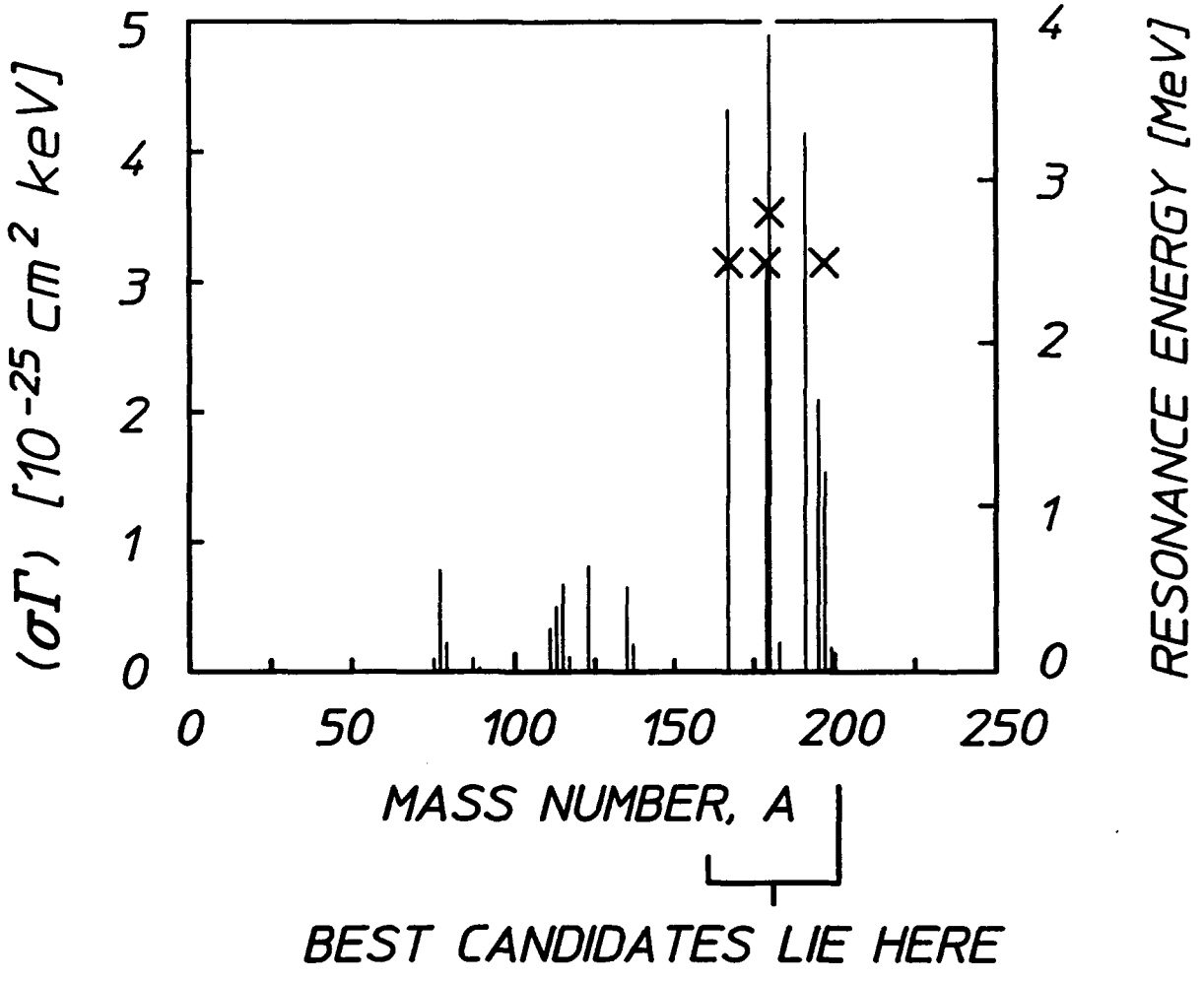
(σΓ) [10⁻²⁵ cm² keV]
RESONANCE ENERGY [MeV]
0
1
2
3
4
5
0
50
100
150
200
250
MASS NUMBER, A
BEST CANDIDATES LIE HERE

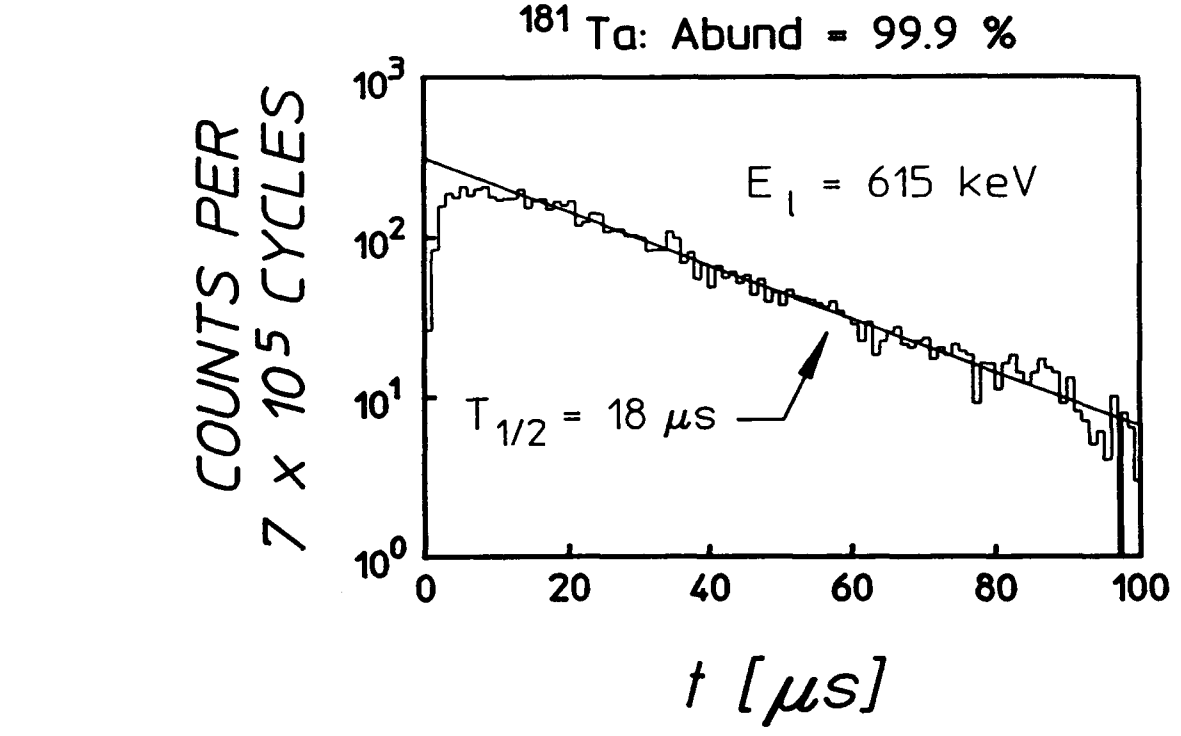
181 Ta: Abund = 99.9 %
COUNTS PER
7 x 10^5 CYCLES
10^3
10^2
10^1
10^0
E_l = 615 keV
T_1/2 = 18 μs
0
20
40
60
80
100
t [μs]

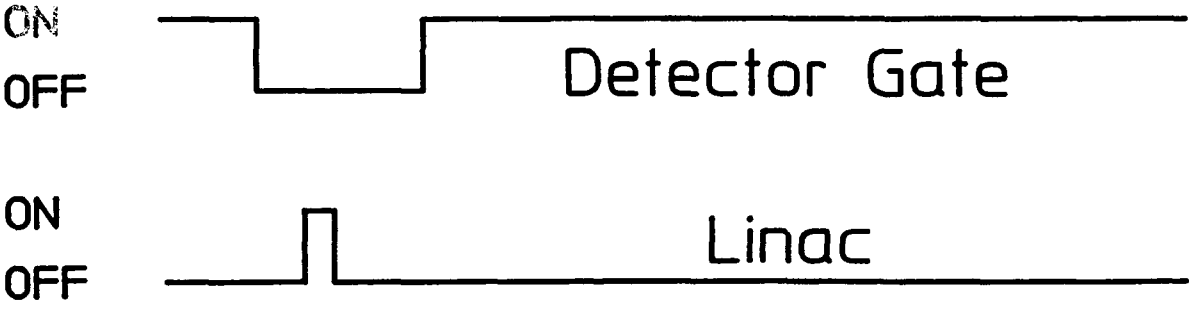
ON
OFF
Detector Gate
ON
OFF
Linac

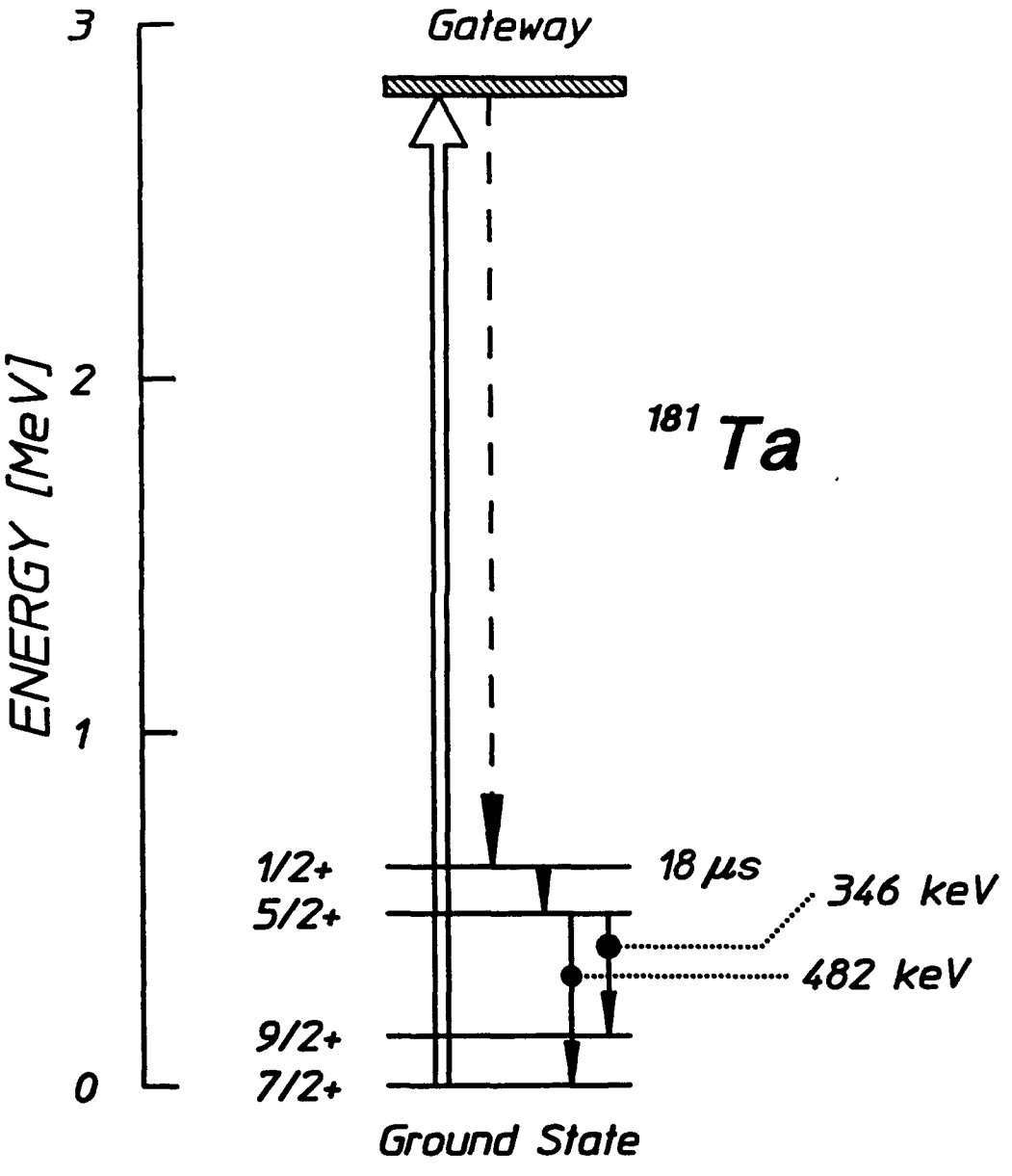
Gateway
3
2
1
0
ENERGY [MeV]
181 Ta
1/2+
5/2+
9/2+
7/2+
18 μs
346 keV
482 keV
Ground State

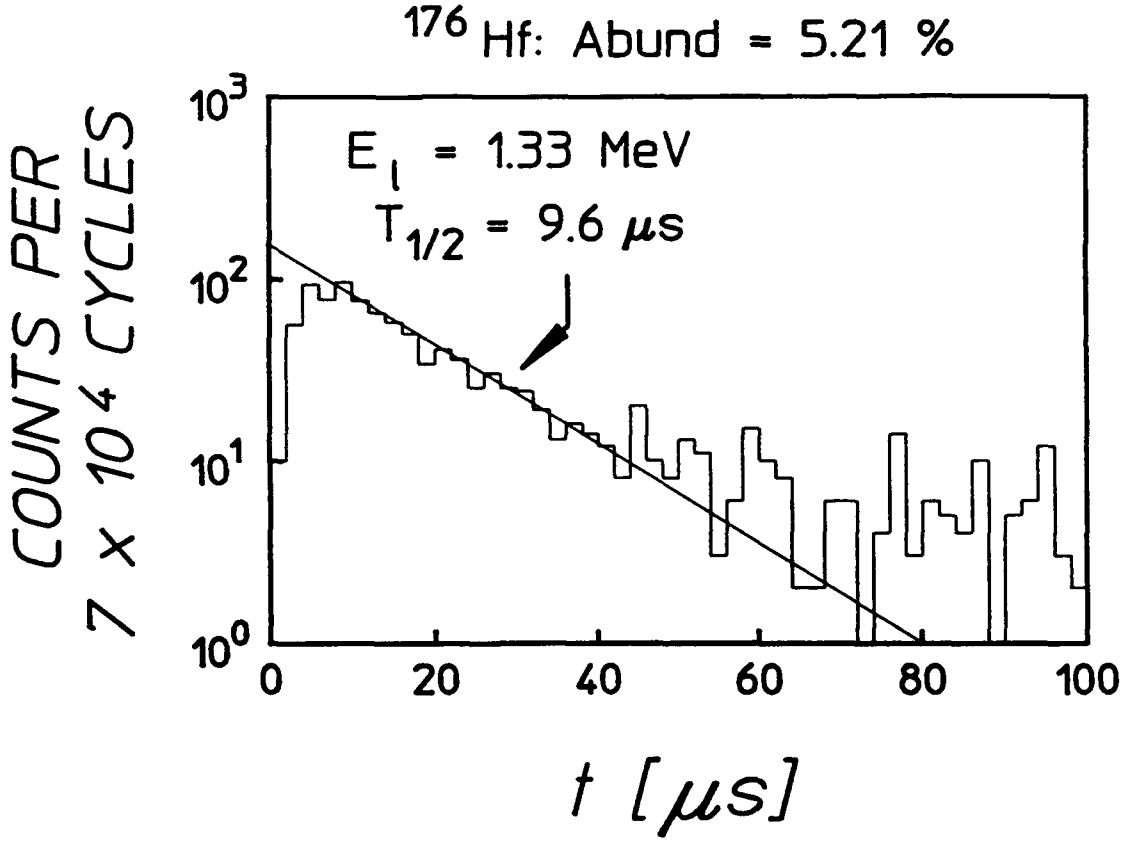
^{176}Hf: Abund = 5.21 %
E_l = 1.33 MeV
$T_{1/2}$ = 9.6 μs
COUNTS PER
7 x 10⁴ CYCLES
10³
10²
10¹
10⁰
0
20
40
60
80
100
t [μs]

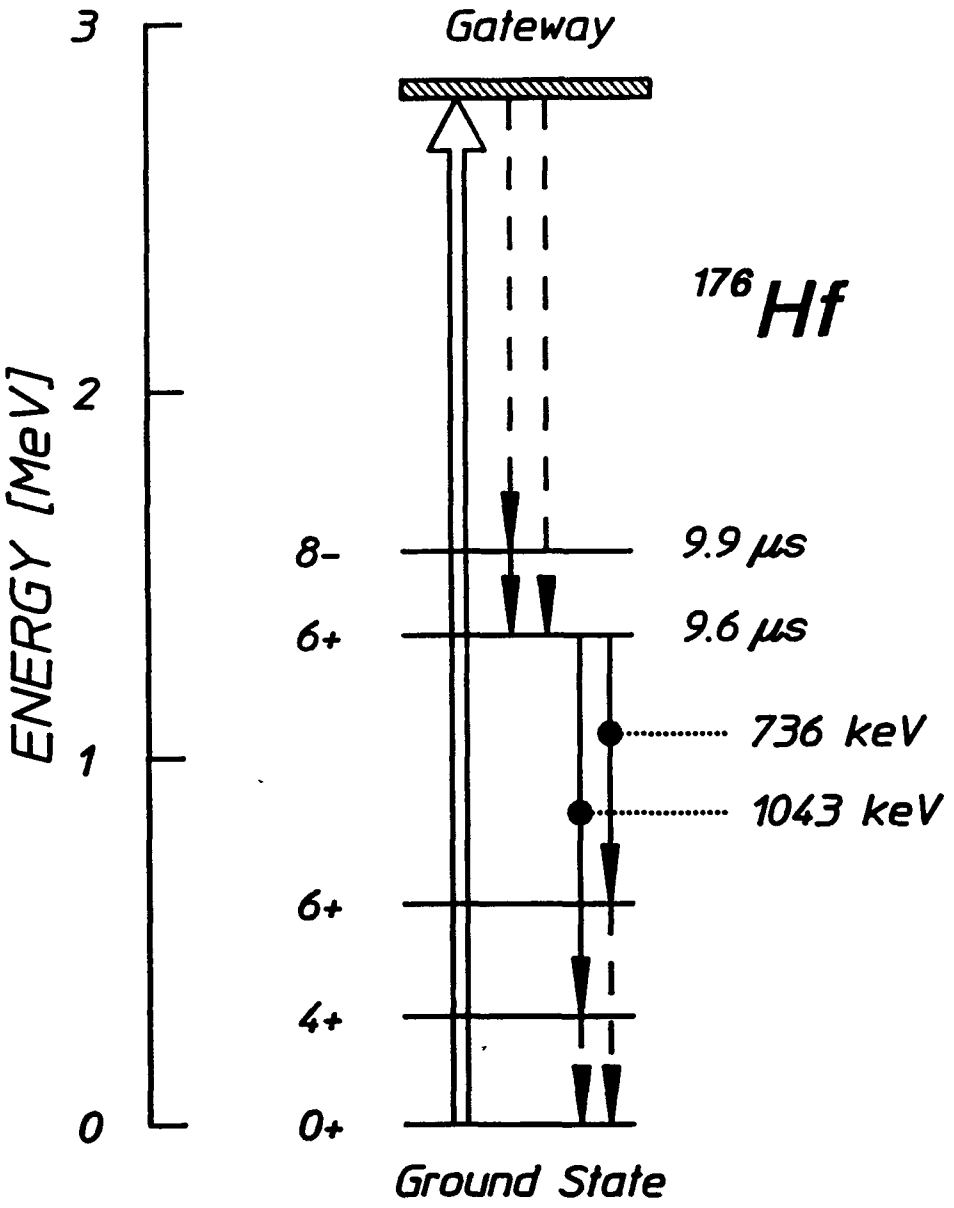
Gateway
^{176}Hf
ENERGY [MeV]
3
2
1
0
8-
6+
9.9 μs
9.6 μs
736 keV
1043 keV
6+
4+
0+
Ground State

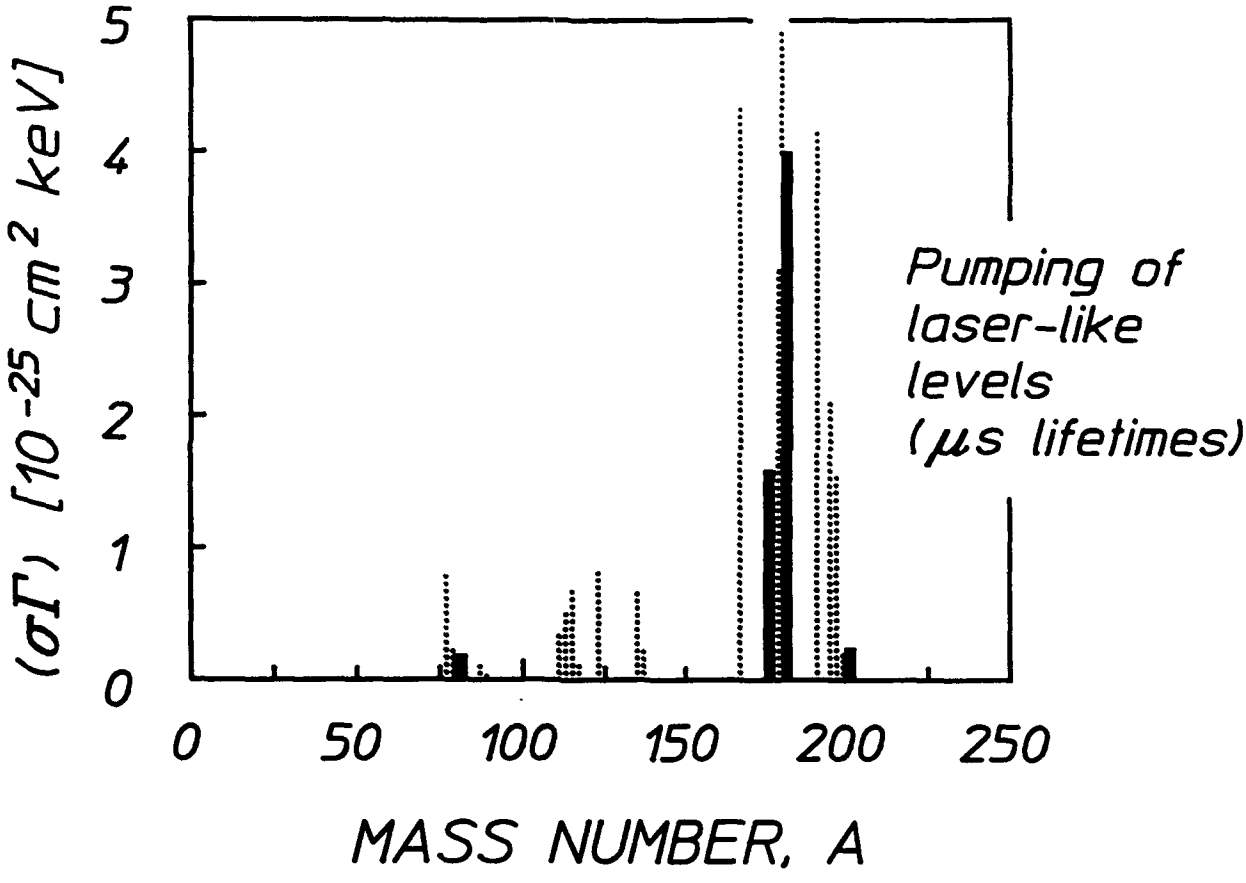
$(\sigma\Gamma)$ $[10^{-25}\,cm^2\,keV]$
0
1
2
3
4
5
0
50
100
150
200
250
MASS NUMBER, A
Pumping of laser-like levels (μs lifetimes)

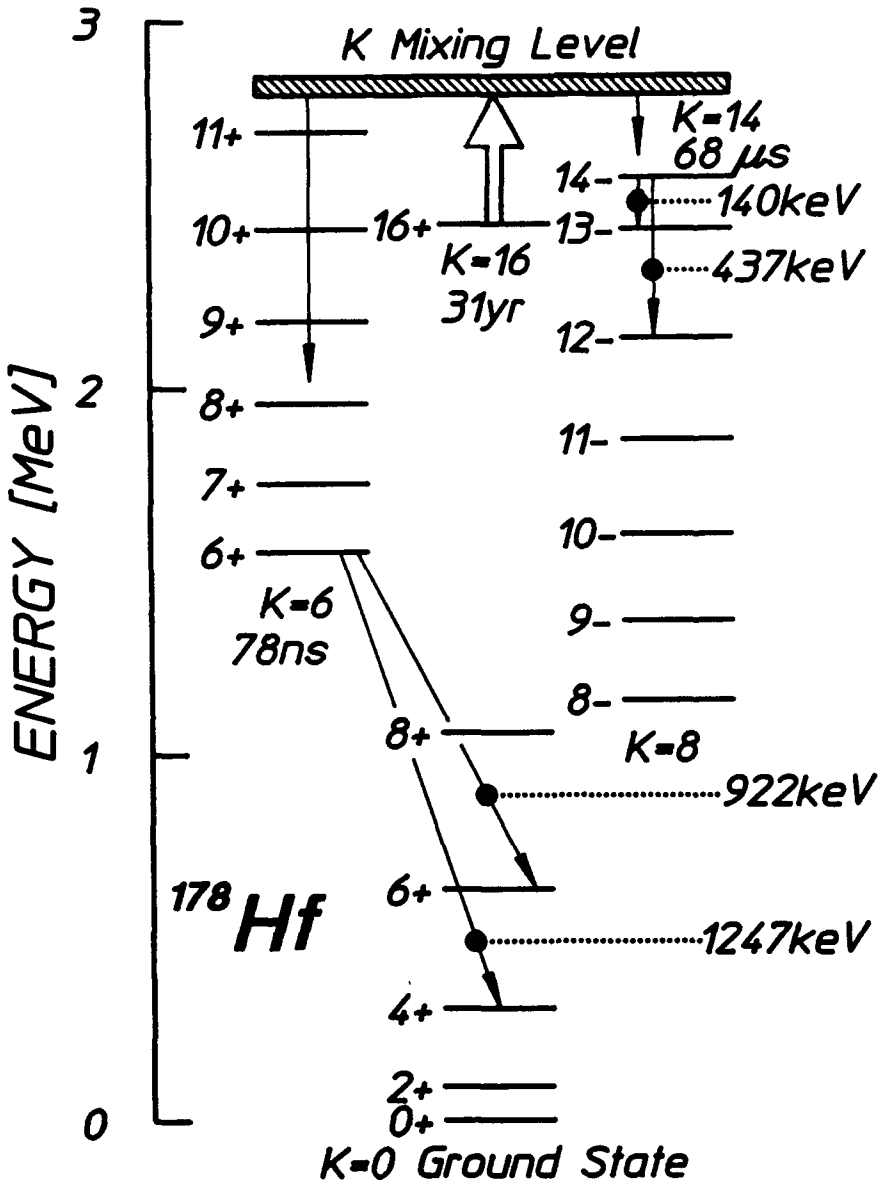
3
2
1
0
ENERGY [MeV]
K Mixing Level
11+
10+
9+
8+
7+
6+
K=6
78ns
16+
K=16
31yr
K=14
68 μs
14-
13-
12-
140keV
437keV
11-
10-
9-
8-
K=8
8+
922keV
6+
1247keV
4+
2+
0+
178 Hf
K=0 Ground State

Intermediate structure in the photoexcitation of $^{77}Se^m$, $^{79}Br^m$, and $^{137}Ba^m$

J. J. Carroll,[1] C. B. Collins,[1] K. Heyde,[2] M. Huber,[3] P. von Neumann-Cosel,[3] V. Yu. Ponomarev,[4] D. G. Richmond,[1] A. Richter,[3] C. Schlegel,[3] T. W. Sinor,[1] and K. N. Taylor[1]

[1]*Center for Quantum Electronics, The University of Texas at Dallas, P.O. Box 830688, Richardson, Texas 75083*

[2]*Institute for Theoretical Physics, Proeftuinstraat 86, B-9000 Gent, Belgium*

[3]*Institut für Kernphysik, Technische Hochschule Darmstadt, Schlossgartenstrasse 9, D-64289 Darmstadt, Germany*

[4]*Laboratory of Theoretical Physics, Joint Institute for Nuclear Research, Dubna, Head Post Office, P.O. Box 79, Moscow, Russia*

(Received 28 June 1993)

Continuing the systematic investigation into the photoexcitation of isomers over wide mass and energy ranges, the production of $^{77}Se^m$, $^{79}Br^m$, and $^{137}Ba^m$ was studied with the bremsstrahlung facility at the superconducting Darmstadt linear accelerator. These isomers have half-lives on the order of seconds. Excitation functions were measured for the (γ,γ') reactions populating the metastable states for energies of 2–7 MeV and the important intermediate states were identified. Nuclear structure calculations with the quasiparticle-phonon model for ^{79}Br and the particle- (hole-) core coupling approach for ^{137}Ba gave satisfactory descriptions for the strength and position of the dominant mediating levels. Admixtures of fragmented outershell single-particle strength shifted to low energies were identified as essential features of the wave functions of those states. Intermediate states in ^{77}Se displayed very large strengths compared to other isomers in the same mass region, providing further support for the correlation between integrated cross sections and ground state deformations recently discovered in the $A = 160-200$ mass region. Such an enhancement would considerably improve the feasibility of a gamma-ray laser based on the sudden deexcitation of isomeric populations in deformed nuclei.

PACS number(s): 25.20.Lj, 27.50.+e, 27.60.+j, 21.90.+f

I. INTRODUCTION

It has been known for more than fifty years that nuclear isomers could be populated by (γ,γ') reactions, yet the greatest progress in the study of this process and the underlying nuclear structure has occurred in the past decade. To a large degree this renaissance has been driven by research directed towards determining the feasibility of a gamma-ray laser whose pump scheme [1,2] would rely on the resonant deexcitation of long-lived nuclear isomers through intermediate states (IS). Such research has required the systematic development of a database describing the population and depopulation of metastable levels. This effort began in earnest [3–10] in 1987 and has recently concentrated [11–16] on the investigation of IS in the largely unexplored excitation energy range of 2–6 MeV.

Applications notwithstanding, the photoactivation of isomers is important in its own right. For example, the integrated cross sections measured for IS can reveal interesting nuclear structures [17–19] since both strong absorption transitions from the ground state and significant cascades to the isomer are needed. In this regard the combination of photoactivation and nuclear resonance fluorescence (NRF) experiments has proven to be a particularly useful tool and the resulting information has been successfully compared with microscopic calculations [13,16]. For deformed nuclei a remarkable discovery [5,11,14] was the appearance of low-lying levels which efficiently couple ground states and isomers differing by as many as eight units in the quantum number K, the projection of the total angular momentum on the major nuclear axis. The properties of IS are important in nuclear astrophysics when stellar nucleosynthesis of a radioisotope is expected to branch to both ground state and isomer which have greatly differing lifetimes [9,11,20]. In a practical field, nuclides with well-known IS can be used to characterize intense bremsstrahlung produced by linear accelerators or pulsed-power machines [21–23].

The systematic investigation of the photoexcitation of isomers was continued in this work by the study of ^{77}Se, ^{79}Br, and ^{137}Ba whose isomers have half-lives on the order of seconds. In addition to the experimental data, nuclear structure calculations are presented for ^{79}Br and ^{137}Ba which permitted a detailed interpretation of the interplay between single-particle and collective properties that provided the observed intermediate states.

II. EXPERIMENTS

A. Methods

The experiments were performed using the injector of the superconducting continuous wave electron accelerator (S-DALINAC) at Darmstadt [24]. Bremsstrahlung for the experiments was produced by electrons which impinged on a 3 mm thick tantalum converter foil. The

TABLE I. Summary of the literature values [25] for the relevant nuclear parameters and transparencies for the escape of fluorescence photons from samples of the nuclides.

Nuclide	g.s. spin J^π	E_{iso} (keV)	Isomer spin J^π	$T_{1/2}$ (s)	Abundance (%)	Principal fluorescence (keV)	Transparency (%)
^{77}Se	$\frac{1}{2}^-$	162	$\frac{7}{2}^+$	17.4	7.6	161.92	76
^{79}Br	$\frac{3}{2}^-$	207	$\frac{9}{2}^+$	4.86	50.69	207.2	76
^{137}Ba	$\frac{3}{2}^+$	662	$\frac{11}{2}^-$	153.12	11.23	661.66	85

electron energies were measured before and after each exposure to an accuracy of 50 keV and were varied from $E_0=2$ to 7 MeV in step sizes of 125 and 250 keV. The proper beam alignment was insured by maximizing the dose registered in a remote ionization chamber which viewed only the central 12 mrad of the bremsstrahlung. Variations in all beam parameters were recorded during each exposure, including the total charge passed to the converter.

Targets consisted of elemental Se and compounds of LiBr and BaF_2 with typical masses of 3–6 g. The materials were contained in hollow aluminum cylinders with 3.5 cm length and 1.4 cm outer diameter. The samples were irradiated axially with their plane faces located 1.3 cm from the converter foil. Nominal electron beam currents were 5 μA and the exposure periods were typically twice the half-life of the isomer being investigated. At the end of each irradiation the samples were transported pneumatically to a well-type NaI(Tl) detector for counting as described in more detail in Refs. [15,16]. To improve the statistical accuracy of the data, measurements were repeated for up to sixteen cycles for each isotope and electron energy. A sample of elemental In was also irradiated at some energies for calibration.

The numbers of isomers produced by these exposures were determined from the counting rates measured in distinctive fluorescence lines. The γ-ray signatures and other relevant parameters for the isomers investigated here are summarized in Table I. The raw numbers of counts within peaks observed in pulse-height spectra were corrected in a standard fashion [15] to account for the isomer half-lives, the detection efficiencies, and the opacities of samples to the escape of fluorescence photons. A typical example of the data is shown in Fig. 1(a) and was obtained from a Se sample following its irradiation with bremsstrahlung having an end-point energy of $E_0=4$ MeV. The isomeric decay signature was clearly identified despite the relatively poor resolution of the NaI spectrometer. In addition to pulse-height spectra, a multichannel analyzer was used to obtain decay curves like that of Fig. 1(b). As shown, there was excellent agreement between measured and adopted [25] values for the isomeric half-lives.

B. Data analysis

Recent investigations have confirmed [11–16,26] that the population of isomers by (γ,γ') reactions at excitation energies below the photoneutron threshold proceeds by the process depicted schematically in Fig. 2. The figure identifies the relevant parameters including the natural width of the intermediate state Γ and the branching ratios b_0 and b_{iso} for decay from the IS directly to the ground state and by unknown cascade to the metastable level, respectively. Along with the Breit-Wigner cross section for the absorption transition, these form the integrated cross section for population of the isomer through the IS,

$$(\sigma\Gamma)_{iso}=\pi^2\left|\frac{\hbar c}{E}\right|^2\frac{2J_{IS}+1}{2J_0+1}b_0b_{iso}\Gamma\ , \tag{1}$$

where J_{IS} and J_0 are the angular momenta of the IS and ground state, respectively, and E is the energy of the absorption transition. The integrated cross section is expressed in usual units of 10^{-29} cm^2 keV, equivalent to 0.01 eV b. This quantity is of primary importance for photoactivation studies since the normalized activation A_f giving the fractional yield of isomers produced by an

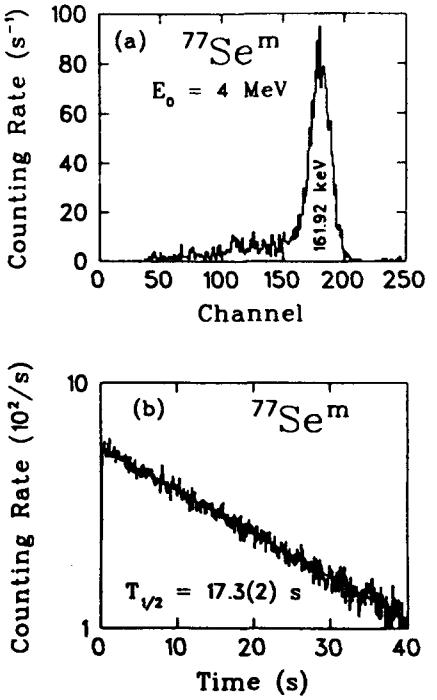

FIG. 1. (a) Pulse-height and (b) time-decay spectra obtained from a Se sample following its irradiation with bremsstrahlung having an end point of 4 MeV. The straight line in (b) represents a best fit (log scale) with $T_{1/2}=17.3\pm0.2$ s which agrees well with the literature value [25] of 17.45 s.

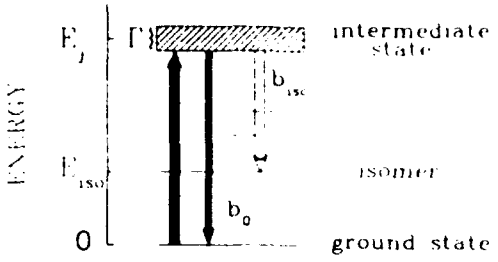

FIG. 2. Schematic representation of the resonant photoexcitation mechanism by which an isomer at an energy of E_{iso} is populated through the hatched intermediate state (IS). The IS is characterized by it excitation energy E_j and its natural width Γ. The branching ratios b_0 and b_{iso} describe the decay of the IS to the ground state and to the isomer, respectively. The latter quantity is the sum of all unknown cascades through the dashed levels which lead to the isomer.

irradiation per incident photon is

$$A_f = \frac{N_{iso}}{N_T \Phi_0} = \sum_j (\sigma\Gamma)^j_{iso} F(E_j, E_0) , \qquad (2)$$

where N_{iso} is the number of isomers produced, N_T is the number of target nuclei, Φ_0 is the total photon flux for the specified end-point energy E_0, and $F(E_j, E_0)$ is the distribution of energies within the bremsstrahlung continuum normalized to 1. The summation in Eq. (2) allows the participation of a plurality of well-spaced gateways.

Values for Φ_0 and $F(E_j, E_0)$ were obtained for each end-point with the well-established EGS4 electron-photon transport code [27], as described in detail elsewhere [11–16]. The calculated spectra were validated with the $^{115}In(\gamma,\gamma')^{115}In^m$ reaction which is characterized sufficiently to serve as a calibration standard [13,23].

III. RESULTS

Figure 3 displays excitation functions of A_f vs end point for the production of $^{77}Se^m$, $^{79}Br^m$, and $^{137}Ba^m$. For comparison, the asterisks represent the experimental results obtained at $E_0 = 6$ MeV from Ref. [10]. The good agreement observed between values measured in completely different experimental environments established confidence in the procedures. Intermediate states were identified by sharp increases in the normalized activation. Integrated cross sections were then extracted by fitting Eq. (2) to the data in such a way as to minimize the residue,

$$R_M(E_0) = A_f(E_0) - \sum_{E_j = E_1}^{E_M} (\sigma\Gamma)^j_{iso} F(E_j, E_0) , \qquad (3)$$

by successively removing contributions from the M lowest-lying IS.

End-point energies below 2 MeV were not accessible in the present work so previously measured experimental values for IS at lesser energies were included in the fitting procedure. In instances where literature values were unavailable or insufficient to reproduce the excitation functions of Fig. 3 up to the energy of the first visible IS, a single intermediate state was introduced at an excitation energy below 2 MeV. Its position and integrated cross section were chosen to remove the baseline level of activation and did not necessarily correspond to that of a real level. Properties of IS which reproduced the excitation functions measured here are summarized in Table II.

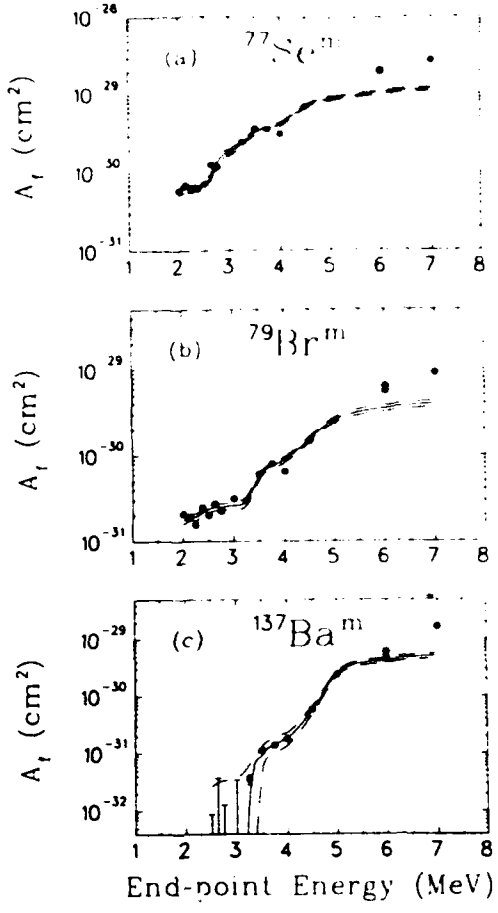

FIG. 3. Normalized yields A_f as functions of electron energy for the populations of (a) $^{77}Se^m$, (b) $^{79}Br^m$, and (c) $^{137}Ba^m$. The asterisks represent experimental results of Ref. [10] obtained at 6 MeV in a completely different environment and agree well with the present data. The solid lines correspond to excitation functions calculated using Eq. (2) with the intermediate states listed in Table II and the dashed lines describe the error bounds of this approach.

The ^{77}Se excitation function at low energies ($E_0 \leq 2.6$ MeV) was partially reproduced by including the 30×10^{-29} cm^2 keV IS at 1.005 MeV of Anderson *et al.* [4], but neglecting the small contributions of the lower-lying levels listed there. The missing strength below 2 MeV was ascribed to an IS at 1.7 MeV of 150×10^{-29} cm^2 keV which served to remove the remaining baseline activation. Boivin *et al.* [28] also examined the production of this isomer up to an excitation energy of 1.7 MeV. Their work indicated three important IS at 1.000, 1.190, and 1.600 MeV with integrated cross sections of 3.2×10^{-29}, 18×10^{-29}, and 52×10^{-29} cm^2 keV, respectively. However, the yield calculated with these values severely underestimated the data. It is noteworthy that

TABLE II. Values of integrated cross sections $(\sigma\Gamma)_{E_0}$ and excitation energies E_j of the intermediate states most important in the production of these isomers by (γ,γ') reactions. Values needed to fit the data were determined in this work by minimizing the residues of Eq. (5). Values available in the literature, where available, were used to reproduce the excitation functions for energies below that of IS clearly identified in this work. Strengths listed above 4 MeV were introduced to account for the excess yield observed toward higher energies and did not necessarily correspond to single levels or groups of levels. No error is given for the 2 MeV state in ^{137}Ba since this level was simply used to estimate the maximum strength corresponding to the baseline activation resulting from null measurements at $E_0 < 3$ MeV.

Isomer	E_j (MeV)	$(\sigma\Gamma)_{E_0}$ (10^{-29} cm^2 keV)	
^{77}Se^m	1.005	30	Ref. [4]
	1.7±0.1	150±15	
	2.6±0.1	1200±120	
	3.2±0.1	3700±370	
	4.0±0.1	5500±1000	
^{79}Br^m	0.761	5.9	Refs. [3,4,29]
	1.8±0.1	65±6	
	3.2±0.1	850±90	
	4.4±0.2	7000±1500	
^{137}Ba^m	2.0	<15	
	3.2±0.1	220±20	
	4.5±0.2	8500±800	

when their integrated cross section at 1.005 MeV was replaced by that of Ref. [4], and with their values for IS at 1.190 and 1.600 MeV, good agreement was obtained between the calculated and measured excitation function below 2.6 MeV.

In the case of ^{79}Br, the well-known level [3,4,29] at 0.761 MeV was included as listed in Table II. The literature does not support the identification of any other IS up to an energy of 1.7 MeV. However, after removing the contribution from the above state the shape of the excitation function of Fig. 3(b) did not indicate a flat baseline but instead followed the isochromat [30] of an IS positioned near 2 MeV. Therefore a level was concluded to lie at 1.8±0.1 MeV as shown in the table.

The data displayed below 3 MeV in the excitation function for ^{137}Ba represent upper bounds on the yield obtained from null measurements for fluorescence from the isomer. This small baseline was consistent with an IS at 2 MeV with less than 15×10^{-29} cm^2 keV for its integrated cross section. For comparison a level at 1 MeV with less than 3×10^{-29} cm^2 keV would have also been allowed. The literature [31] describing excited states lying below 2.6 MeV does not support the identification of any IS so it was concluded that the first intermediate state of significant strength was located at 3.2±0.1 MeV.

The results of the application of Eqs. (2) and (3) that included the low-lying levels discussed above are shown as the solid lines in Fig. 3. The dashed lines define bands describing the errors in the values given in Table II and those quoted in the literature.

IV. MODEL CALCULATIONS

A. ^{79}Br

The photoexcitation of ^{79}Br^m, an odd-even nucleus, was studied in the quasiparticle-phonon model (QPM). The method for treating such nuclei in this theoretical framework is described in detail in Ref. [32] and has been successfully applied to the calculation of NRF and isomer photoexcitation [16] in ^{89}Y. Calculations of the properties of the ^{81}Br$(\gamma,\gamma')^{81}$Br^m reaction are also available [19] which should show very similar structure to those for ^{79}Br since both nuclei have the same g.s. and isomer spins. The two extra neutrons in ^{81}Br are not expected to significantly change the average field.

Calculations were performed with the wave function

$$\Psi_\nu(JM)=C_J^\nu\left[\alpha_{JM}^\dagger+\sum_{\lambda\mu i}D_j^{\lambda i}(J\nu)(\alpha_{jm}^\dagger Q_{\lambda\mu i}^\dagger)_{JM}\right]\Psi_0\,, \qquad (4)$$

for states with angular momentum J and projection M. In Eq. (4), $\alpha_{JM}^\dagger$ denotes the one quasiparticle and $Q_{\lambda\mu i}^\dagger$ the phonon creation operator for angular momentum λ, projection μ, and random phase approximation root number i. The g.s. wave function of the even-even core is denoted by Ψ_0 and ν is the number within a sequence of states of given J^π.

The effective QPM Hamiltonian includes the average field, pairing interactions, and a residual interaction between quasiparticles. The latter was adjusted to reproduce the energy and strength of the 2_1^+ and 3_1^+ phonons in the neighboring even-even nuclei. A Woods-Saxon potential with the parametrization of Ref. [33] was used to describe the average field. Phonons with $J^\pi=1^\pm,2^\pm,3^\pm,4^\pm,5^-,6^+$, including the collective as well as two-quasiparticle states, were considered in the summation of the second term of Eq. (4). The complete configuration space up to $E_x=12$ MeV was taken into account to avoid truncation effects.

Numerical calculations were performed with the code PHOQUS [34]. The calculations were restricted to one-phonon coupled states, since the total electromagnetic

strength is known to be unaffected by the inclusion of multiphonon coupled configurations. An effective spin g factor $g^s_{\rm eff}=(0.8)g^s_{\rm free}$ was used. Effective charges $e^p_{\rm eff}=(N/A)e$ and $e^n_{\rm eff}=-(Z/A)e$ were introduced for $E1$ transitions to separate the central mass motion.

B. ^{137}Ba

The single-hole configuration of the unpaired neutron in ^{137}Ba relative to the $N=82$ shell closure suggested that the hole-core coupling model [35], called the unified model (UM), would be a useful approach. In the comparable case of ^{115}In (one proton hole relative to $Z=50$), encouraging results were obtained both for the description of NRF and for the isomer photoexcitation [13]. Also a detailed UM study of ^{143}Nd (one particle relative to $N=82$) has recently been reported which successfully accounted for all major features of the low-energy spectrum [36].

The configuration space consisted of 1h (one-hole) states (with respect to the semimagic ^{138}Ba nucleus) and 1p-2h (one-particle–two-hole) states (with respect to ^{136}Ba). The g.s. wave function of ^{136}Ba relative to the neutron closed shell at $N=82$ was calculated with the pairing interaction of the Hamiltonian. A realistic approximation to the ^{136}Ba g.s. wave function was essential, because important contributions to the electromagnetic excitations would have been missed using a simple pure two-hole $(s_{1/2})^{-2}_{0^+}$ configuration as suggested by the independent-particle model.

Single-particle energies were taken from systematics of the odd-mass Ba nuclei and the single-particle space was coupled to collective 2^+ and 3^- phonons in the neighboring even nuclei [37]. Excitation energies and transition strengths for those phonons were adopted from experimental data. The energy shift between 1h states and 1p-2h states across the shell closure was estimated from the neutron separation energy differences [35] between the ^{137}Ba and ^{139}Ba nuclei.

An effective charge $e^p_{\rm eff}=(1.5)e$ and effective g factor $g^s_{\rm eff}=(0.7)g^s_{\rm free}$ were used for the calculations of electromagnetic transitions. A collective limit $g_R=Z/A$ was assumed for the gyromagnetic ratio. As was the case [13] for ^{115}In, strong transitions were hardly affected by using other g_R values, e.g., $g_R=0$.

The results of the UM calculations were validated against the low-energy spectrum [31] up to $E_x=2$ MeV. The $J^\pi=\frac{11}{2}^-$ isomer energy was found to be 150 keV too high, but this was sensitive to the $h_{11/2}$ single-particle energy and the 3^-_1 coupling strength in ^{136}Ba. Transitions between low-lying states ($E2$ transitions only) were reproduced within a factor of 2 for the scarce information available in the literature.

V. DISCUSSION

A. ^{77}Se

The nucleus ^{77}Se shows a very complex structure at low excitation energies [38,39] and no calculations are available for electromagnetic transitions above 1 MeV. The activation function in Fig. 3(a) is dominated by a transition at 2.6 MeV. The integrated cross section of Table II may be converted into a decay width and the corresponding reduced transition probabilities are $B(E1)\geq 2.9\times10^{-3}$ W.u., $B(M1)\geq 0.17$ W.u., and $B(E2)\geq 33.0$ W.u., depending on the assumed nature of the excitation step. These values are lower limits only, since the largest possible product of branching ratios, $b_0b_{\rm iso}=0.25$ was used. Typically, the branching ratio factor could be expected to be about 2–5 times smaller than this value.

It is interesting to note that yields obtained for ^{77}Se^m are much larger than those in other isomers in the same mass region (^{79}Br, ^{81}Br, ^{87}Sr, ^{89}Y). A large g.s. deformation ($\beta=-0.28$) has been derived [39] for ^{77}Se from Coriolis coupling calculations and therefore this provides another hint for the peculiar role of deformation in the variations of integrated cross sections for the population of isomers in different nuclei [15].

B. ^{79}Br

The ground state and isomer have spin structures of $\frac{3}{2}^-$ and $\frac{9}{2}^+$, respectively, so the isomer can be reached by either an $E2$ excitation to a $J^\pi=\frac{7}{2}^-$ IS followed by an $E1$ decay, or the reversed scheme of an $E1$ excitation to a $J^\pi=\frac{5}{2}^+$ IS with subsequent $E2$ decay. Intermediate states found in the QPM calculations are compared to the experimental data in Fig. 4 and show this behavior. Only two strong IS are observed and the contributions of all other levels are at least two orders of magnitude smaller.

A difficulty in the model results was the poor reproduc-

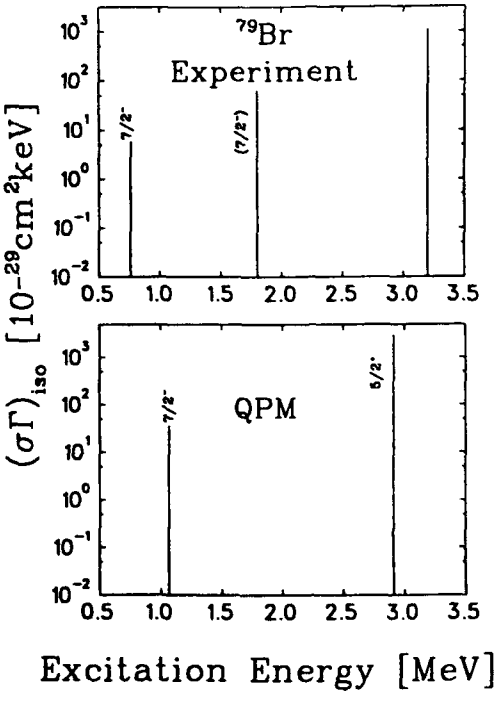

FIG. 4. Positions and strengths of intermediate states in ^{79}Br measured experimentally (upper) and calculated using the quasiparticle-phonon model as described in the text (lower).

tion of the $\frac{9}{2}^+$ isomer excitation energy, 1.270 MeV, which strongly distorted the energy-dependent integrated cross sections. Therefore, the experimental value of 0.127 MeV was used as the basis for electromagnetic transitions. A similar problem occurred in the ^{81}Br calculations [19]. There it was shown that the inclusion of two-phonon coupled configurations shifted the lowest $\frac{9}{2}^+$ state to roughly the correct position without strongly affecting the strength of the intermediate states.

The calculated low-energy IS has $J^\pi=\frac{7}{2}^-$, in agreement with the established 0.761 MeV level. Assuming the experimental 1.8 MeV state also to be $J^\pi=\frac{7}{2}^-$, a very good correspondence was obtained for the total energy-independent isomer population strength below $E_x=2$ MeV. Such a fragmentation would have naturally emerged from the model calculations if more complex configurations had been considered. Thus it was concluded that all IS below 2 MeV had $J^\pi=\frac{7}{2}^-$ and that the intermediate strength had a common excitation-decay structure.

The microscopic structure was extracted from the $\frac{7}{2}^-$ state wave function

$$\Psi_1(\tfrac{7}{2}^-)=(0.34)2f_{7/2}+(0.85)(2p_{3/2}\otimes 2_1^+)+\cdots .$$

The excitation occurred through the 2^+ phonon component coupled to the main g.s. configuration while the decay to the isomer took place in a $2f_{7/2}\rightarrow 1g_{9/2}$ $E1$ single-particle transition.

The strong experimental IS at 3.2 MeV was well reproduced by the QPM. The calculated $\sigma\Gamma$ was a factor of 3 larger, but again inclusion of many-phonon states would have been expected to bring the values into closer agreement. The QPM predicted $J^\pi=\frac{5}{2}^+$ for the IS and a reversed excitation-deexcitation sequence compared to the $\frac{7}{2}^-$ state. Analysis of the wave function

$$\Psi_1(\tfrac{5}{2}^+)=(0.38)2d_{5/2}+(0.90)(1g_{9/2}\otimes 2_1^+)\cdots$$

revealed that a $2p_{3/2}\rightarrow 2d_{5/2}$ $E1$ transition was responsible for the excitation and phonon coupling to the dominant isomer configuration provided an $E2$ decay.

The common feature in the intermediate levels of the QPM results is the presence of single-particle components in the wave functions belonging to strength having a centroid energy lying much higher. These configurations from the next major shell are strongly damped by coupling to collective excitations [32] and this pushes fragments to low energies. Exactly these components were found to be crucial for the isomer population in ^{79}Br.

C. ^{137}Ba

The experimental data showed evidence for only a single IS up to 4.3 MeV. Within the experimental limits, no contribution was observed below 2 MeV in agreement with the literature [31]. Thus, photoexcitation of ^{137}Ba^m has proven to be particularly important for the bremsstrahlung characterization technique of Ref. [22] since the isomer yield directly provides the photon flux at a single energy.

The results of the UM calculations are displayed in the middle part of Fig. 5 and indicate a strong transition at 2.75 MeV. Within the limitations of the model it appeared justified to assign this to the experimentally determined level 450 keV higher in energy at 3.2 MeV. The integrated cross section of the state was overpredicted by a factor of about 2–3, depending on whether the experimental or model excitation energy was used. However, similar to the ^{79}Br case this was probably due to the basis truncation and larger configuration spaces would be expected to bring the results closer to experiment.

An analysis of the wave functions of the IS identified $2d_{3/2}\rightarrow 2f_{5/2}$ single-particle $E1$ transitions as the common excitation mechanism. Because of the large spin difference, $\Delta J=4$ between g.s. and isomer, the decay occurs by complicated cascades which cannot be easily summarized.

A particular problem of the UM calculations already discussed for the ^{115}In$(\gamma,\gamma')^{115}$In^m reaction was a systematic deviation for the average $E1$ and $E2$ transition strengths with respect to experimental systematics in this mass region [40]. Good correspondence of the distribution shapes was obtained by comparing the reduced transition probabilities of all possible transitions up to 4 MeV in the model with Ref. [40]. However, the maximum had to be normalized with factors of $f(E1)=0.2$ and $f(E2)=50$ while absolute $M1$ strengths were reproduced well.

A reanalysis of the isomer population implementing

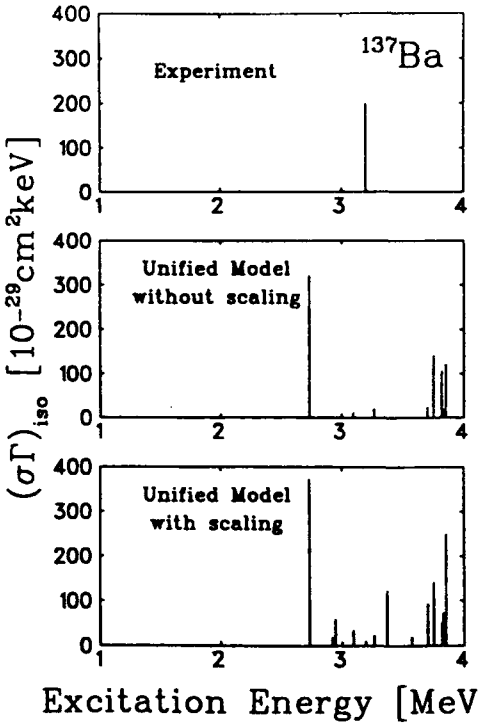

FIG. 5. Positions and strengths of intermediate states in ^{137}Ba measured experimentally (upper), calculated with the unified model (middle) and calculated with the unified model using empirically introduced correction factors for the average transition strengths (lower). Those factors were $f(E1)=0.02$ and $f(E2)=50$.

the normalization factors is shown in the lower part of Fig. 5. Surprisingly little change was observed with the main difference being some additional strength at 3–3.5 MeV. The $E2$ correction factor seemed unrealistically large considering how well the low-energy transitions were described. It is important to note that many of the weaker $E2$ transitions resulted from destructive interference of the collective and single-particle parts of the transition operator. The renormalization factor for $E1$ transitions seemed more realistic due to the sensitivity to smaller amplitudes of the wave functions which would have been smeared out in an enlarged configuration space. Accordingly, the best description might lie somewhere between the two extremes displayed in Fig. 5. However, the strong IS at 2.75 MeV which likely corresponds to the experimental 3.2 MeV level was hardly affected by these variations in the UM calculation.

VI. CONCLUSIONS

Excitation functions were measured for the photoactivation of $^{77}Se^m$, $^{79}Br^m$, and $^{137}Ba^m$ using bremsstrahlung with end-point energies in the range 2–7 MeV. This permitted the identification of intermediate states and the extraction of their integrated cross sections.

A particularly strong IS at 2.6 MeV was observed for the population of $^{77}Se^m$. Its transition strength significantly exceeds 10^{-3} W.u. for an $E1$ excitation or 0.1 W.u. for an $M1$ excitation, both of which are quite large values. In fact the magnitude of $^{77}Se^m$ yields compared to other isomers in this mass region provide further support for a correlation between integrated cross sections and the g.s. deformation. Such a correlation was recently discovered in the $A=160$–200 mass region [15] and is important to gamma-ray laser research since many candidate nuclei are well deformed.

The appearance of strong intermediate states requires a special combination of properties including a large partial g.s. width and significant mixing in the wave function. Thus the number of important levels is typically very small at energies below about 5 MeV as confirmed by the model results. The calculations further emphasized the importance of a delicate interplay of single-particle and collective amplitudes in the IS wave functions. In all examples analyzed so far (Refs. [13,19] and this work) the decisive factor has been the appearance of fragments of outer-shell single-particle strength at low energies. It would be of interest to compare these conclusions with findings in other valence-shell regions and in nuclei with large g.s. deformations. Experimental and theoretical work along these lines is underway.

ACKNOWLEDGMENTS

The authors gratefully acknowledge the valuable support of H.-D. Gräf and the S-DALINAC crew for providing excellent beams, W. Ziegler for assistance in conducting the experiments, and C. Spieler for help with the data analysis. One of us (P.v.N.-C.) would like to thank the group at the Center for Quantum Electronics for their hospitality during the stay when the present work was completed. This work was sponsored by the Department of Defense through the Naval Research Laboratory and the Bundesministerium für Forschung und Technologie, Contract No. 06DA641I. Partial support was received by NATO research Grant CRG92/0011 (K.H.) and by a grant of the Heisenberg-Landau program (V.Yu.P.).

[1] C. B. Collins, F. W. Lee, D. M. Shemwell, B. D. DePaola, S. Olariu, and I. I. Popescu, J. Appl. Phys. 53, 4645 (1982).
[2] C. B. Collins, in *CRC Handbook of Laser Science and Technology, Supplement 1: Lasers*, edited by M. J. Weber (CRC Press, Boca Raton, FL 1991), p. 561.
[3] J. A. Anderson and C. B. Collins, Rev. Sci. Instrum. 58, 2157 (1987).
[4] J. A. Anderson and C. B. Collins, Rev. Sci. Instrum. 59, 414 (1988).
[5] C. B. Collins, C. D. Eberhard, J. W. Glesener, and J. A. Anderson, Phys. Rev. C 37, 2267 (1988).
[6] C. B. Collins, J. A. Anderson, Y. Paiss, C. D. Eberhard, R. J. Peterson, and W. L. Hodge, Phys. Rev. C 38, 1852 (1988).
[7] J. A. Anderson, M. J. Byrd, and C. B. Collins, Phys. Rev. C 38, 2838 (1988).
[8] J. A. Anderson, C. D. Eberhard, M. J. Byrd, J. J. Carroll, C. B. Collins, E. C. Scarbrough, and P. P. Antich, Nucl. Instrum. Methods B40/41, 452 (1989).
[9] J. J. Carroll, J. A. Anderson, J. W. Glesener, C. D. Eberhard, and C. B. Collins, Astrophys. J. 344, 454 (1989).
[10] J. J. Carroll, M. J. Byrd, D. G. Richmond, T. W. Sinor, K. N. Taylor, W. L. Hodge, Y. Paiss, C. D. Eberhard, J. A. Anderson, C. B. Collins, E. C. Scarbrough, P. P. Antich, F. J. Agee, D. Davis, G. A. Huttlin, K. G. Kerris, M. S. Litz, and D. A. Whittaker, Phys. Rev. C 43, 1238 (1991).
[11] C. B. Collins, J. J. Carroll, T. W. Sinor, M. J. Byrd, D. G. Richmond, K. N. Taylor, M. Huber, N. Huxel, P. von Neumann-Cosel, A. Richter, C. Spieler, and W. Ziegler, Phys. Rev. C 42, 1813 (1990).
[12] J. J. Carroll, T. W. Sinor, D. G. Richmond, K. N. Taylor, C. B. Collins, M. Huber, N. Huxel, P. von Neumann-Cosel, A. Richter, C. Spieler, and W. Ziegler, Phys. Rev. C 43, 897 (1991).
[13] P. von Neumann-Cosel, A. Richter, C. Spieler, W. Ziegler, J. J. Carroll, T. W. Sinor, D. G. Richmond, K. N. Taylor, C. B. Collins, and K. Heyde, Phys. Lett. B 266, 9 (1991).
[14] J. J. Carroll, C. B. Collins, P. von Neumann-Cosel, D. G. Richmond, A. Richter, T. W. Sinor, and K. N. Taylor, Phys. Rev. C 45, 470 (1992).
[15] C. B. Collins, J. J. Carroll, K. N. Taylor, D. G. Richmond, T. W. Sinor, M. Huber, P. von Neumann-Cosel, A. Richter, and W. Ziegler, Phys. Rev. C 46, 952 (1992).
[16] M. Huber, P. von Neumann-Cosel, A. Richter, C. Schlegel, R. Schulz, J. J. Carroll, K. N. Taylor, D. G. Richmond, T. W. Sinor, C. B. Collins, and V. Yu. Ponomarev, Nucl. Phys. A559, 253 (1993).
[17] E. C. Booth and J. Brownson, Nucl. Phys. A98, 529 (1967).
[18] A. P. Dubenskij, V. V. Dubenskij, A. A. Boikova, and L.

Malov, Bull. Acad. Sci. USSR, Ser. Phys. **54**, 166 (1990).
[19] V. Ponomarev, A. P. Dubenskij, V. P. Dubenskij, and E. A. Boykova, J. Phys. G **16**, 1727 (1990).
[20] N. Klay, F. Käppeler, H. Beer, and G. Schatz, Phys. Rev. C **44**, 2839 (1991); K. T. Lesko, E. B. Norman, R.-M. Larimer, B. Sur, and C. D. Beausang, *ibid.* **44**, 2850 (1991).
[21] J. A. Anderson, C. D. Eberhard, K. N. Taylor, J. M. Carroll, J. J. Carroll, M. J. Byrd, and C. B. Collins, IEEE Trans. Nucl. Sci. **36**, 241 (1989).
[22] J. J. Carroll, D. G. Richmond, T. W. Sinor, K. N. Taylor, C. Hong, J. D. Standifird, C. B. Collins, N. Huxel, P. von Neumann-Cosel, and A. Richter, Rev. Sci. Instrum. **64**, 2298 (1993).
[23] P. von Neumann-Cosel, N. Huxel, A. Richter, C. Spieler, J. J. Carroll, and C. B. Collins (submitted to Nucl. Instrum. Methods).
[24] K. Alrutz-Ziemssen, D. Flasche, H-D. Gräf, V. Huck, M. Knirsch, W. Lotz, A. Richter, T. Rietdorf, P. Schardt, E. Spamer, A. Staschek, W. Voigt, H. Weise, and W. Ziegler, Part. Acc. **29**, 53 (1990).
[25] E. Browne and R. B. Firestone, in *Table of Radioactive Isotopes*, edited by V. S. Shirley (Wiley, New York, 1986); *Evaluated Nuclear Structure Data File* (Brookhaven National Laboratory, Upton, New York, 1986).
[26] P. von Neumann-Cosel, A. Richter, J. J. Carroll, and C. B. Collins, Phys. Rev. C **44**, 554 (1991).
[27] *Monte Carlo Transport of Photons and Electrons*, edited by T. M. Jenkins, W. R. Nelson, and A. Rindi (Plenum, New York, 1988).
[28] M. Boivin, Y. Cauchois, and Y. Heno, Nucl. Phys. **A137**, 520 (1969).
[29] B. Singh and D. A. Viggars, Nucl. Data Sheets **37**, 393 (1982).
[30] J. Guth, Phys. Rev. **59**, 325 (1941).
[31] L. K. Peker, Nucl. Data Sheets **59**, 767 (1990).
[32] S. Gales, Ch. Stoyanov, and A. I. Vdovin, Phys. Rep. **166**, 125 (1988).
[33] V. Yu. Ponomarev, V. G. Soloviev, Ch. Stoyanov, and A. I. Vdovin, Nucl. Phys. **A323**, 446 (1979).
[34] Ch. Stoyanov and C. Q. Khuong, JINR Dubna Report P-4-81-234, 1981 (unpublished).
[35] K. Heyde, P. van Isacker, M. Waroquier, J. L. Wood, and R. A. Mayer, Phys. Rep. **102**, 291 (1983).
[36] L. Trache, K. Heyde, and P. von Brentano, Nucl. Phys. **A554**, 118 (1993).
[37] S. Raman, W. C. Nestor, Jr., S. Kahane, and K. H. Bhatt, At. Data Nucl. Data Tables **42**, 1 (1989).
[38] S. L. Heller and J. N. Friedman, Phys. Rev. C **10**, 1509 (1974); **12**, 1006 (1975).
[39] S. E. Larsson, G. Leander, and I. Ragnarsson, Nucl. Phys. **A307**, 189 (1978).
[40] P. M. Endt, At. Data Nucl. Data Tables **26**, 47 (1981).

Mössbauer effect measurement of the recoil-free fraction for ^{57}Fe implanted in a nanophase diamond film

T. W. Sinor,[a] J. D. Standifird, F. Davanloo, K. N. Taylor, C. Hong, J. J. Carroll, and C. B. Collins
Center for Quantum Electronics, University of Texas at Dallas, P. O. Box 830688, Richardson, Texas 75083-0688

(Received 9 September 1993; accepted for publication 8 December 1993)

The Mössbauer effect was used to investigate films of nanophase diamond (NPD) implanted with isotopically pure ^{57}Fe at a dose of 5×10^{16} atoms/cm^2 and an energy of 20 keV. When defects and voids created by the implantation were repaired with an overcoating layer of NPD, the recoil-free fraction at room temperature for these samples was found to be $f_{dia}=0.94\pm0.06$ with a corresponding Debye temperature of 1140 K. This relatively high value for f makes NPD films a promising host matrix for microgram quantities of Mössbauer isotopes.

The principal figure of merit for a matrix in which Mössbauer nuclei are embedded is the fraction f of events which can occur without any recoil of a nucleus emitting or absorbing gamma rays. The probability for the recoilless emission or absorption of gamma rays is related to the mean-square vibrational amplitude of an atom in the direction of observation and is given by the relation $f=\exp(-k^2\langle x^2\rangle)$ where $k=2\pi/\lambda$. Since the wave number k is determined for a given transition, an increase in f can only be accomplished by decreasing the mean-square vibrational amplitude of atoms in the host lattice. Such a change may be accomplished by either reducing the temperature of the lattice, or by increasing the interatomic binding energy. In practice, the latter can be done by substituting the Mössbauer nuclei of interest into a rigid lattice.

In the Debye theory of solids, rigid lattices have high Debye oscillator frequencies, ω_D, and correspondingly high Debye temperatures, θ_D related by $k_B\theta_D=\hbar\omega_D$. The recoil-free fraction is related to θ_D and the temperature, T of the sample by[1]

$$f=\exp\left\{-\frac{3E_R}{2k_B\theta_D}\left[1+4\left(\frac{T}{\theta_D}\right)^2\int_0^{\theta_D/T}\frac{x}{e^x-1}\,dx\right]\right\} \quad (1)$$

where E_R is the recoil energy for a free nucleus. Clearly f increases asymptotically as a function of temperature with increasing θ_D. For pure samples of materials containing only the nuclei of interest for Mössbauer spectroscopy, typical Debye temperatures are on the order of a few hundred degrees Kelvin.

In contrast, natural diamond has a Debye temperature of $\theta_D=2230$ K, the highest in nature.[2] It is therefore one of the most attractive of the host lattices with the potential for supporting Mössbauer nuclei. Because of the convenience arising from the use of a single device to accelerate ions, separate isotopes, and decelerate the desired fraction, our interests have been focused upon implantation as a means of introducing Mössbauer nuclei into hosts. Numerous studies involving the implantation of Mössbauer nuclei into natural diamond have been reported in the literature.[3–7]

Recently, substantial progress has been made in the development of different types of pure carbon films having many of the properties of diamond. These films appear to be combinations of the various polytypes of diamond and often have mechanical and thermal properties similar to those of natural diamond.

Nanophase diamond (NPD) films are unique among the growing class of these new diamondlike materials and offer a number of important solid-state properties.[8–12] As used here, these NPD films were condensed from ions of carbon produced by the laser ablation of graphite at intensities sufficient to impart kinetic energies in excess of 0.5 keV. They were prepared in vacuum on substrates at room temperatures without hydrogen or other catalysts and without columnar patterns of growth. Such layers of NPD nominally contain 75%–85% diamondlike sp^3 bonds concentrated into nodules of 20–30 nm in diameter as determined by STM and confirmed by TEM.[13] The bulk properties of these films closely approach those of natural diamond in the areas of thermal management and hardness.[14] These films can also be deposited on a wide variety of different substrates. In this work, we investigate the utility of these films as host matrices for targets containing microgram quantities of Mössbauer isotopes by performing comparative measurements of the recoil-free fractions for ^{57}Fe implanted into a film of NPD and for iron foils enriched in ^{57}Fe.

The ^{57}Fe implanted sample was prepared by depositing a 1 μm thick film of nanophase diamond on a Ti substrate with a diameter of 25 mm and a thickness of 3 mm. Titanium was chosen since its bonding properties to NPD films have been characterized and reported in the literature.[13] The bonding of NPD to Ti is particularly strong because of the formation of an interfacial layer of TiC which is 20–30 nm thick. After deposition, the film was ion implanted with 5×10^{16} atoms/cm^2 of isotopically pure ^{57}Fe at an energy of 20 keV. The iron atoms penetrated to a depth of approximately 20 nm in the film as determined by Rutherford backscattering spectroscopy (RBS) and represented a concentration of about 10%. With an effective implantation area of 3.3 cm^2, a total mass of 15.5 mg of ^{57}Fe was present in the sample.

[a]Present address: Advanced Materials, Varo Inc. IMO Industries, Garland, TX 75046-9015.

 0003-6951/94/64(10)/1221/3/$6.00

In order to account for the effects of ^{57}Fe impurity atoms in the NPD matrix, it is customary to define an effective Mössbauer Debye temperature, θ_M which, for a monatomic, regular lattice is given by[7,17]

$$\theta_M = \theta_D \left(\frac{m_0 \gamma_0}{m \gamma} \right)^{1/2}, \quad (2)$$

where θ_D is the Debye temperature of the host lattice, and γ_0, γ are the force constants for the interaction between the host atoms and impurity atoms of mass m_0 and m, respectively. As a first approximation, we assume that the force constants are nearly equal.[15,16] In the case of the implanted NPD sample, $m_0 = 12$ amu for the C atoms, and $m = 57$ amu for the ^{57}Fe atoms. Setting $\gamma_0 = \gamma$, we find that the Debye temperature for the NPD lattice is a factor of 2.18 more than the average effective Debye temperature of the iron sites, as would be determined from the Mössbauer effect.

In addition to the reduced effective Debye temperature for the ^{57}Fe, the relatively low number of atoms implanted in the diamond film, combined with the presence of the Ti substrate, made the use of standard spectroscopic techniques relying on the transmission of gamma rays impractical. To observe the resonant effects produced by the ^{57}Fe nuclei required the use of a backscattering technique. In this work, both conversion electron Mössbauer spectroscopy (CEMS) and photon scattering techniques were used to collect data for the f measurements. The CEMS is advantageous because of the large internal conversion coefficient for ^{57}Fe. However, it is only sensitive to a small surface layer in the sample with a thickness on the order of the mean escape depth for electrons in the material. For conversion electrons in metallic iron, this depth[18] is 57 nm and is probably greater in NPD. Since the thickness of the implanted layer is only 20 nm the mean escape depth is greater in either case.

Mössbauer spectra were collected using a He-CH_4 gas flow proportional counter with an approximate flow rate of 5 ml per minute of 4% CH_4 in He. A typical Mössbauer spectrum of the ^{57}Fe in NPD sample is shown in Fig. 1 directly as measured. The spectrum consists of two components; a quadrupole split doublet and a singlet. The doublet appears to arise from iron atoms located in low symmetry or interstitial sites between the sp^3 nodules whereas the singlet corresponds to substitutional or high-symmetry sites in the sp^3 hard nodules themselves.[4,7]

A relative measurement of the recoilless fraction for the ^{57}Fe in NPD was made using the photon scattering geometry. This arrangement was used because it is sensitive to the entire volume of the sample, unlike CEMS. The measurement was performed by comparing the resonant scattering intensity from the implanted NPD sample with that from metallic iron targets having a known recoil-free fraction of $f = 0.69$ at room temperature.[19] The same ^{57}Co(Pd) source was used for all of the targets[20,21] and made the measurements independent of its recoil-free fraction. The recoil-free fraction of the NPD sample was determined by comparing the experimental areas under the resonance peaks in the spectra. This comparison is based upon the assumption that such an optically thin sample is free from spurious additional absorptions and has the additional advantage of canceling errors due to purely instrumental effects.

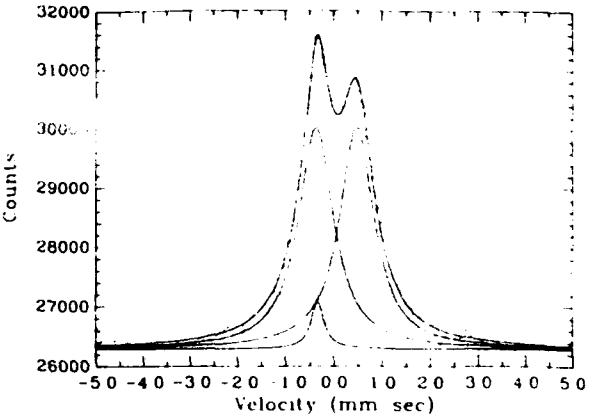

FIG. 1. Conversion electron Mössbauer spectrum of 5×10^{16} atoms/cm^2 of ^{57}Fe implanted in a 1 μm thick film of nanophase diamond. After implantation the sample was overcoated with 47 nm of NPD to partially repair implantation-induced damage. The spectrum is composed of three lines, a symmetric doublet with a quadrupole splitting of 0.850 mm/s and an isomer shift of +0.062 mm/s due to atoms in low symmetry interstitial sites and a singlet with an isomer shift of −0.326 mm/s which can be attributed to nuclei in high symmetry substitutional sites in the sp^3 hard nodules. The source was ^{57}Co(Pd) with a nominal activity of 2 mCi.

Data were collected for a variety of calibration foils having different masses of ^{57}Fe. The total counts in the resonance lines were plotted as a function of the total mass of ^{57}Fe in each sample. This calibration curve is shown in Fig. 2. As expected, the count rate increases linearly with the amount of ^{57}Fe in each sample. The total signal count rate for the ^{57}Fe implanted in the nanophase diamond film is plotted against the calibration curve and direct comparison indicates that the fluorescent signal from the ^{57}Fe in the nanophase diamond is greater than would be expected for a corresponding metallic absorber having the same number of Mössbauer nuclei. From the calibration data with $f_{Fe} = 0.69$, a value of $f_{dia} = 0.94 \pm 0.06$ is obtained. This value for the recoil-free fraction corresponds to an effective Debye temperature of

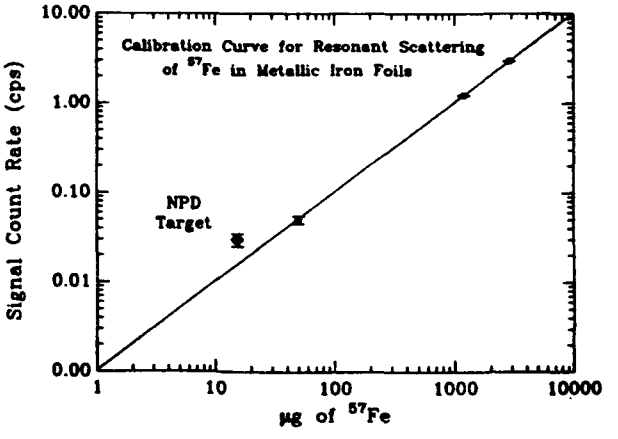

FIG. 2. Calibration curve for the resonant counting rate of the metallic samples as a function of the mass of Mössbauer nuclei contained in them. From these data the lower limit on the recoil-free fraction of the nanophase diamond film is $f_{dia} = 0.94 \pm 0.06$.

$\theta_M = 523$ K for the ^{57}Fe atoms in NPD. Using Eq. (2), we obtain a Debye temperature of 1140 K for the NPD film itself. By comparison, the Debye temperature for metallic Fe is 470 K.[2]

Although the measured Debye temperature for the NPD lattice is much greater than that for typical metallic host matrices, it is still below the Debye temperature for natural diamond. A possible explanation for this is that the implantation of ^{57}Fe nuclei into the lattice could result in partial graphitization of the sp^3 component of the film. The sp^2 graphitic bond is more thermodynamically stable than the sp^3 diamondlike bond so that any excessive energy transferred to the lattice from the implantation could tend to change the sp^3 bonds to sp^2.[22]

For natural diamond, implantation-induced damage can be partially repaired by heat treating the sample either during or after the implantation.[5] We have found that the deposition of an additional thin layer of nanophase diamond after implantation accomplishes a similar effect, probably by filling voids by the condensation of additional material. In this case the ease with which implantation-induced damage can be repaired provides an additional advantage for the use of NPD films as host matrices for small amounts of Mössbauer nuclei.

The results obtained with the ^{57}Fe implanted NPD sample closely parallel the results obtained by Sawicki *et al.*[7] In that work, ^{57}Co was implanted into natural diamond at a dose of 2×10^{13} atoms/cm^2 and an energy of 50 keV. The Debye temperature for the high symmetry substitutional sites was found to be 1300 K while that for the low symmetry interstitial sites was 550 K. Our result of $\theta_D = 1140$ K for the NPD film shows that its rigidity is comparable to that of natural diamond in spite of the orders of magnitude higher dose of 5×10^{16} atoms/cm^2 used in the preparation of the sample.

Comparing the best of the data[7] from the literature for natural diamond with the result for NPD shows the two to be reasonably equivalent in terms of the effective Debye temperatures experienced by the implanted ^{57}Fe nuclei. If the NPD offers an advantage, it is to be found in cost and practicality. In the work reported here a 3.3 cm^2 area of NPD was doped to a concentration of 10% ^{57}Fe. Such high concentrations over large areas of natural diamond would seem to lie outside the realm of practicality. Moreover, the use of NPD may support the implantation of other Mössbauer nuclei such as ^{119}Sn and ^{125}Te. If comparable successes were realized the recoil-free fractions would be ~0.7 at 300 K in both cases.

The authors gratefully acknowledge the support of this work by SDIO/TNI through NRL and preparation of the sample by General Coherent Technology, Inc.

[1] U. Gonser, *Mössbauer Spectroscopy*, edited by U. Gonser (Springer, New York, 1975), p. 15.
[2] C. Kittel, *Introduction to Solid State Physics*, 6th ed. (Wiley, New York, 1986), p. 110.
[3] M. Van Rossum, J. De Bruyn, G. Langouche, M. de Potter, and R. Coussement, Phys. Lett. 73A, 127 (1979).
[4] B. D. Sawicka, J. A. Sawicki, and H. de Waard, Phys. Lett. 85A, 303 (1981).
[5] M. de Potter and G. Langouche, Z. Phys. B Condensed Matter 53, 89 (1983).
[6] J. A. Sawicki and B. D. Sawicka, Nucl. Instrum. Methods 194, 465 (1982).
[7] J. A. Sawicki and B. D. Sawicka, Nucl. Instrum. Methods Phys. Res. B 46, 38 (1990).
[8] S. S. Wagal, E. M. Juengerman, and C. B. Collins, Appl. Phys. Lett. 53, 187 (1988).
[9] C. B. Collins, F. Davanloo, E. M. Juengerman, W. R. Osborn, and D. R. Jander, Appl. Phys. Lett. 54, 216 (1989).
[10] C. B. Collins, F. Davanloo, E. M. Juengerman, W. R. Osborn, D. R. Jander, and T. J. Lee, Texas J. Sci. 41, 343 (1989).
[11] F. Davanloo, E. M. Juengerman, D. R. Jander, T. J. Lee, and C. B. Collins, J. Appl. Phys. 67, 2081 (1990).
[12] F. Davanloo, E. M. Juengerman, D. R. Jander, T. J. Lee, and C. B. Collins, J. Mater. Res. 5, 2398 (1990).
[13] C. B. Collins, F. Davanloo, T. J. Lee, D. R. Jander, J. H. You, H. Park, and J. C. Pivin, J. Appl. Phys. 71, 3260 (1992).
[14] C. B. Collins, F. Davanloo, D. R. Jander, T. J. Lee, J. H. You, and H. Park, Diamond Films Technol. 2, 25 (1992).
[15] V. A. Bryukhanov, N. N. Delyagin, and V. S. Shpinel, Sov. Phys. JETP 20, 55 (1965).
[16] Yu. Kagan and Ya. A. Iosilevskii, JETP 42, 259 (1962).
[17] J. P. Schiffer, P. N. Parks, and J. Herberle, Phys. Rev. 133, A1553 (1964).
[18] J. A. Sawicki, *Industrial Applications of the Mössbauer Effect*, edited by G. J. Long and J. G. Stevens (Plenum, New York, 1986), p. 83.
[19] P. Debrunner and R. J. Morrison, Rev. Mod. Phys. 36, 463 (1964).
[20] D. A. Shirley, M. Kaplan, and P. Axel, Phys. Rev. 123, 816 (1961).
[21] G. Lang, Nucl. Instrum. Methods 24, 425 (1963).
[22] M. S. Dresselhaus and R. Kalish, *Ion Implantation in Diamond, Graphite, and Related Materials* (Springer, New York, 1992), p. 21.

Nuclear Instruments and Methods in Physics Research A 338 (1994) 425–431
North-Holland

NUCLEAR INSTRUMENTS & METHODS IN PHYSICS RESEARCH
Section A

Absolute calibration of low energy, thick target bremsstrahlung **

P. von Neumann-Cosel [a,*], N. Huxel [a], A. Richter [a], C. Spieler [a], J.J. Carroll [b], C.B. Collins [b]

[a] Institut für Kernphysik, Technische Hochschule Darmstadt, Schlossgartenstr. 9, D-64289 Darmstadt, Germany
[b] Center for Quantum Electronics, The University of Texas at Dallas, P.O. Box 830688, Richardson, Texas 75083, USA

(Received 5 April 1993)

The applicability of the Monte Carlo program GEANT3 for the calculation of low energy, thick target bremsstrahlung is investigated. The results of GEANT3, version 15, show very good correspondence to those of the well established EGS4 code. In contrast it is shown that GEANT3, version 11, leads to erroneous angular distributions, total intensities and even spectral shapes for angles far from the critical angle. The use of the $^{115}In(\gamma,\gamma')^{115}In^{m}$ reaction for an absolute calibration of bremsstrahlung spectra is also demonstrated. This method relies on the reconstruction of the isomer yield excitation function from a set of ^{115}In levels with well characterized properties. It can be utilized for continuous photon spectra up to about 3 MeV.

1. Introduction

Recently considerable interest has been shown in the field of resonant photoabsorption experiments using thick target bremsstrahlung with energies of several MeV. This has been motivated by the discovery [1] of low-lying collective magnetic dipole transitions, the so called "scissors mode" [2], as well as the observation of enhanced electric dipole transitions in heavy deformed nuclei [3]. For both problems nuclear resonance fluorescence (NRF) provides an ideal experimental tool [4]. Another field of experimental activity is the investigation of resonant photoexcitation of isomers [5] which has an impact on fields as varied as γ-ray laser research [6], nuclear astrophysics [7–10] and nuclear structure [11–14].

While the study of (γ,γ') reactions has a long history, its usefulness has always been hampered by the lack of experimental methods with adequate accuracy for an absolute calibration of fluxes and spectral distributions of intense photon continua. Commonly these continua are thick target bremsstrahlung or Compton spectra of strong radioactive sources. It has therefore become increasingly popular to use Monte Carlo (MC) simulations which provide an appropriate solution even for complex geometries [15].

In NRF experiments independent data of "reference" nuclei with well measured transition strengths covering the relevant excitation energy region can be used for a sampling of the unknown photon spectra and for a normalization of the flux. It was found [16,17] that a simulation with the MC program GEANT3 [18] described the shapes of the forward thick target bremsstrahlung spectra rather well. However, investigations of the photoexcitation of isomers usually involve more complex geometries which lead to a sensitivity not only on the spectral shapes, but also on the spectral distributions. Additionally, the total flux must be known to calibrate the experimental results (see e.g. refs. [5,13]). In this work, the analysis was based on another electron–photon shower MC program, EGS4 [19]. The code is widely used in medical physics and its basic correctness has been verified experimentally [20].

A thorough comparison of the results obtained with both programs for identical geometries revealed massive differences which questioned the conclusions drawn in refs. [16,17]. Therefore, one purpose of the present work is a detailed presentation of results from the calculations of thick target bremsstrahlung with the MC codes GEANT3 and EGS4. In particular, results from the recently released version 15 of GEANT3 are compared to those of the earlier version 11, on which the calculations described in refs. [16,17] were based.

In the second part an experimental method for the absolute calibration of thick target bremsstrahlung spectra applicable up to endpoint energies $E_0 \approx 3$ MeV is presented. It relies on the measurement of the yield excitation function of the ^{115}In isomer obtained in

* Corresponding author.
** Work supported by the Bundesministerium für Forschung und Technologie (BMFT) under contract number 06DA641I and by the Department of Defense through the Naval Research Laboratory,.

SSDI 0168-9002(93)E1089-G

bremsstrahlung irradiations with varying endpoint energy [12,21]. The importance of accurate methods for the absolute calibration of continuous photon spectra might be inferred from Table 1 of ref. [22]. There, all available data on the photoexcitation of $^{115}In^{m}$ through a single intermediate level at 1078 keV are summarized. This represents the most studied photoexcitation reaction in the literature. Yet, the large scattering of cross sections even in this particularly simple case is obvious.

Furthermore, the method provides a valuable tool for the characterization of nuclear simulators where the extremely high dose outputs in a single cycle disable many conventional calibration methods [23]. A similar application for photon energies limited to $E_\gamma \approx 1.5$ MeV and using photoexcitation of the ^{77}Se and ^{79}Br isomers is described in refs. [24,25].

2. Monte Carlo simulations

Simulations of thick target bremsstrahlung were performed with the MC codes GEANT3 and EGS4. These codes include all electron/positron and photon interactions relevant at MeV energies. The experimental setup is represented by building blocks of various basic geometries which can consist of different materials. Because of the significant differences between the results of EGS4 and GEANT3, version 11 (or briefly GEANT3.11), calculations with the improved version 15 are also presented. The incorporated geometry reproduced the bremsstrahlung facility [14] at the injector of the S-DALINAC electron accelerator in Darmstadt. It consisted of a 100 μm Al vacuum exit window, an air path of 2 cm and a 3 mm thick Ta radiator which is capabable of a complete stopping of electrons with energies up to 9 MeV. Based on experimental findings a beam spot of 2 mm diameter with a Gaussian distribution was assumed for the electrons incident on the radiator. Further details of the experimental environment can be found in Fig. 1 of ref. [14]. The spectral distributions were recorded an a circular plane at a distance of 4.77 cm at which a radius of 4 cm corresponded to an opening angle of 80°.

Calculations were performed for electron energies $E_0 = 1$, 2, 3, 5 and 7 MeV. In most cases the spectra correspond to 10^7 initial electrons which were sampled with 50 keV binsize. Polynomials up to fourth order were then fitted to the histogram spectra to average out statistical fluctuations and show the main features more clearly. For the 1 MeV calculations the number of triggers was increased to 4×10^7 in order to keep statistical errors at a level comparable to the higher energies. Below an energy cutoff $E_c = 600$ keV the computations were stopped for electrons and photons. This threshold was chosen since EGS4 spectra for the above energies were already available from the data analysis of the photoactivation experiments [8,12–14,26] where the information at lower energies was not needed. For a test of the programs down to the lowest energies, a seperate run was performed with $E_c = 10$ keV for an electron energy of 1 MeV.

Angular distributions of the energy integrated bremstrahlung flux are displayed in Fig. 1 for the various electron energies. In this and the following figures EGS4 results are displayed as solid lines, GEANT3.11 as dotted and GEANT3.15 as dashed lines. Note that the data for very small angles (0–2°) are left out. They show large fluctuations because of poor statistics combined with a large areal weighting factor in the conversion of radial to angular distributions. The differences obtained with GEANT3.11 and EGS4 are dramatic. The GEANT3.11 angular distribution is very narrow with a maximum roughly at the critical angle $\Theta_c = m_e c^2/E_0$ and a minimum under 0° in contradiction to experimental results for thick target bremsstrahlung [15]. On the other hand the improved GEANT3.15 version shows very good agreement with EGS4. Differences are observed at small angles only where EGS4 intensities tend to be somewhat higher, but typically less than 10% except for the $E_0 = 1$ MeV results.

In Fig. 2 the total intensity radiated into the 80° opening angle is depicted as a function of electron energy E_0. While at the highest energy reasonable agreement of all three calculations is obtained, GEANT3.11 leads to significantly larger intensities with increasing deviations towards lower energies. The GEANT3.15 and EGS4 curves are very close except for at $E_0 = 1$ MeV where the former calculation is about 25% larger.

Bremstrahlung spectra for $E_0 = 3$ MeV corresponding to different angular regions are displayed in Fig. 3. Again, excellent agreement of GEANT3.15 and EGS4 is observed, in particular for smaller angles (upper two figures). At larger angles (lower two figures) EGS4 predicts slightly higher intensities near the endpoint energy. The shape of spectra calculated with GEANT3.11 is much too steep at larger angles. However, the total spectrum is dominated by the most forward angles and in the region around the critical angle the spectral shape produced with GEANT3.11 coincides reasonably well with the other results. At other electron energies a behaviour similar to Fig. 3 is observed. Thus, despite the erroneous description of the angular distributions and total fluxes the conclusions of refs. [16,17] are not affected, since they depend on only the angle integrated shape.

The results in Figs. 1–3 demonstrate a very good correspondence of the GEANT3.15 and EGS4 results. Because of various inherent approximations in the codes the comparison is most critical at low electron

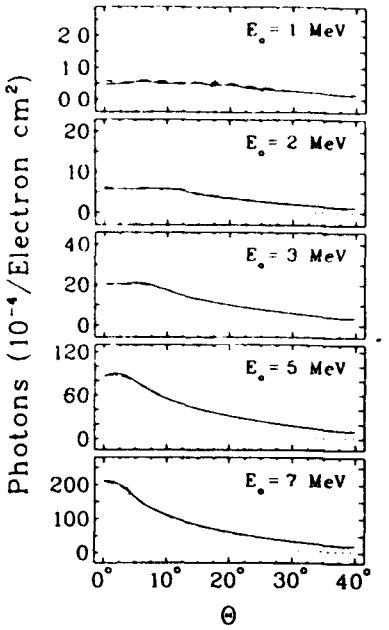

Fig. 1. Angular distributions relative to the beam axis of the energy-integrated bremstrahlung intensity from a 3 mm Ta radiator and for electron energies E_0 = 1, 2, 3, 5 and 7 MeV. The EGS4 results are displayed as solid lines, the GEANT3.11 results as dotted lines and the GEANT3.15 results as dashed lines.

energies. Fig. 4 presents angle integrated spectra for E_0 = 1 MeV calculated down to a cutoff E_c = 10 keV. Because of self absorption in the thick target no photons are registered below 200 keV. The overall intensity of the GEANT3.15 spectrum is about 30% larger as already seen in Fig. 2 and in the 400–800 keV region the spectrum decreases faster than the EGS4 results. Close to the endpoint energy a larger relative yield is observed with EGS4 in accordance with the general trend in all calculations.

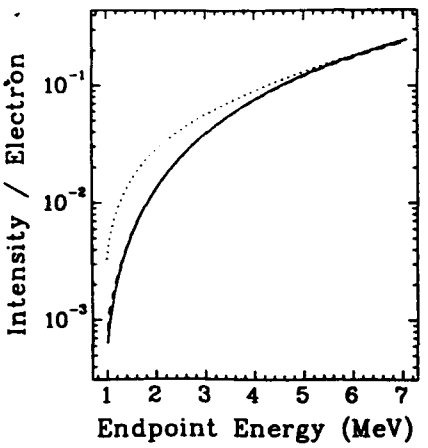

Fig. 2. Total intensity of the bremsstrahlung emitted in a 80° forward opening angle as a function of electron energy. The EGS4 results are displayed as solid line, the GEANT3.11 results as dotted line and the GEANT3.15 results as dashed line.

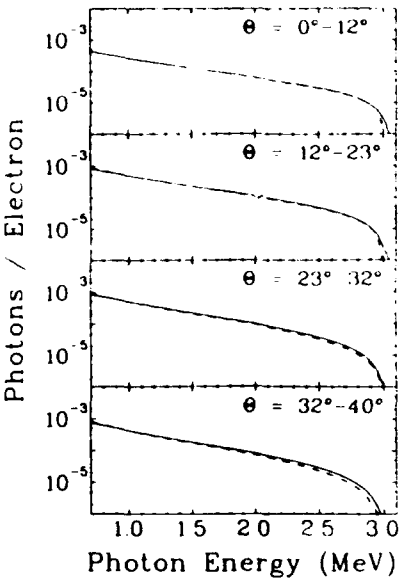

Fig. 3. Bremstrahlung spectra for different angular regions at E_0 = 3 MeV. The EGS4 results are displayed as solid lines, the GEANT3.11 results as dotted lines and the GEANT3.15 results as dashed lines.

For comparison, the analytical approximation of Schiff [27] for thin target bremsstrahlung into forward direction is shown as dashed-dotted line. The thin target assumption limits the comparison to energies where self absorption is negligible ($E \geq 300$ keV). Similar to the findings of ref. [16] at higher electron energies the MC spectral shape at intermediate energies is well reproduced, but the high-energy part is severly overestimated.

3. Experimental bremsstrahlung calibration with the ^{115}In(γ,γ')^{115}In^{m} reaction

The photoexcitation of isomer proceeds via resonant photoabsorption into higher-lying intermediate states (IS) which subsequently decay with a certain probability to the metastable level, either directly or in a cascade. In the case of a continuous photon source like bremsstrahlung, information about the energy and integrated cross sections of IS can be obtained from the isomer yield excitation function [5,8,11–14,26]. Alternatively, if the relevant properties of the IS are known from other experiments the measured yield can

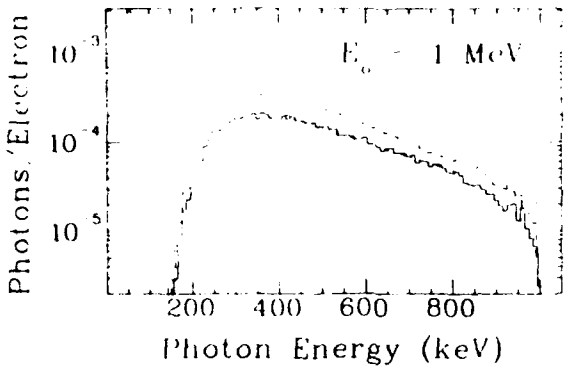

Fig. 4. Angle-integrated bremsstrahlung spectra for $E_0 = 1$ MeV. The histogram binsize is 10 keV. The cutoff energy in the calculations was lowered to $E_c = 10$ keV. The EGS4 results are displayed as solid histogram and the GEANT3.15 results as dashed histogram. The dashed-dotted line corresponds to a calculation with the Schiff formula [28] for a thin target.

be utilized to deduce the photon field $\Phi(\Theta, E_R, E_0)$ for a given endpoint energy E_0. Here, Θ is the angle relative to the incident electron beam and E_R represents the energy of the resonant IS. As described below, the latter method is applicable for the ^{115}In$(\gamma,\gamma')^{115}$In^m reaction at photon energies up to ≈ 3 MeV.

An investigation of the ^{115}In isomer photoexcitation was performed for electron energies $E_0 = 2$–6 MeV at the injector of the S-DALINAC electron accelerator [28] in Darmstadt. Disks of nominally 1 g of natural indium with a diameter of 3.8 cm were placed in the beam direction at a distance of 6.43 cm from the converter. After an irradiation of typically 4 h with an average electron current of 20 μA the characteristic isomeric transition ($E = 336$ keV, $T_{1/2} = 4.486$ h) of ^{115}In was recorded with a Ge(Li) detector. These values were transformed into yields including the corrections described in ref. [8]. A detailed description of the data analysis can be found in ref. [21].

The isomeric yield N_f can be expressed as

$$N_f = N_T \int_{E_c}^{E_0} \sigma(E) \frac{d\Phi(E, E_0)}{dE}\, dE, \qquad (1)$$

where N_T denotes the number of target atoms, $d\Phi/dE$ describes the spectral intensity per energy of the photon field for an endpoint energy E_0, and $\sigma(E)$ is the resonant absorption cross section. Note that the Θ dependence of the spectral distribution is implicitly considered in the definition of the target geometry in the MC calculations.

The typical widths of resonant intermediate states are small enough to assume that $d\Phi/dE$ is constant over each resonance. Then, Eq. (1) can be simplified to

$$N_f = N_T \sum_i (\sigma\Gamma)_{iso} \Phi(E_i, E_0). \qquad (2)$$

with $(\sigma\Gamma)_{iso}$ giving the integrated cross section of the ith level. We note that nonresonant cross sections, which would inhibit the use of Eq. (2), are not considered. Claims of important nonresonant contributions [29] to the photoexcitation of isomers have recently been disproven [30] and shown to have resulted from the omission of intense contributions to the photon fields in those experiments due to environmental Compton scattering.

The integrated cross section of an IS is related to its level properties by

$$(\sigma\Gamma)_{iso} = \pi^2 \left(\frac{\hbar c}{E_i}\right)^2 \frac{2J_{IS}+1}{2J_0+1} b_0 b_{iso} \Gamma. \qquad (3)$$

$J_{0,IS}$ are the spins of the g.s. and the intermediate state, Γ describes the total width and b_0, b_{iso} denote the branching ratios for decay into the g.s. and isomeric state, respectively. If the relevant level properties Γ, b_0, b_{iso}, E_i and J of *all* intermediate levels are known, Eq. (2) can be inverted and information on the spectral intensities at the resonance energies can be extracted. For ^{115}In the available data base [31] provides a complete characterization of all levels contributing to the isomer yield up to $E_x = 1.65$ MeV. The adopted data and derived integrated cross sections are summarized in Table 1. A theoretical yield function can be constructed from the MC photon spectra and tested against the measured results.

This method was used in ref. [12] to determine the contribution of low-lying levels and to extract information on previously unknown IS at higher excitation energies. Here, we are concerned with the quality of reproduction of the experimental yield curve at low

Table 1
Properties of ^{115}In levels contributing to the population of the 0.336 MeV isomer for $E_x \le 2$ MeV (from ref. [31])

E_x (MeV)	J^π	$T_{1/2}$ (ps)	b_0 (%)	b_{iso} (%)	$(\sigma\Gamma)_{iso}$ (meV b)
g.s.	$9/2^+$	6×10^{14} [a]	–	–	–
0.336	$1/2^-$	4.486 h	–	–	–
0.934	$7/2^+$	57(7)	99.3(3)	0.5(2)	0.0133(12)
0.941	$5/2^+$	15.1(1.4)	88.0(6)	12.0(16)	0.83(8)
1.078	$5/2^+$	0.99(5)	83.4(6)	15.5(4)	118(6)
1.449	$9/2^+$	0.35(4)	84.7(7)	0.2(1)	3.3(4)
1.463	$7/2^+$	0.063(10)	93.5(7)	0.91(8)	89(14)
1.486	$9/2^+$	0.44(6)	79.6(6)	0.45(9)	6.5(9)
1.497	$7/2^+$	0.167(20) [a]	78.1(8)	21.9(8)	639(80)
1.608	$7/2^+$	0.113(18) [a]	69.0(7)	4.8(2)	160(26)

[a] Partial g.s. width from ref. [32], branching ratios from ref. [31].

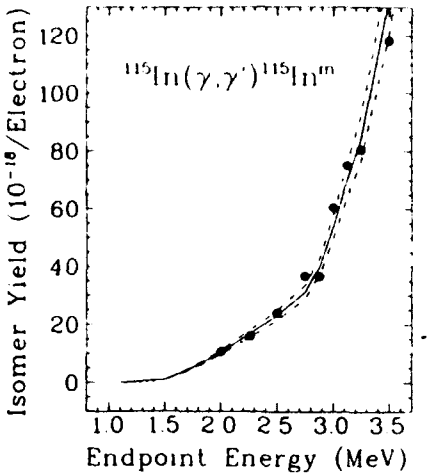

Fig. 5. Yield excitation function of the ^{115}In(γ,γ')^{115}In^{m} reaction. The solid line describes a calculation using the energies and integrated cross sections of Table 1 and GEANT3.15 bremsstrahlung spectra. The dashed lines give the relative error of the data summarized in Table 1

energies using the MC generated photon spectra. Fig. 5 displays the data and theoretical results (solid line) using the GEANT3.15 spectra described in section 2. The dashed lines give the relative error of the calculation introduced by the experimental data of Table 1. Since the lowest technically feasible electron energy was $E_0 = 2$ MeV and the level information above $E_x = 1.65$ MeV is incomplete, some problem could arise from the presence of additional, yet unknown IS with $1.65 \le E_x \le 2$ MeV. However, Fig. 5 clearly shows that the yield variation for $E_0 = 2$–2.8 MeV is well described by the calculations including only the IS of Table 1. We conclude that no additional IS with a significant contribution to the isomer yield is present up to 2.8 MeV excitation energy. The clear break in the excitation function at 2.9 MeV is attributed to a new IS (see ref. [12]).

The other important criterion is the reproduction on an absolute scale. If one performs a least-square fit to the experimental data points below 3 MeV, an overall normalization factor $F = 1.27$ results for the GEANT3.15 spectra. The corresponding result with EGS4 spectra is $F = 1.13$. Due to problems described below a systematic error of ±30% must be assumed. Within this error, calculations with EGS4 and GEANT3.15 are able to quantitatively describe the yields obtained for the ^{115}In(γ,γ')^{115}In^{m} reaction.

The main contribution to the error comes from the efficiency calibration of the Ge(Li) detector. The ^{115}In isomeric decay was measured in close proximity (the disks were placed on the detector cap) which leads to a strong sensitivity on details of the detector geometry. The energy dependence of the detection efficiency was measured with a set of pointlike γ calibration sources in a distance of 10 cm from the detector cap. Since most γ sources could not be used in the close geometry without severe deadtime effects we had to rely on a MC simulation of the absolute efficiency of the 336 keV isomeric transition. Also there was an inaccurate knowledge of the precise detector crystal size and of the distance from the crystal surface to the Al window and some discrepancies between the measured efficiencies at large and small distance and the calculations. Therefore, we estimate the accuracy to be no better than 30%. Unfortunately, in the meantime the detector has suffered from severe neutron damage and no repetition of the efficiency calibration is possible to resolve this problem.

4. Discussions and conclusions

The present work addresses two questions related to the problem of an absolute calibration of thick target bremsstrahlung for electron energies of several MeV. The calculation of the electron-photon cascade with the MC codes EGS4 and GEANT3 are compared. While the results of EGS4 are reasonably verified against experimental results [20], no such tests have been reported to date for this application of GEANT3. The Figs. 1–4 demonstrate the extreme differences of GEANT3, version 11, compared to EGS4 in all but one aspects: the angle integrated shape of the bremsstrahlung spectra agrees reasonably well. Thus, concerns about the use of GEANT3.11 spectra in the calibration of NRF experiments [16,17] are removed.

On the other hand, results obtained with GEANT3, version 15, reveal very good agreement with EGS4 over most of the investigated energy range. At energies $E_0 \ge 2$ MeV the remaining differences are small enough to permit interchangeable use of the results obtained with both programs for most practical purposes. It seems worthwile to extend the test of GEANT3 to higher energies used in medical applications, since a recent comparison of the 10–30 MeV region reports considerable differences between EGS4 and other MC codes [33]. The differences observed at low energies might be partly due to the fact that EGS4 neglects the Coulomb correction (Elwert factor [34]), which increases the cross sections considerably at $E_0 = 1$ MeV, while GEANT3.15 is based on the recent parametrization of bremsstrahlung cross sections of Berger and Seltzer [35] using exact partial wave calculations [36] at energies below 2 MeV.

An experimental method for absolute calibration of thick target bremsstrahlung spectral distributions with endpoint energies up to about 3 MeV is presented. It relies on the measurement of the excitation function of the ^{115}In(γ,γ')^{115}In^{m} reaction. Since the properties of

all IS in ^{115}In with $E_x \leq 2.8$ MeV contributing to the isomer population are known, the yield curve can be calculated using MC results. The distribution of IS at several excitation energies is sensitive to the spectral shapes and the variation with endpoint energy tests the energy dependence of the total flux. Also, angular distributions can be measured with the In samples placed off-axis.

The results described here indicate that the MC programs tested above are capable of reproducing the experimental spectral shapes and absolute intensities in the MeV range. Due to the uncertainties in the efficiency determination of the Ge(Li) detector used for detection of the ^{115}In isomeric transition, a relatively large systematic error of about 30% remains for the absolute normalization. In the light of possible applications like the characterization of unknown photon fields of new bremsstrahlung facilities or nuclear simulators and the calibration of isomer excitation experiments it would be worthwhile to repeat and extend the above described experiments in order to determine an absolute calibration of the MC generated spectra with improved accuracy.

Nevertheless, these results already constitute a benchmark for the series of recent photoexcitation experiments [5,8,12–14,26]. The confirmation of absolute values of the integrated cross sections of IS at higher excitation energies extracted from the MC generated photon spectra can be utilized for an extension of the calibration method towards higher photon energies. As a result of the improved nuclear data this method, called "X-ray activation of nuclei" [23–25,37], has now be markedly improved as discussed in ref. [38].

Acknowledgements

We would like to thank H.-D. Gräf and the S-DALINAC crew for providing excellent beams. The help of M. Huber, T.W. Sinor and W. Ziegler in the data taking is appreciated. We are indebted to C. Bähr, M.J. Byrd, S. Lindenstruth, A. Stiller and O. Titze for support in the installation of the Monte Carlo programs.

References

[1] D. Bohle, A. Richter, W. Steffen, A.E.L. Dieperink, N. Lo Iudice, F. Palumbo and O. Scholten, Phys. Lett. B 137 (1984) 27.

[2] A. Richter, Nucl. Phys. A 522 (1991) 139c.

[3] H. Friedrichs, B. Schlitt, J. Margraf, S. Lindenstruth, C. Wesselborg, R.D. Heil, H.H. Pitz, U. Kneissl, P. von Brentano, R.D. Herzberg, A. Zilges, D. Häger, G. Müller and M. Schumacher, Phys. Rev. C 45 (1992) R892.

[4] U. Kneissl, Prog. Part. Nucl. Phys. 24 (1990) 31.

[5] J.J. Carroll, M.J. Byrd, D.G. Richmond, T.W. Sinor, K.N. Taylor, W.T. Hodge, Y. Paiss, C.D. Eberhard, J.V. Anderson, C.B. Collins, J.C. Scarbrough, P.P. Antich, H.J. Agee, D. Davis, G.A. Huttlin, K.G. Kerris, S.M. Lutz and D.A. Whittacker, Phys. Rev. C 43 (1991) 1238.

[6] C.B. Collins, F.W. Lee, D.M. Shemwell, B.D. DePaola, S. Olariu and I. Popescu, J. Appl. Phys. 53 (1982) 4645.

[7] J.J. Carroll, J.A. Anderson, J.W. Glesener, C.D. Eberhard and C.B. Collins, Astrophys. J. 344 (1989) 454.

[8] C.B. Collins, J.J. Carroll, T.W. Sinor, M.J. Byrd, D.G. Richmond, K.N. Taylor, M. Huber, N. Huxel, P. von Neumann-Cosel, A. Richter, C. Spieler and W. Ziegler, Phys. Rev. C 42 (1990) R1813.

[9] N. Klay, F. Käppeler, H. Beer and G. Schatz, Phys. Rev. C 44 (1991) 2839.

[10] Zs. Németh, F. Käppeler and G. Reffo, Astrophys. J. 392 (1992) 277.

[11] V.Yu. Ponomarev, A.P. Dubenskij, V.P. Dubenskij and E.A. Boykova, J. Phys. G 16 (1990) 1727.

[12] P. von Neumann-Cosel, A. Richter, C. Spieler, W. Ziegler, J.J. Carroll, T.W. Sinor, D.G. Richmond, K.N. Taylor, C.B. Collins and K. Heyde, Phys. Lett. B 266 (1991) 9.

[13] C.B. Collins, J.J. Carroll, K.N. Taylor, D.G. Richmond, T.W. Sinor, M. Huber, P. von Neumann-Cosel, A. Richter and W. Ziegler, Phys. Rev. C 46 (1992) 952.

[14] M. Huber, P. von Neumann-Cosel, A. Richter, C. Schlegel, R. Schulz, J.J. Carroll, K.N. Taylor, D.G. Richmond, T.W. Sinor, C.B. Collins and V. Yu. Ponomarev, Nucl. Phys. A 559 (1993) 253.

[15] W.P. Swanson, Radiological Safety Aspects of the Operation of Electron Linear Accelerators (IAEA, Vienna, 1979).

[16] S. Lindenstruth, A. Degener, R.D. Heil, A. Jung, U. Kneissl, J. Margraf, H.H. Pitz, P. Schacht, U. Seemann, R. Stock and C. Wesselborg, Nucl. Instr. and Meth. A 300 (1991) 293.

[17] W. Ziegler, N. Huxel, P. von Neumann-Cosel, C. Rangacharyulu, A. Richter, C. Spieler, C. De Coster and K. Heyde, Nucl. Phys. A 564 (1993) 366.

[18] R. Brun, F. Bruyart, M. Maire, A.C. McPherson and P. Zanarini, GEANT3, CERN report DD/EE/84-1 (1987).

[19] W.R. Nelson, H. Hirayama and D.W.O. Rogers, EGS4, SLAC report 265 (1985).

[20] D.W.O. Rogers and A.F. Bielajev, in: Monte Carlo Transport of Electrons and Photons, eds. T.M. Jenkins, W.R. Nelson and A. Rindi (Plenum, New York, 1988) p. 307.

[21] C. Spieler, Diploma thesis, Darmstadt (1992).

[22] C.B. Collins, J.A. Anderson, Y. Paiss, C.D. Eberhard, R.J. Peterson and W.L. Hodge, Phys. Rev. C 38 (1988) 1852.

[23] J.A. Anderson, C.D. Eberhard, K.N. Taylor, J.M. Carroll, J.J. Carroll, M.J. Byrd and C.B. Collins, IEEE Trans. Nucl. Sci. NS-36 (1989) 241.

[24] J.A. Anderson and C.B. Collins, Rev. Sci. Instr. 58 (1987) 2157.

[25] J.A. Anderson and C.B. Collins, Rev. Sci. Instr. 59 (1988) 414.

[26] J.J. Carroll, T.W. Sinor, D.G. Richmond, K.N. Taylor,

C.B. Collins, M. Huber, N. Huxel, P. von Neumann-Cosel, A. Richter, C. Spieler and W. Ziegler, Phys. Rev. C 43 (1991) 897.

[27] L.I. Schiff, Phys. Rev. 83 (1951) 252.

[28] K. Afrutz Ziemssen, D. Flasche, H.D. Graf, V. Huck, M. Knirsch, W. Lotz, A. Richter, T. Rietdorf, P. Schardt, I. Spamer, A. Stascheck, W. Voigt, H. Wersé and W. Ziegler, Part. Acc. 29 (1990) 53.

[29] A. Ljubičić, K. Pisk and B.A. Logan, Phys. Rev. C 23 (1981) 2238;
M. Krčmar, A. Ljubičić, B.A. Logan and M. Bistrović, Phys. Rev. C 33 (1986) 293;
M. Krčmar, S. Kaučić, T. Tustonić, A. Ljubičić, B.A. Logan and M. Bistrović, Phys. Rev. C 41 (1990) 771.

[30] P. von Neumann-Cosel, A. Richter, J.J. Carroll and C.B. Collins, Phys. Rev. C 44 (1991) 554.

[31] J. Blachot and G. Marguier, Nucl. Data Sheets 51 (1987) 565.

[32] Y. Gauchois, H. Beil, M.-C. Duzy, R. Kosiek and C. Schlocsing-Moller, J. Phys. G 7 (1981) 1539.

[33] B.A. Faddegon and D.W.O. Rogers, Nucl. Instr. and Meth. A 327 (1993) 550.

[34] G. Elwert, Ann. Phys. 34 (1939) 178.

[35] M.J. Berger and S.M. Seltzer, Nucl. Instr. and Meth. B 12 (1985) 95.

[36] R.H. Pratt and H.K. Tseng, Atomic Inner Shell Physics, ed. B. Crasemann (Plenum, New York, 1985) p. 533.

[37] J.A. Anderson, F.M. Carroll, K.N. Taylor, H.E. Garrett, M.L. Byrd, F.W. Smith, C.B. Collins, H.E. Acree, G.A. Huttlin, H.G. Kerris, M.S. Lutz, D.A. Whittaker, N.R. Pereira and S.G. Gorbics, Nucl. Instr. and Meth. B 40–41 (1989) 1187.

[38] J.J. Carroll, D.G. Richmond, F.W. Smith, K.N. Taylor, C. Hong, J.D. Standiford, C.B. Collins, N. Huxel, P. von Neumann-Cosel and A. Richter, Rev. Sci. Instr. 64 (1993) 2298.

Low-energy conversion electron Mössbauer spectroscopy using a chevron microchannel plate detector

T. W. Sinor, J. D. Standifird, K. N. Taylor, C. Hong, J. J. Carroll, and C. B. Collins
Center for Quantum Electronics, University of Texas at Dallas, P. O. Box 830688, Richardson, Texas 75083-0688

(Received 2 March 1993; accepted for publication 12 June 1993)

A detection system for conversion electron Mössbauer spectroscopy is described. A chevron microchannel plate assembly attached to a two-stage electrostatic lens is used to preferentially detect electrons with energies <15 eV. Mössbauer spectra collected with these electrons can provide information about a variety of solid-state surface phenomena.

I. INTRODUCTION

Conversion electron Mössbauer spectroscopy[1-4] (CEMS) is a low-noise spectroscopic technique based on the detection of conversion, Auger, and secondary electrons emitted from a material as a result of the deexcitation of Mössbauer nuclei. It provides information about the environment in which these sensitive nuclei are embedded. However, the range which can be probed with the method is limited by the escape depth of the electrons in the material. For ^{57}Fe the mean electron range in metallic iron has been reported to be 57 and 36 nm for the 7.3 and 5.4 keV conversion and Auger electrons, respectively.[1] It has been shown that the component with energies <15 eV comprises about 50% of the total signal and provides information from the top 5 nm of the sample.[5-7] Because the range of those electrons is so short, they can provide specific information about a variety of solid-state surface phenomena and aid in the characterization of implanted layers.[8-10]

In this article we discuss the design and construction of a relatively simple spectrometer that was used to selectively and efficiently detect this low-energy component. It was based upon a chevron microchannel plate (MCP) assembly with an active diameter of 25 mm that served as the detector. A two-stage electrostatic lens was used to preferentially focus and accelerate low-energy electrons from the target to the detector. This acceleration increased the energy of the electrons to a level more compatible with the sensitivity of the input microchannel plate.

The detection of higher energy signal electrons, which escape from and provide information about deeper regions of the target, could serve as a source of "contamination" to the signal in that they carry little or no information about the surface effects being investigated. The number of these electrons detected was reduced to negligible levels by minimizing the geometrical solid angle between the Mössbauer target and the MCP assembly. This was possible since the trajectories of the more energetic electrons were not significantly focused by the relatively weak electrostatic fields of the lens.

II. EXPERIMENTAL DETAIL

A. Apparatus

Figure 1 shows the experimental arrangement used in these measurements. A ^{57}Co(Pd) source with a nominal activity of 10 mCi was mounted on a Doppler motor external to the vacuum chamber containing the sample and electron detector and provided the 14.4-keV Mössbauer radiation. To optimize the passage of resonant γ rays into the target chamber a thin entrance window was constructed from titanium. The 14.4-keV γ rays were only slightly attenuated but the window efficiently filtered out a significant number of the lower energy x rays that were produced by the decay of source nuclei. Without filtering, these x rays would have seriously degraded the performance of the detection system.

Low-energy electrons emitted from the target were collected with a two-stage aperture lens. The MCP, target, electrical feedthrough, and electrostatic lens were mounted as an integral unit on a 6-in. vacuum flange. This provided for convenient mounting and removal of the entire assembly from the vacuum chamber for adjustments to the target geometry. The angular position of the Mössbauer target with respect to the direction of the source γ rays was adjusted by rotating it about the vertical axis. Data were typically collected with the target at a 45° angle with respect to the detector axis and the incident radiation.

The chamber was initially evacuated with an Alcatel CFF-450 turbomolecular pump (TMP) to a pressure of about 3×10^{-7} Torr. However, vibrations from the TMP seriously degraded the resonant absorption in the absorber and could not be used to maintain the vacuum necessary to operate the chevron. To provide for vibrationless pumping, a 140 ℓ/s Varian diode VacIon pump was used to maintain the required pressure of 2×10^{-6} Torr. It is important to note that such pumps operate by ionizing gas in a magnetically confined cold-cathode discharge. Thus proper precautions had to be taken to prevent neutral and charged particles, as well as hard ultraviolet radiation from escaping from the VacIon pump and degrading the performance of the detector. To avoid this difficulty a line-of-sight baffle was used that consisted of six successive aperture plates.

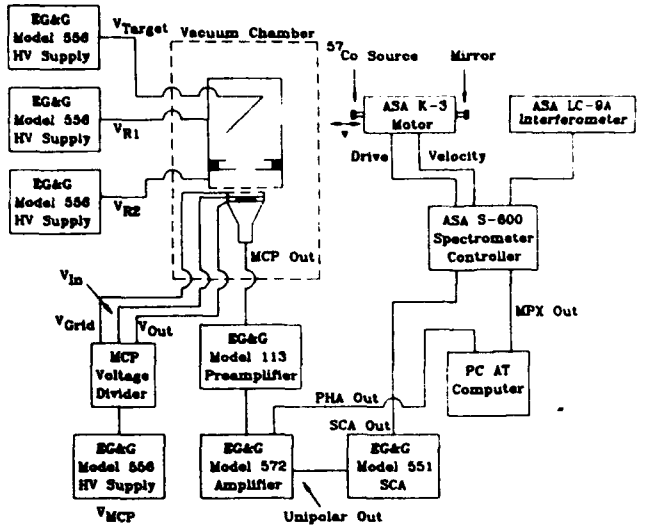

FIG. 1. Schematic diagram of the experimental arrangement.

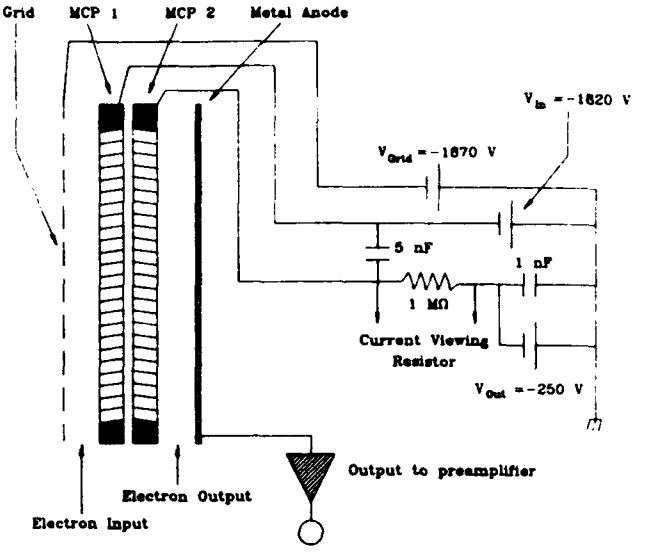

FIG. 3. Circuit diagram of the supporting electronics for the chevron microchannel plate assembly.

This was inserted between the VacIon pump and target chamber with the apertures staggered in a helical pattern.

B. Lens design

The structure and dimensions of the lens used in this work are shown in Fig. 2. The steering of the electrons was performed primarily by the potential gradients established between two annular rings mounted inside a wire cylinder. The rings had a common outer diameter of 12.7 cm and inner diameters of 2.5 and 6.4 cm, respectively. The overall length of the lens was 14 cm. It not only served to focus and accelerate electrons to the detector, but also as a Faraday shield isolating the lens elements from the ground potential of the chamber walls due to the inclusion of endcaps on the assembly. This minimized the number of noise photoelectrons produced inside the chamber that entered the sensitive region of the detector.

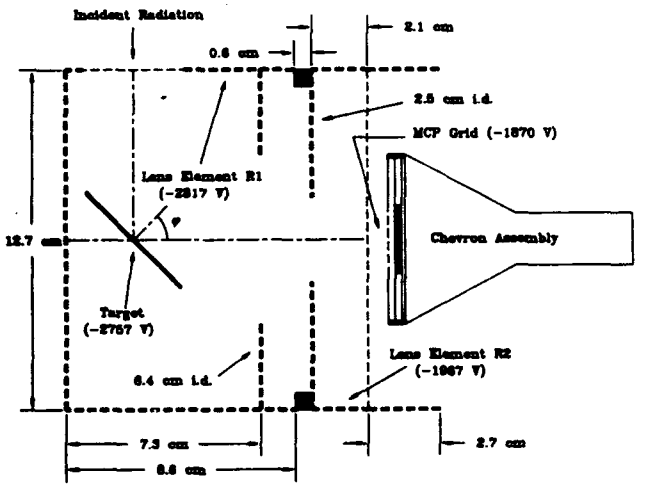

FIG. 2. Drawing of the two-element electron lens designed to efficiently collect electrons having energies <15 eV. The steering of the electrons was performed primarily by the potential gradients established between R_1 and R_2. With the inclusion of the endcaps on the assembly, the lens system not only served to focus and accelerate electrons to the detector input plate, but also as a Faraday cage in shielding the lens elements from the ground potential and noise electrons of the chamber walls. The optimum operating biases for the lens were found to be $V_{R_1} = -2817$ V, $V_{R_2} = -1967$ V, and $V_{target} = -2757$ V when the chevron was operated at -1616 V and the MCP grid at -1870 V.

To model the lens and to determine the optimum potentials for the various elements the program EGN2C was employed which is traceable to SLAC.[11] This program is designed to calculate trajectories of charged particles in electrostatic and magnetostatic fields and is capable of including effects due to space-charge and self-magnetic fields. In this work these effects were not investigated. Input to the program included electrode boundary conditions and initial conditions for electrons emitted from the surface of the target.

Various electron emission configurations including plane waves and point sources were simulated for electrons with energies ranging from 15 eV to 7.3 keV. Biases were found that achieved an effective solid angle for collection of nearly 2π steradians for electrons with energies below 15 eV and are indicated in Fig. 2. A circuit diagram of the supporting electronics for the MCP assembly is shown in Fig. 3. Simulations indicated that the lens had a negligible effect on the trajectories of electrons with energies greater than about 100 eV for the biases used. The detection efficiency for these electrons was then solely defined by the geometrical solid angle between the detector and the target.

C. Noise reduction

To obtain Mössbauer spectra with large signal-to-noise ratios, proper collimation of the source was critical to reduce nonresonant scattering inside the chamber. Various collimator designs were used in these experiments but the best performance was realized with a 1.25 cm thick lead

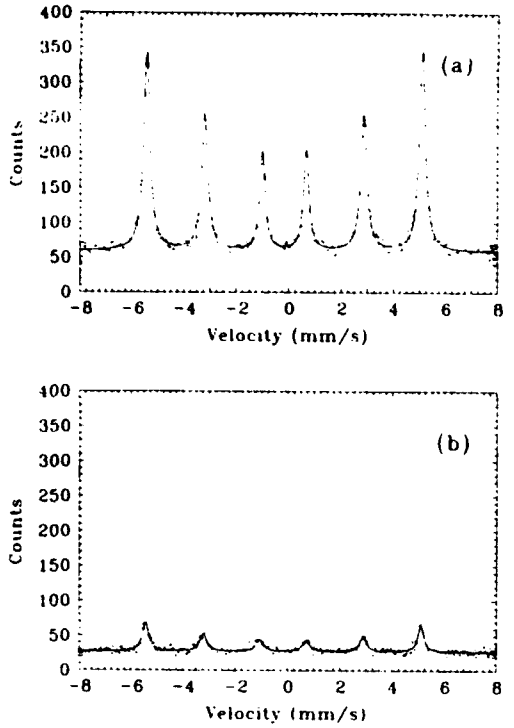

FIG. 4. Conversion electron Mössbauer spectra for a 93.55% enriched ^{57}Fe target: (a) Lens in a focusing or active mode and collected for 3.4 h with a counting rate of 2.47 cps. (b) With the lens in a passive, field-free mode possessing no focusing or accelerating properties the signal counting rate dropped to 0.087 cps. The data were collect five times longer than in (a). The geometrical collection of the lens accounted for less than 3.5% of the signal when the lens was operated at optimum biases.

plate that had a circular aperture at its center. The aperture was tapered so that its diameter increased in the direction of propagation of the radiation to reduce scattering from the collimator walls.

Radiation scattering inside the chamber was minimized by providing an exit window diametrically opposite the entrance window. This window had a diameter of 10 cm and was constructed of mylar to avoid significant backscattering of photons and photoelectrons. The beam size of γ rays from the ^{57}Co source was optimized by proper collimation to illuminate the entire target without expanding to a diameter that would impede its exit from the output window.

To further reduce scattering in the system the lens was constructed from a copper mesh which had an open area of 69% and a wire diameter of 250 μm. Perturbations of the electric field resulting from the use of a mesh instead of a continuous sheet of metal have been shown to be negligible at distances greater than the wire separation.[12] The percentage of open area was further increased by alternately removing wires in the region of the lens that were in the direct path of the input radiation.

III. RESULTS

The target foil used to evaluate the effectiveness of the lens was a $5.0\times5.0\times2\times10^{-4}$ cm iron foil with ^{57}Fe nuclei enriched to 93.55%. For purposes of comparison, data were collected with the electron lens operating in an "active" mode at the optimum potentials for low-energy electrons and in a passive mode where there were no accelerating fields. Data collected with the lens in the focusing or active mode are shown in Fig. 4(a). The total collection time for the data was 3.44 h and the total signal counting rate was 2.47 counts per second. The data with the lens in the passive, field-free mode are shown in Fig. 4(b). There the signal counting rate was 0.087 counts per second. The data were collected five times longer than the corresponding data with the lens active to obtain reasonable statistics.

Operation of the lens in a passive mode helped determine the geometrical collection efficiency for the system. In this geometry it was concluded from the data of Fig. 4 that the lens increased the signal count rate by a factor of 28 while the background signal increased by only a factor of 11. For the biases used in the active mode the trajectories of the higher energy signal electrons were defined solely by the geometrical solid angle between the target and MCP assembly and were the same for both bias configurations. This contribution to the signal counting rate could have been reduced further by simply increasing the distance between the target and detector assembly.

IV. DISCUSSION

Detection of electrons with energies <15 eV can provide detailed information about a variety of surface phenomena in the top 5 nm of a material. In this article we have described the design and construction of a detection system for conversion electron Mössbauer spectroscopy. This device preferentially detects electrons with energies <15 eV and has the potential for providing a simple alternative to more complex and expensive electron detectors which are currently used in energy-resolved Mössbauer spectroscopy.

It was shown that the detection efficiency of higher energy conversion and Auger electrons can be minimized by choosing an appropriate geometry. Numerous computer simulations using plane-wave and point-source electron configurations showed that the electrostatic lens gave an effective solid angle of almost 2π steradians for the signal electrons having appropriately low energies.

Although not pursued in this work, it is possible with the current design to collect virtually all the electrons emitted from the target. This could be accomplished if the potential difference between the input of the chevron and target foil is made sufficiently large. Furthermore, if a retarding field analyzer is positioned between the target and MCP the lower energy electrons can be efficiently filtered out.[13] In this manner it is possible to obtain energy-resolved Mössbauer spectra over a wide range of electron energies.

ACKNOWLEDGMENTS

The authors gratefully acknowledge the support of this work by SDIO/TNI through NRL.

[1] For a good review see, J. A. Sawicki, in *Industrial Applications of the Mössbauer Effect*, edited by G. J. Long and J. G. Stevens (Plenum, New York, 1986), p. 83.
[2] Z. Bonchev, A. Jordanov, and A. Minkova, Nucl. Instrum. Methods **70**, 36 (1969).
[3] J. Fenger, Nucl. Instrum. Methods **69**, 268 (1969).
[4] K. R. Swanson and J. J. Spijkerman, J. Appl. Phys. **41**, 3155 (1970).
[5] W. Jones, J. M. Thomas, R. K. Thorpe, and M. J. Tricker, Appl. Surf. Sci. **1**, 388 (1978).
[6] J. A. Sawicki and T. Tyliszczak, Nucl. Instrum. Methods **216**, 501 (1983).
[7] J. S. Zabinski and B. J. Tatarchuk, Nucl. Instrum. Methods B **42**, 379 (1989).
[8] J. S. Zabinski and B. J. Tatarchuk, Nucl. Instrum. Methods B **31**, 576 (1988).
[9] G. Klingelhöfer and E. Kankeleit, Hyperfine Interactions **57**, 1905 (1990).
[10] J. S. Zabinski and B. J. Tatarchuk, Thin Solid Films **166**, 213 (1988).
[11] W. B. Herrmannsfeldt, *EGUN. An Electron Optics and Gun Design Program*, Stanford Linear Accelerator Center, Stanford, CA, SLAC-Report-331 (1988).
[12] See, for example, R. P. Feynman, R. B. Leighton, and M. Sands, *The Feynman Lectures in Physics* (Addison-Wesley, Reading, MA, 1964), Vol II, p. 7–10.
[13] H. Sato and M. Mitsuhashi, Hyperfine Interactions **58**, 2535 (1990)

Quantum interference asymmetries in the multiphoton radio-frequency sideband spectra of ^{57}Fe

S. Olariu,* T. W. Sinor and C. B. Collins

Center for Quantum Electronics
University of Texas at Dallas
P.O. Box 830688
Richardson, TX 75083-0688

ABSTRACT

We determine the intensity of the nuclear multiphoton sidebands to the forbidden components of the 14.4 keV Mössbauer transition in ^{57}Fe, generated by the application of radio-frequency magnetic fields to ferromagnetic samples in the presence of static magnetic fields. Further we determine the intensity of the second-order sidebands to the 14.4 keV transition in the case known as the radio-frequency collapse, when the entire hyperfine magnetic field acting on the ^{57}Fe nuclei follows the oscillations of the applied radio-frequency field. Then we discuss a number of characteristic asymmetries due to quantum interference, appearing in the multiphoton radio-frequency sideband spectra.

*Permanent address: Str. Fizicienilor nr 2, bloc M6, apt. 5, 76900 Bucharest/Magurele, Romania

I. INTRODUCTION

We consider in this work a class of nuclear multiphoton processes involving the simultaneous interaction with a nucleus of a gamma-ray photon and of radio-frequency photons from an applied oscillatory magnetic field, the intermediate states being the magnetic sublevels of the nuclear states. The ratio of the intensity of a two-photon transition to the intensity of the single gamma-ray transition between the same nuclear states is of the order of the square of the ratio of the interaction energy of the radio-frequency magnetic field with the nucleus and the frequency of this field.

The first experimental demonstration of a nuclear transition involving simultaneously a gamma-ray photon and a radio-frequency photon is due to West and Matthias in 1978,[1] for the 6.2 keV state of ^{181}Ta under an applied radio-frequency magnetic field of 23 mT having a frequency of 0.94 MHz. A similar nuclear two-photon process has been demonstrated in 1988 by Ikonen et al.[2-4] for the 93 keV state of ^{67}Zn under an applied radio-frequency magnetic field of 13.4 mT at the frequencies 3.1 kHz and 9.3 kHz.

When we consider the possibility to observe such simultaneous gamma radio-frequency transitions in ^{57}Fe, we have to take into consideration the fact that the half-life of the 14.4 keV transition in ^{57}Fe is 98 ns, compared to a 6.8 μs half-life for the 6.2 keV transition in ^{181}Ta, and a 9.2 μs half-life for the 93 keV transition in ^{67}Zn. Moreover, the spins and the nuclear magnetic moments of the ground and the excited states are respectively 1/2, $0.090\mu_n$ and 3/2, $-0.155\mu_n$ for ^{57}Fe, compared to

7/2, 2.37μ_n and 9/2, 5.3μ_n for ^{181}Ta, and 5/2, 0.87μ_n and 1/2, 0.58μ_n for ^{67}Zn, where μ_n = 5.05 x 10^{-27} J/T. Thus, the energy of interaction of an applied radio-frequency field with a ^{57}Fe nucleus is considerably smaller than the coupling of the same field to ^{181}Ta or ^{67}Zn nuclei. Therefore, a two-photon experiment for ^{57}Fe, without any enhancement mechanism, would require applied magnetic fields with an amplitude of the order of 0.1 T at a frequency of a few MHz, which is difficult to produce.

However, if a ^{57}Fe nucleus is in a ferromagnetic environment, the direction of the hyperfine magnetic field acting on the nucleus is determined by the direction of the magnetization in the sample, and the orientation of the bulk magnetization can be controlled with the aid of applied static and radio-frequency magnetic fields. This approach has been used by Heiman et al.[5-6] who observed the spectrum of the gamma rays scattered by finely powdered metallic iron under the action of an oscillatory magnetic field whose frequency of 26 MHz was equal to the hyperfine splitting of the upper, 14.4 keV state of ^{57}Fe. The incident gamma rays were themselves resonant to one of the allowed transitions between the magnetic nuclear sublevels, and the arrangement has been referred to by the authors as an excited-state nuclear magnetic resonance experiment. As a result of the application of the radio-frequency magnetic field to the iron-powder scatterer, lines appeared in the spectrum of the scattered gamma radiation at the position of the other known transitions of ^{57}Fe.

On the theoretical side, the effects of circularly-polarized radio-frequency magnetic fields on the Mössbauer spectra of ^{57}Fe have been analyzed by Gabriel.[7]

Initially Heiman et al. have tried to use a metallic iron *foil* for the scatterer,[8] but they have found that the application of the radio-frequency magnetic field produced in this case additional lines at positions which did not correspond to any known transition in ^{57}Fe. They have suggested[9] that the observed sidebands, occurring in a foil but with negligible intensity in a powder, result from the acoustic vibrations generated in the foil by the applied radio-frequency magnetic field. Similar observations have been reported by Asti et al.[10,11]

The fact that the hyperfine magnetic field acting on a ^{57}Fe nucleus in a ferromagnetic environment can be made to oscillate between opposing directions by the application of radio-frequency fields has been demonstrated by the radio-frequency collapse effect discovered by Pfeiffer in 1971.[12,13] He found that, as a result of the application of an oscillatory magnetic field with an amplitude of 1.5 mT and frequencies of 39 MHz, 61 MHz and 106 MHz to a 6-μm-thick permalloy foil, the six-line hyperfine pattern of ^{57}Fe disappeared and has been replaced by a single central line, accompanied by a number of sidebands displaced on a frequency scale by multiples of the applied frequency.

Pfeiffer attributed the presence of the sidebands in his collapse experiments entirely to the acoustic vibrations generated in the permalloy foil by the radio-frequency field.

However, Olariu et al.[14] pointed out that the oscillation through large angles of the hyperfine magnetic field acting on the ^{57}Fe nuclei, produced by the application of the radio-frequency field to the permalloy sample, results necessarily in the generation of nuclear multiphoton sidebands whose transition intensities are comparable to those observed by Pfeiffer. The fact that the entire hyperfine magnetic field can be made to follow the direction of the applied radio-frequency field, and the reduced amplitude of the mechanical vibrations in the permalloy sample, due to the small magnetostrictive constant of permalloy, show that it is possible to observe nuclear multiphoton transitions for ^{57}Fe nuclei in a ferromagnetic environment.

The radio-frequency collapse effect has been further investigated by Kopcewicz et al. in ferromagnetic amorphous metals,[15,16] in $FeBO_3$,[17] and in Fe-Ni alloys,[18] with the conclusion that for sufficiently intense radio-frequency fields, of the order of 1.5 mT, the hyperfine magnetic field acting on the ^{57}Fe nuclei follows the direction of the applied field. The sidebands observed in these experiment have been in general attributed to acoustic modulation.

As a corollary of their studies on the magnetic modulation of the phase of ^{67}Zn nuclei, Ikonen et al.[2] have reiterated the previous prediction[14] that if the hyperfine field acting on ^{57}Fe nucleus can be switched between two opposite directions at a rate determined by the frequency of the applied radio-frequency field, this will generate sidebands without any mechanical motion.

The intensities of the nuclear multiphoton sidebands for the six allowed transitions of ^{57}Fe have been calculated by Olariu[19] for ^{57}Fe nuclei embedded in thin ferromagnetic films under static and radio-frequency magnetic fields. He remarked that the use of a thin ferromagnetic film having a thickness of a few thousand angstroms, instead of a foil, is likely to minimize the mechanical vibrations, and moreover would allow the determination with reasonable accuracy of the time evolution of the magnetization of the sample.

The role played by the spin waves in the generation of the radio-frequency sidebands has been emphasized by Sinor et al.[20] who showed that it is possible to produce a modulation of the phase of ^{57}Fe nuclei in paramagnetic media by transporting spin waves of large amplitude from ferromagnetic sources.

The resonance line splitting of hyperfine lines of ^{57}Fe nuclei in radio-frequency magnetic field, caused by Rabi oscillations, predicted in a number of papers,[7,19,21] has been recently observed by Vagizov[22] and independently by Tittonen et al.[23] Special precautions have been taken in these works to minimize the mechanical vibrations.

It is apparent from this survey of previous work on radio-frequency sidebands that, while the ferromagnetic foil samples can provide the required large radio-frequency fields, in the form of oscillatory hyperfine magnetic fields, the observation of the nuclear multiphoton processes is often hindered by the ease with which mechanical vibrations can be induced in ferromagnetic samples through magnetostriction, especially at lower

frequencies. The importance of nuclear multiphoton processes becomes apparent when we refer to recent developments in atomic multiphoton processes, where problems like inversionless amplification[24,25] or electromagnetically-induced transparency[26-28] are under active consideration.

The purpose of this work is to bring into evidence a number of characteristic properties of nuclear multiphoton processes involving gamma-ray and radio-frequency photons. Thus, in Section II we determine the intensity of the nuclear multiphoton sidebands to the forbidden components of the 14.4 keV transition of ^{57}Fe, generated by the application of radio-frequency magnetic fields to ferromagnetic samples, in the presence of a static field. In Section III we determine the intensity of the second-order sidebands to the 14.4. keV transition of ^{57}Fe in the case of the radio-frequency collapse, when the entire hyperfine magnetic field follows the oscillations of the applied radio-frequency field. In Section IV we discuss a number of characteristic asymmetries due to quantum interference, appearing in the multiphoton radio-frequency sideband spectra.

II. Intensity of the first-order sidebands to the forbidden $e, 3/2 \rightarrow g, -1/2$ and $e, -3/2 \rightarrow g, 1/2$ transitions in ^{57}Fe

The intensities of the first-order sidebands to the six allowed transitions between the 14.4 keV excited state e and the ground state g of ^{57}Fe nuclei have been determined in Ref. 19 as a function of the direction and polarization of the gamma rays for a linear and a circular polarization of the applied radio-

frequency magnetic field. The transitions e, $3/2 \rightarrow g$, $-1/2$ and e, $-3/2 \rightarrow g$, $1/2$ are forbidden as single gamma-ray processes, but these forbidden transitions have in general non-vanishing multiphoton sidebands, the intensity of which we shall calculate in this section.

The intensity of the sidebands to the forbidden hyperfine transition of ^{57}Fe has been reported previously[29] in the particular case of a linearly-polarized radio-frequency mangetic field B_0^h, and for a direction of propagation of the gamma rays which was perpendicular to the static and radio-frequency magnetic fields. In the previous paper[29] it has been also pointed out that sidebands to the forbidden hyperfine transition of ^{57}Fe can be identified in the Mössbauer spectra of ^{57}Fe nuclei in permalloy recently reported by Tittonen et al.[23] The presence of the sidebands to the forbidden hyperfine transitions of ^{57}Fe constitute the unequivocal proof that nuclear multiphoton processes are inded taking place in ^{57}Fe nuclei subject to radio-frequency magnetic fields, as predicted repeatedly.[2,7,14,19,30]

We shall determine the probability for the transition e, $3/2 \rightarrow g$, $-1/2$ in a ^{57}Fe nucleus by the emission of a linearly polarized gamma-ray quantum, the orientation of the magnetic gamma-ray field $\vec{B}_\gamma$ and of the wave vector $\vec{k}_\gamma$ being shown in Fig. 1, under the action of a static hyperfine magnetic field B_0^h, oriented along the z axis, and of a radio-frequency magnetic field having the x component $B_{rf,x} \cos(\omega_{rf} t)$ and the y component $B_{rf,y} \cos(\omega_{rf} t + \alpha_{rf})$. The positive direction of the z axis is

chosen to coincide with the direction of the static hyperfine magnetic field effectively acting on the ^{57}Fe nuclei, so that the magnetic sublevels, in order of increasing energy, are g, 1/2; g, -1/2; and e, -3/2; e, -1/2; e, 1/2; e, 3/2.

It can be shown that the transition amplitudes b_k are solutions of the Hamiltonian equations

$$i\hbar\frac{db_k}{dt}=\sum_n F_{kn}(t)b_n \tag{1}$$

The non-vanishing matrix elements are given by

$$F_{g,\frac{1}{2};g,-\frac{1}{2}}(t)=-\frac{\hbar\omega_g}{2B_0^h}Y(t)^*\exp(-i\omega_g t), \tag{2a}$$

$$F_{e,-\frac{1}{2};e,-\frac{1}{2}}(t)=\frac{\hbar\omega_e\sqrt{3}}{2B_0^h}Y(t)\exp(-i\omega_e t), \tag{2b}$$

$$F_{e,-\frac{1}{2};e,\frac{1}{2}}(t)=\frac{\hbar\omega_e}{2B_0^h}Y(t)\exp(-i\omega_e t), \tag{2c}$$

$$F_{e,\frac{1}{2};e,\frac{3}{2}}(t)=\frac{\hbar\omega_e\sqrt{3}}{2B_0^h}Y(t)\exp(-i\omega_e t), \tag{2d}$$

where

$$Y(t)=B_{rf,x}\cos(\omega_{rf}t)+iB_{rf,y}\cos(\omega_{rf}t+\alpha_{rf}), \tag{3}$$

and by

$$F_{g,-\frac{1}{2};e,-\frac{1}{2}}(t)=\frac{\sqrt{6}}{2}AB_\gamma\cos(\omega_\gamma t+\phi_\gamma)Z\exp\left[-i\left(\frac{E_e-E_g}{\hbar}-\frac{3\omega_e}{2}-\frac{\omega_g}{2}-\frac{i\Gamma}{2}\right)t\right], \tag{4a}$$

$$F_{g,-\frac{1}{2};e,-\frac{1}{2}}(t)=\sqrt{2}AB_\gamma\cos(\omega_\gamma t+\phi_\gamma)\sin\theta\cos\upsilon\exp\left[-i\left(\frac{E_e-E_g}{\hbar}-\frac{\omega_e}{2}-\frac{\omega_g}{2}-\frac{i\Gamma}{2}\right)t\right], \tag{4b}$$

$$F_{g,-\frac{1}{2};e,\frac{1}{2}}(t) = -\frac{\sqrt{2}}{2} AB_\gamma \cos(\omega_\gamma t + \phi_\gamma) Z^* \exp\left[-i\left(\frac{E_e - E_g}{\hbar} + \frac{\omega_e}{2} - \frac{\omega_g}{2} - \frac{i\Gamma}{2}\right)t\right], \tag{4c}$$

$$F_{g,\frac{1}{2};e,-\frac{1}{2}}(t) = \frac{\sqrt{2}}{2} AB_\gamma \cos(\omega_\gamma t + \phi_\gamma) Z \exp\left[-i\left(\frac{E_e - E_g}{\hbar} - \frac{\omega_e}{2} + \frac{\omega_g}{2} - \frac{i\Gamma}{2}\right)t\right], \tag{4d}$$

$$F_{g,\frac{1}{2};e,\frac{1}{2}}(t) = \sqrt{2} AB_\gamma \cos(\omega_\gamma t + \phi_\gamma) \sin\theta \cos\upsilon \exp\left[-i\left(\frac{E_e - E_g}{\hbar} + \frac{\omega_e}{2} + \frac{\omega_g}{2} - \frac{i\Gamma}{2}\right)t\right], \tag{4e}$$

$$F_{g,\frac{1}{2};e,\frac{3}{2}}(t) = -\frac{\sqrt{6}}{2} AB_\gamma \cos(\omega_\gamma t + \phi_\gamma) Z^* \exp\left[-i\left(\frac{E_e - E_g}{\hbar} + \frac{3\omega_e}{2} + \frac{\omega_g}{2} - \frac{i\Gamma}{2}\right)t\right], \tag{4f}$$

where A is a reduced matrix element, and

$$Z = \sin\varphi \sin\upsilon - \cos\varphi \cos\theta \cos\upsilon + i(\cos\varphi \sin\upsilon + \sin\varphi \cos\theta \cos\upsilon). \tag{5}$$

In Eqs. (2) and (4), ω_e, $\omega_g > 0$ represent the separations, on a frequency scale, of the magnetic sublevels of the excited state e and respectively of the ground state g due to the static hyperfine field B_0^h, and $\Gamma = 1/\tau$, where the mean life is $\tau = 1.4 \times 10^{-7}$ s for the 14.4 keV level of ^{57}Fe. E_e and E_g are the energies of the excited and ground states in the absence of any applied magnetic field.

The Eq. (1) can be solved by a perturbation series, and the second-order contribution, which gives the amplitudes of the first-order sidebands to the gamma-ray transitions, is

$$b^{(2)}_{gm;em_0} = -\frac{1}{\hbar^2} \sum_k \int_0^\infty F_{gm,k}(t)dt \int_0^t F_{k;em_0}(\zeta)d\zeta. \tag{6}$$

Substituting in Eq. (6) the expression of the appropriate matrix elements from Eqs. (2) - (5), and neglecting non-resonant terms, we obtain an expression for the intensity of the first-order sidebands for a linear polarization of the radio-frequency field, when $B_{rf,y} = 0$, that is given by

$$\left|\left\langle g,-\tfrac{1}{2}\middle|e,\tfrac{3}{2}\right\rangle_{\pm}^{(L)}\right|^2 = \frac{3|A|^2 B_\gamma^2}{32\hbar^2\Gamma^2}(\sin^2\upsilon+\cos^2\theta\cos^2\upsilon)\left(\frac{B_{rf,x}}{B_0^h}\right)^2\left(\frac{\omega_e}{\pm\omega_{rf}+\omega_e}+\frac{\omega_g}{\pm\omega_{rf}-\omega_g}\right)^2, \tag{7}$$

$$for \quad \omega_\gamma = \frac{E_e-E_g}{\hbar}+\frac{3\omega_e}{2}-\frac{\omega_g}{2}\pm\omega_{rf.}$$

where the alternate signs should be read along the upper line or the lower line.

If the radio-frequency field has a right circular polarization, so that $B_{rf,x} = B_{rf,y} = B_{rf}$ and $\alpha_{rf} = -\pi/2$, the intensity of the sidebands, obtained from Eq. (6), is

$$\left|\left\langle g,-\tfrac{1}{2}\middle|e,\tfrac{3}{2}\right\rangle_{+}^{(CR)}\right|^2 = 0 \quad , \tag{8a}$$

$$for \quad \omega_\gamma = \frac{E_e-E_g}{\hbar}+\frac{3\omega_e}{2}-\frac{\omega_g}{2}+\omega_{rf} \quad ,$$

$$\left|\left\langle g,-\tfrac{1}{2}\middle|e,\tfrac{3}{2}\right\rangle_{-}^{(CR)}\right|^2 = \frac{3|A|^2 B_\gamma^2}{8\hbar^2\Gamma^2}(\sin^2\upsilon+\cos^2\theta\cos^2\upsilon)\left(\frac{B_{rf}}{B_0^h}\right)^2\left(\frac{\omega_e}{\omega_{rf}-\omega_e}+\frac{\omega_g}{\omega_{rf}+\omega_g}\right)^2, \tag{8b}$$

$$for \quad \omega_\gamma = \frac{E_e-E_g}{\hbar}+\frac{3\omega_e}{2}-\frac{\omega_g}{2}-\omega_{rf} \quad .$$

If the radio-frequency field has a left circular polarization, so the $B_{rf,x} = B_{rf,y} = B_{rf}$ and $\alpha_{rf} = \pi/2$, the intensity of the sidebands, obtained from Eq. (6), is

$$\left|\left\langle g,-\tfrac{1}{2}\middle|e,\tfrac{3}{2}\right\rangle_{+}^{(CR)}\right|^2 = \frac{3|A|^2 B_y^2}{8\hbar^2\Gamma^2}(\sin^2\upsilon+\cos^2\theta\cos^2\upsilon)\left(\frac{B_{rf}}{B_0^h}\right)^2\left(\frac{\omega_e}{\omega_{rf}+\omega_e}+\frac{\omega_g}{\omega_{rf}-\omega_g}\right)^2, \tag{9a}$$

$$for \quad \omega_\gamma = \frac{E_e-E_g}{\hbar}+\frac{3\omega_e}{2}-\frac{\omega_g}{2}+\omega_{rf} \quad ,$$

$$\left|\left\langle g,-\tfrac{1}{2}\middle|e,\tfrac{3}{2}\right\rangle_{-}^{(CR)}\right|^2 = 0 \quad , \tag{9b}$$

$$for \quad \omega_\gamma = \frac{E_e-E_g}{\hbar}+\frac{3\omega_e}{2}-\frac{\omega_g}{2}-\omega_{rf} \quad .$$

It can be shown that the intensities of the first-order sidebands to the forbidden transition e, -3/2 → g, 1/2 are connected to the previous intensities by the relations

$$\left|\left\langle g,\tfrac{1}{2}\middle|e,-\tfrac{3}{2}\right\rangle_{+}^{(2)}\right|^2 = \left|\left\langle g,-\tfrac{1}{2}\middle|e,\tfrac{3}{2}\right\rangle_{-}^{(2)}\right|^2, \tag{10a}$$

$$\left|\left\langle g,\tfrac{1}{2}\middle|e,-\tfrac{3}{2}\right\rangle_{-}^{(2)}\right|^2 = \left|\left\langle g,-\tfrac{1}{2}\middle|e,\tfrac{3}{2}\right\rangle_{+}^{(2)}\right|^2, \tag{10b}$$

for all polarizations of the applied radio-frequency field, where the superscript (2) refers to the second-order contribution in the perturbation series.

As was the case with the sidebands of the allowed transitions,[19] the intensity of the sidebands towards higher

frequencies of a parent line is in general different from the intensity of the sideband towards lower frequencies of the same parent line. This asymmetry becomes particularly striking in the case of a circular polarization of the radio-frequency field, when not only the parent forbidden line has a zero intensity, but the intensity of one of the sidebands is also equal to zero.

By combining the results of Ref. 19 and the present work, we obtain the intensities of the sidebands towards higher frequencies, labelled by the subscript +, which are shown in Fig 2 for linear, right circular and left circular polarizations of the radio-frequency magnetic field. The intensity of the unperturbed transition e, 1/2 $\rightarrow$ g, 1/2, averaged over the polarization of the gamma rays, and observed at the angle $\theta = \pi/2$, was chosen as unity. The remarkable aspect of the pattern in Fig. 2 is the appearance of the supplementary lines which are the sidebands of the forbidden parent transitions. The appearance of these lines in a spectrum is characteristic of the multiphoton generation of the radio-frequency sidebands.

If the ^{57}Fe nucleus is under the action of a circularly polarized magnetic field but the static field $B_0^{\hbar}$ is equal to zero, the intensity of the first-order sidebands, at $\omega_\gamma = (E_e - E_g)/\hbar \pm \omega_{rf}$, can be shown to be

$$I_1^{(C)} = \frac{|A|^2 B_\gamma^2}{2\hbar^2 I^2}\left(\frac{\mu_e B_{rf}}{J_e \hbar \omega_{rf}}\right)^2 \left[\sin^2\theta\cos^2\upsilon\,(7+4f+f^2)+(\sin^2\upsilon+\cos^2\theta\cos^2\upsilon)(4+3f+f^2)\right], \quad (11)$$

where

$$f = -\frac{\mu_g J_e}{\mu_e J_g} > 0.$$

The ratio of the intensity of the first-order sideband to the parent line, at the angle of observation $\theta = 0$, is then, for a circular polarization of the radio-frequency field,

$$R_1^{(C)} = \frac{1}{8}\left(\frac{\mu_e B_{rf}}{J_e \hbar \omega_{rf}}\right)^2 (4 + 3f + f^2). \qquad (12)$$

The results in Eqs. (11) and (12) differ from the corresponding expressions, Eqs. (32) and (33) of Ref. 19, by the contribution of the sidebands to the forbidden lines, evaluated in this section.

III. Intensity of the second-order sidebands in the case of radio-frequency collapse for ^{57}Fe

While the second-order perturbation calculations are in general sufficient to describe the generation of radio-frequency sidebands at frequencies of the order of 100 MHz or higher, the third-order contribution to the perturbation series is needed to describe the second-order sidebands which become observable at lower frequencies. In this section we shall determine the intensity of the second-order sidebands for the case of the radio-frequency collapse, when the hyperfine magnetic field acting on the ^{57}Fe nuclei follows the oscillations of the applied radio-frequency field, so that the static hyperfine field is $B_0^h = 0$.

The third-order contribution to the transition amplitude is given by

$$b^{(3)}_{g m_g, e m_e} = \frac{i}{\hbar^3} \sum_k \int_0^\infty F_{g m_g, l}(t)\,dt \int_0^t F_{l,k}(\eta)\,d\eta \int_0^\eta F_{k, e m_e}(\zeta)\,d\zeta \quad . \tag{13}$$

We shall assume, as in the previous section, that the applied radio-frequency field is in the x,y plane, and shall evaluate the right-hand side of Eq. (13) for gamma rays emitted perpendicularly to the x,y plane, so that we shall consider that $\theta = 0$, $\varphi = 0$.

The non-vanishing matrix elements for the present problem are

$$F_{g,\frac{1}{2};g,-\frac{1}{2}}(t) = -\frac{\mu_g}{2J_g} Y^*(t), \tag{14a}$$

$$F_{e,-\frac{1}{2};e,-\frac{1}{2}}(t) = -\frac{\mu_e \sqrt{3}}{2J_e} Y(t), \tag{14b}$$

$$F_{e,-\frac{1}{2};e,\frac{1}{2}}(t) = -\frac{\mu_e}{J_e} Y(t), \tag{14c}$$

$$F_{e,\frac{1}{2};e,\frac{3}{2}}(t) = -\frac{\mu_e \sqrt{3}}{2J_e} Y(t), \tag{14d}$$

where $Y(t)$ is the function defined in Eq. (3), and

$$F_{g,-\frac{1}{2};e,-\frac{3}{2}}(t) = -\frac{\sqrt{6}}{4} AB_\gamma e^{i\phi_\gamma - i\upsilon} e^{i\left(\omega_\gamma - \omega_0 + i\frac{\Gamma}{2}\right)t}, \tag{15a}$$

$$F_{g,-\frac{1}{2};e,\frac{1}{2}}(t) = \frac{\sqrt{2}}{4} AB_\gamma e^{i\phi_\gamma + i\upsilon} e^{i\left(\omega_\gamma - \omega_0 + i\frac{\Gamma}{2}\right)t}, \tag{15b}$$

$$F_{g,\frac{1}{2};e,-\frac{1}{2}}(t) = -\frac{\sqrt{2}}{4} AB_\gamma e^{i\phi_\gamma - i\upsilon} e^{i\left(\omega_\gamma - \omega_0 + i\frac{\Gamma}{2}\right)t}, \tag{15c}$$

$$F_{g,\frac{1}{2};e,\frac{1}{2}}(t) = \frac{\sqrt{6}}{4} AB_\gamma e^{i\phi_\gamma + i\upsilon} e^{i\left(\omega_\gamma - \omega_0 + i\frac{\Gamma}{2}\right)t}, \tag{15d}$$

where $\omega_0 = \left(E_e - E_g\right)/\hbar$. Since according to Eqs. (14) and (15) the matrix elements are non-vanishing only for $\Delta m = \pm 1$, there is a non-vanishing third-order contribution to the amplitude $b^{(3)}_{gm;em}$ for the 14.4 keV transition only when $|m - m_0| = 1$, so that the transitions to be considered are e, 3/2 → g, 1/2; e, 1/2 → g, -1/2; e, -1/2 → g, 1/2 and e, -3/2 → g, -1/2. From the symmetry of the matrix elements in Eqs. (14) and (15) it results that it is sufficient to evaluate $b^{(3)}_{g,1/2;e,3/2}$ and $b^{(3)}_{g,-1/2;e,1/2}$ at $\omega_\gamma = \omega_0 \pm 2\omega_{rf}$. There are four channels contributing to $b^{(3)}_{g,1/2;e,3/2}$, and there are six channels contributing to $b^{(3)}_{g,-1/2;e,1/2}$. Thus, we obtain for the intensity of the second-order sidebands, at $\omega_\gamma = \omega_0 \pm 2\omega_{rf}$, averaged over the polarization υ of the gamma rays,

$$I_2 = \frac{1}{256} \frac{|A|^2 B_\gamma^2}{\hbar^2 \Gamma^2} \left(\frac{\mu_e}{J_e \hbar \omega_{rf}}\right)^2 \left[B_1 B_1^* B_2 B_2^* \left(19 + 30f + 20f^2 + 6f^3 + f^4\right) + 2\left[\left(B_1 B_1^*\right)^2 + \left(B_2 B_2^*\right)^2\right]\left(3 + 3f + f^2\right)\right], \tag{16}$$

where

$$B_1 = B_{rf,x} + iB_{rf,y} e^{i\alpha_{rf}} \tag{17a}$$

$$B_2 = B_{rf,x} + iB_{rf,y} e^{-i\alpha_{rf}} \tag{17b}$$

For a linear polarization of the radio-frequency field, when $B_{rf,y} = 0$, the ratio of the second-order sideband, averaged over

gamma-ray polarization, to the unperturbed partent intensity is, for $\omega_\gamma = \omega_o \pm 2\omega_{rf}$,

$$R_2^{(L)} = \frac{1}{1024}\left(\frac{\mu_e B_{rf,x}}{J_e \hbar \omega_{rf}}\right)^4 (31+42f+24f^2+6f^3+f^4), \tag{18}$$

where $f = -\mu_g J_e/\mu_e J_g$. This expression is equivalent to the result reported previously in Eq. (17) of Ref. 14.

If the radio-frequency field acting on the nucleus can be described as a superposition of two independent orthogonal modes, so that $B_{rf,x} = B_{rf,y} = B_{rf}$ and the relative phase α_{rf} is random, then the ratio of the intensity of the second-order sideband, averaged over gamma-ray polarization, to the parent intensity, is

$$R_2^{(x,y)} = \frac{1}{256}\left(\frac{\mu_e B_{rf}}{J_e \hbar}\right)^4 (31+42f+24f^2+6f^3+f^4) \quad . \tag{19}$$

If the radio-frequency field is circularly polarized, so that $B_{rf,x} = B_{rf,y} = B_{rf}$ and $|\alpha_{rf}| = \pi/2$, the ratio of the intensity of the second-order sideband, averaged over the polarization of the gamma rays, to the unperturbed parent intensity is

$$R_2^{(C)} = \frac{1}{32}\left(\frac{\mu_e B_{rf}}{J_e \hbar \omega_{rf}}\right)^4 (3+3f+f^2) \quad . \tag{20}$$

If, as a result of the application of an oscillatory magnetic field of frequency ω_{rf}, the hyperfine field assumes

alternatively two opposite values $\pm B_s$, the Fourier component of this hyperfiene field at the frequency ω_{rf} will have the enhanced amplitude $(4/\pi)B_s$. The amplitude of the component of the afore-mentioned hyperfine field at the frequency $2\omega_{rf}$ is equal to zero, but the amplitude of the component at the frequency $3\omega_{rf}$ will be $4B_s/3\pi$, and can produce, at low frequencies, a sizable sideband. These considerations lose their applicability if the passages between the opposing values of the hyperfine field are rounded off.

Combining the results of Ref. 14 and the results of the present work, we have represented in Fig. 3 the emission gamma-ray spectrum with sidebands in the case of radio-frequency collapse for ^{57}Fe nuclei in a permalloy sample, for a linear polarization of the applied oscillatory magnetic field at several frequencies, assuming that the amplitude of the oscillating hyperfine field is equal to its static value. Moreover, in Fig. 4 we have represented the emission gamma-ray spectrum with sidebands at a fixed frequency for several configurations of the applied radio-frequency field. The intensities in parts (a) and (b) of Fig. 4 are calculated according to the Bessel-function formula of Ref. 14, and the intensities in part (c) and (d) are calculated according to the perturbation expressions of Ref. 14 and the present work. It is apparent from Figs. 3 and 4 that if the hyperfine field follows the applied radio-frequency, as it is supposed to be the case for the radio-frequency collapse spectra, the generation of nuclear multiphoton sidebands can be very intense.

IV. Quantum interference effects in the radio-frequency multiphoton spectra of ^{57}Fe

While the intensity of the acoustic sidebands of a given order is a decreasing function of frequency, the intensity of the multphoton sidebands of a given order, in the presence of static magnetic fields, can <u>increase</u> in certain frequency ranges. The increase with frequency of the intensity of the multiphoton transition can arise from the fact that some of the transition amplitudes have resonances when the applied frequency becomes equal to the separation in frequency units between the magnetic sublevels of the ground or excited states, i.e. when a real intermediate state in the nucleus coincides with the position of the virtual multiphoton level.

This pattern is encountered for example to the first-order sideband towards lower frequencies of the transition e, 1/2 → g, 1/2, in the presence of a static magnetic field B_0^h and of a linearly polarized radio-frequency magnetic field. If the emitted gamma rays are observed along a direction perpendicular to the plane of the applied fields, $\theta = \pi/2$, $\varphi = \pi/2$, then the ratio of the first-order sideband intensity $I_{b,-}^{(L)}$ to the intensity of the unperturbed parent transition I_b, both averaged over the gamma-ray polarization, becomes[19]

$$\frac{I_{b,-}^{(L)}}{I_b} = \left(\frac{B_{rf,x}}{B_0^h}\right)^2 \left(\frac{3}{8}\frac{\omega_e}{\omega_e + \omega_{rf}} + \frac{1}{4}\frac{\omega_e}{\omega_e - \omega_{rf}} - \frac{1}{8}\frac{\omega_g}{\omega_g - \omega_{rf}}\right)^2 . \qquad (21)$$

The resonances of the relative sideband intensity $I_{b,-}^{(L)}/I_b$, occurring at $\omega_{rf} = \omega_e$ and $\omega_{rf} = \omega_g$, are shown in Fig. 5 for ^{57}Fe nuclei in iron.

Another circumstance which can lead to an increase with frequency of the intensity of the sidebands is the cancellation for certain frequencies of the partial amplitudes contributing to the total transition amplitude. This pattern is encountered for example to the first-order sidebands towards lower frequencies of the transition e, 1/2 → g, 1/2 in the presence of a static magnetic field B_0^h and of a left circular-polarized radio-frequency field of rotating amplitude B_{rf}. The ratio of the first-order sideband intensity $I_{b,-}^{(CL)}$ to the intensity I_a of the unperturbed transition e, 3/2 → g, 1/2 is[19]

$$\frac{I_{b,-}^{(CL)}}{I_a} = \frac{1}{12}\left(\frac{B_{rf}}{B_0^h}\right)^2\left(\frac{3\omega_e}{\omega_{rf}+\omega_e} - \frac{\omega_g}{\omega_g-\omega_{rf}}\right)^2, \qquad (22)$$

for all gamma-ray polarizations and directions of observation. The zero in the relative sideband intensity $I_{b,-}^{(CL)}/I_a$, occurring at $\omega_{rf} = 2\omega_e\omega_g/(3\omega_e + \omega_g)$, can be seen in Fig. 6 for ^{57}Fe nuclei in an iron environment, when the zero occurs at ω_{rf} = 19.1 MHz, assuming that B_{rf} is small compared to B_0^h.

An interesting example of cancellation of amplitudes is encountered for the first-order sidebands of the forbidden gamma-ray transition e, 3/2 → g, → 1/2. In this case the cancellation of amplitudes occurs at ω_{rf} = 0, so that the intensity of the first-order sidebands at ω_{rf} = 0 is, according

to Eqs. (7) - (9), equal to zero for all polarizations of the applied radio-frequency field while, on the other hand, the generation of acoustic sidebands is supposed to increase in intensity at lower frequencies. For example, the ratio of the first-order sideband intensity $\left|\langle g,-\tfrac{1}{2}|e,\tfrac{3}{2}\rangle_{\pm}^{(L)}\right|^2$ to the intensity I_a of the unperturbed transition e, 3/2 → g, 1/2, in the presence of a static magnetic field B_0^h and for a linear polarization of the ratio-frequency field, is, according to Eq. (7),

$$\frac{\left|\langle g,-\frac{1}{2}|e,\frac{3}{2}\rangle_{\pm}^{(L)}\right|^2}{I_a}=\frac{1}{16}\left(\frac{B_{rf,x}}{B_0^h}\right)^2\left(\frac{\omega_e}{\pm\omega_{rf}+\omega_e}+\frac{\omega_g}{\pm\omega_{rf}-\omega_g}\right)^2, \tag{23}$$

for all gamma-ray polarization and directions of observation. The intensity of these sidebands are represented in Fig. 7 for ^{57}Fe nuclei in iron.

V. CONCLUSIONS

In this paper we have demonstrated a number of asymmetries characteristic of the nuclear multiphoton generation of radio-frequency sidebands to gamma-ray transitions in ^{57}Fe nuclei. We have pointed out that these are sidebands of observable intensity to the forbidden 14.4 keV gamma-ray transitions e, 3/2 → g, -1/2 and e, -3/2 → g, 1/2, and have calculated the intensities of the first-order sidebands for a linear and a circular polarization of the applied radio-frequency field. Then we have determined the intensity of the second-order sidebands in the case of the radio-frequency collapse, and have evaluated the sideband intensities for a number of configurations of the applied magnetic field.

Finally, we have remarked that unlike the decreasing patterns of the intensity of the acoustic sidebands, the intensity of the nuclear multiphoton sidebands can increase with frequency over certain frequency ranges, this being a consequence of the resonances extant in the multiphoton transition amplitudes, and also of the cancellation for certain frequencies of the interfering amplitudes.

REFERENCES

1. P. J. West and E. Matthias, Z. Physik A288, 369 (1978).
2. E. Ikonen, P. Helistö, J. Hietaniemi and T. Katila, Phys. Rev. Lett. 60, 643 (1988).
3. E. Ikonen, J. Hietaniemi and T. Katila, Phys. Rev. B 38, 6380 (1988).
4. E. Ikonen, J. Hietaniemi, T. Katila, J. Lindén and I. Tittonen, Hyperfine Interactions 47, 139 (1989).
5. N. D. Heiman, J. C. Walker and L. Pfeiffer, Phys. Rev. 184, 281 (1969).
6. N. D. Heiman, J. C. Walker and L. Pfeiffer, in Mössbauer Effect Methodology Vol 6, edited by I. J. Gruverman (Plenum Press, New York, 1971), p. 123.
7. H. Gabriel, Phys. Rev. 184, 359 (1969).
8. Ref. 6, p. 133.
9. N. D. Heiman, L. Pfeiffer and J. C. Walker, Phys. Rev. Lett. 21, 93 (1968).
10. G. Asti, G. Albanese and C. Bucci, Nuovo Cimento 57B, 531 (1968).
11. G. Asti, G. Albanese and C. Bucci, Phys. Rev. 184, 260 (1969).
12. L. Pfeiffer, J. Appl. Phys. 42, 1725 (1971).
13. L. Pfeiffer, in Mössbauer Effect Methodology, Vol 7, edited by I. J. Gruverman (Plenum, New York, 1971), p. 263.
14. S. Olariu, I. I. Popescu and C. B. Collins, Phys. Rev C 23, 1007 (1981).

15. M. Kopcewicz, H. G. Wagner and U. Gonser, J. Magn. Magn. Mat. 40, 139 (1983).

16. M. Kopcewicz, H. G. Wagner and U. Gonser, J. Magn. Magn. Mat. 51, 225 (1985).

17. M. Kopcewicz, H. Engelmann, S. Stenger, G. V. Smirnov, U. Gonser and H. -G. Wagner, Appl. Phys. A 44, 131 (1987).

18. M. Kopcewicz, M. El Zayat and U. Gonser, Hyperfine Interactions 42, 1123 (1988).

19. S. Olariu, Phys. Rev. B 37, 7698 (1988).

20. T. W. Sinor, P. W. Reittinger and C. B. Collins, Phys. Rev. Lett. 62, 2547 (1989).

21. M. N. Hack and M. Hamermesh, Nuovo Cimento XIX, 546 (1961).

22. F. G. Vagizov, Hyperfine Interactions 61, 1359 (1990).

23. I. Tittonen, M. Lippmaa, E. Ikonen, J. Linden and T. Katila, Phys. Rev. Let. 69, 2815 (1992).

24. S. E. Harris, Phys. Rev. Lett. 62, 1033 (1989).

25. O. Kocharovskaya, P. Mandel and Y. V. Radeonychev, Phys. Rev. A 45, 1997 (1992).

26. M. O. Scully, Phys. Rev. Lett. 67, 1855 (1991).

27. J. E. Field, K. H. Hahn and S. E. Harris, Phys. Rev. Lett. 67, 3062 (1991).

28. S. E. Harris, Phys. Rev. Lett. 70, 552 (1993).

29. S. Olariu, T. W. Sinor and C. B. Collins, Phys. Rev. B. (pending).

30. A. V. Mitin, Zh. Eksp. Teor. Fiz. 52, 1596 (1967) [Sov. Phys. JETP 25, 1062 (1967)].

Figure Captions

Fig. 1. Orientation of the magnetic field $\vec{B}_\gamma$ and of the wave vector $\vec{k}_\gamma$ of a quantum of gamma radiation emitted by a ^{57}Fe nucleus.

Fig. 2 Intensities of the sidebands towards higher frequencies for the gamma-ray emission spectrum of ^{57}Fe nuclei under a static magnetic field B_0^h and of an oscillatory magnetic field of frequency $\omega_{rf}/\omega_e = 4$, averaged over the polarization of the gamma rays for different configurations of the radio- frequency fields. (a) The radio-frequency field is linearly polarized, $B_{rf,x}/B_0^h = 1/10$, and the direction of observation is perpendicular to the plane of the applied field, $\theta = \pi/2$, $\varphi = \pi/2$. (b) The radio-frequency field has a right circular polarization, $\alpha_{rf} = \pi/2$, and $B_{rf}/B_0^h = 1$. The spectrum is observed along the direction of the static field, $\theta = 0$. (c) The radio-frequency field has a left circular polarization, $\alpha_{rf} = \pi/2$, and $B_{rf}/B_0^h = 1$. The spectrum is observed along the direction of the static field, $\theta = 0$.

Fig. 3. Gamma-ray emission spectrum with sidebands in the case of radio-frequency collapse for ^{57}Fe nuclei in a permalloy sample for a linear polarization of the applied magnetic field for several frequencies ω_{rf} of the oscillatory field. It is assumed that the amplitude of the oscillating hyperfine field is equal to the static hyperfine field. The direction of observation is

perpendicular to a plane containing the oscillatory field. These intensities are given by

$$R^{(N)} = \left(\tfrac{1}{8}\right) J_N^2\left(\left(\omega_g - \omega_e\right)/2\omega_{rf}\right) + \left(\tfrac{1}{2}\right) J_N^2\left(\left(\omega_g + \omega_e\right)/2\omega_{rf}\right) + \left(\tfrac{3}{8}\right) J_N^2\left(\left(\omega_g + 3\omega_e\right)/2\omega_{rf}\right),$$

where J_N is the Bessel function of order N.

Fig. 4. Gamma-ray emission spectrum with sidebands in the case of radio-fequency collapse for ^{57}Fe nuclei in a permalloy sample for different configurations of the applied radio-frequency field at the frequency ω_{rf} = 61 MHz. (a) The hyperfine oscillatory field is polarized linearly and its amplitude is equal to the static hyperfine field B_S. (b) The hyperfine field is polarized linearly and its amplitude is $4B_S/\pi$. (c) The hyperfine field is a superposition of two orthogonal components of amplitude B_S, uncorrelated in phase. (d) The hyperfine field is polarized circularly, and the rotating amplitude is equal to B_S. In all cases, the direction of observation is perpendicular to a plane containing the oscillatory field.

Fig. 5. Relative first-order sideband intensity $I_{b,-}^{(L)}/I_b$ for a static magnetic field $B_0^{\prime}$ and a linearly polarized magnetic field of amplitude $B_{rf,x}$, for ^{57}Fe nuclei in iron. The relative intensity $I_{b,-}^{(L)}/I_b$ has resonances at $\omega_{rf} = \omega_e$, $\omega_{rf} = \omega_g$. The direction of observation is perpendicular to the plane of the applied field. The gamma-ray intensities are averaged over polarization.

Fig. 6. Relative first-order sideband intensity $I_{b,-}^{(CL)}/I_a$, for a static magnetic field B_0^h and a left circular polarized radio-frequency field B_{rf}, for ^{57}Fe nuclei in iron. The relative intensity $I_{b,-}^{(CL)}/I_a$ has a zero when $\omega_{rf} = 2\omega_e\omega_g/(3\omega_e + \omega_g)$, or ω_{rf} = 19.1 MHz. B_{rf} is assumed to be small compared to B_0^h.

Fig. 7. Relative first-order sideband intensities $\left|\langle g,-\tfrac{1}{2}|e,\tfrac{3}{2}\rangle_+^{(CL)}\right|^2/I_a$ (full line) and $\left|\langle g,-\tfrac{1}{2}|e,\tfrac{3}{2}\rangle_-^{(CL)}\right|^2/I_a$ (dotted line), for a static magnetic field B_0^h and a linearly polarized radio-frequency field $B_{rf,x}$ for ^{57}Fe nuclei in iron. The intensity of these sidebands are equal to zero for $\omega_{rf} = 0$.

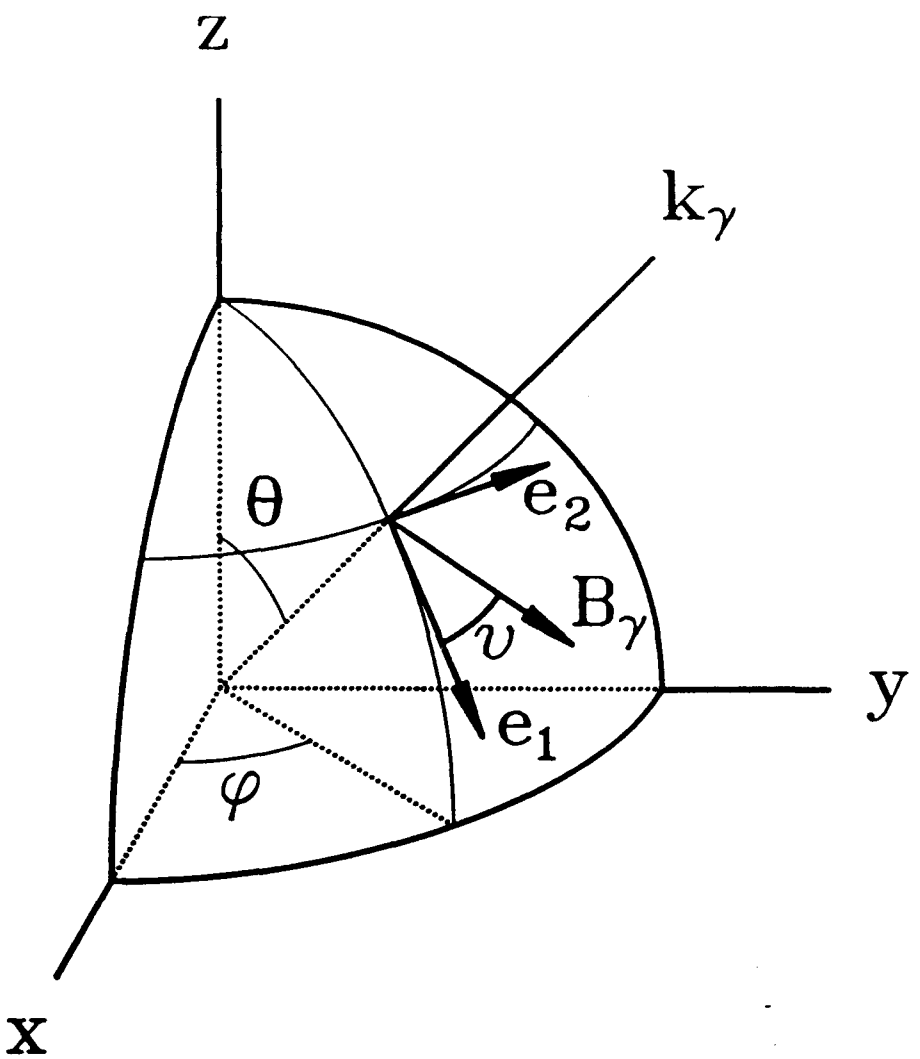
z
k_γ
θ
e_2
B_γ
υ
y
e_1
φ
x

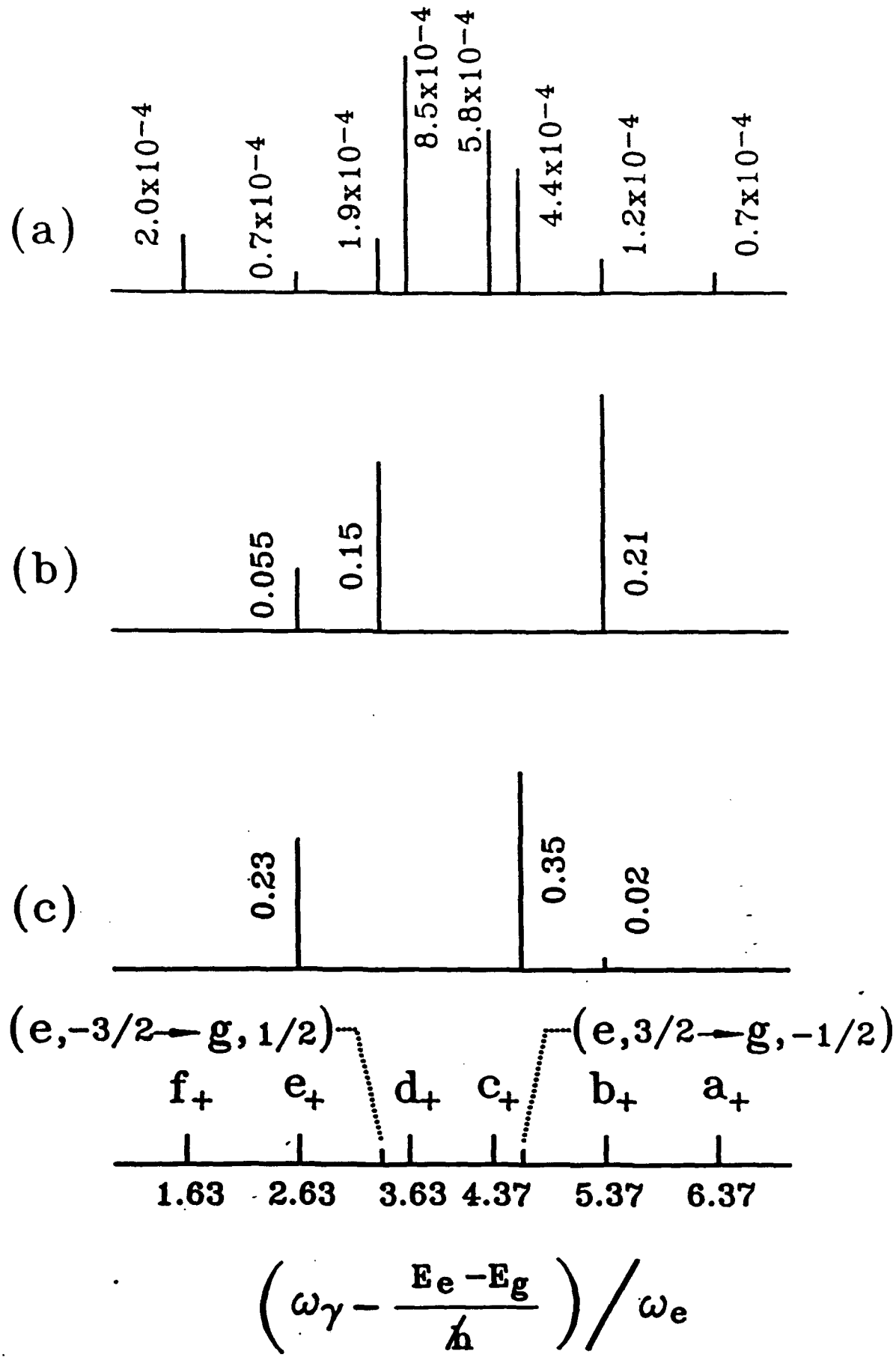
(a)
2.0x10⁻⁴
0.7x10⁻⁴
1.9x10⁻⁴
8.5x10⁻⁴
5.8x10⁻⁴
4.4x10⁻⁴
1.2x10⁻⁴
0.7x10⁻⁴
(b)
0.055
0.15
0.21
(c)
0.23
0.35
0.02
(e,-3/2→g,1/2)
(e,3/2→g,-1/2)
f+ e+ d+ c+ b+ a+
1.63 2.63 3.63 4.37 5.37 6.37
$\left(\omega_\gamma - \frac{E_e - E_g}{\hbar}\right) / \omega_e$

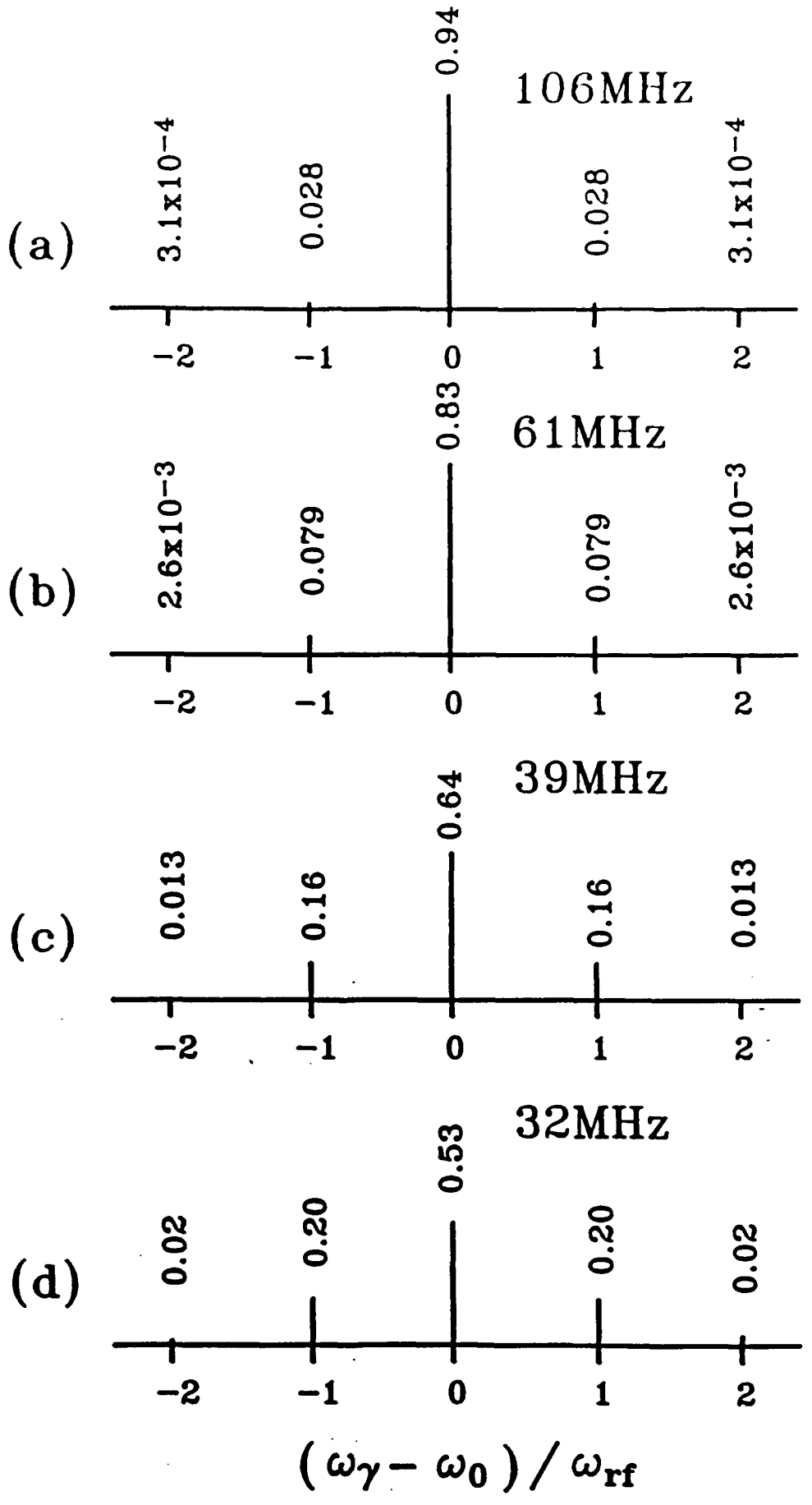
(a)
106MHz
0.94
3.1x10⁻⁴
0.028
0.028
3.1x10⁻⁴
(b)
61MHz
0.83
2.6x10⁻³
0.079
0.079
2.6x10⁻³
(c)
39MHz
0.64
0.013
0.16
0.16
0.013
(d)
32MHz
0.53
0.02
0.20
0.20
0.02
−2
−1
0
1
2
(ωγ − ω0) / ωrf

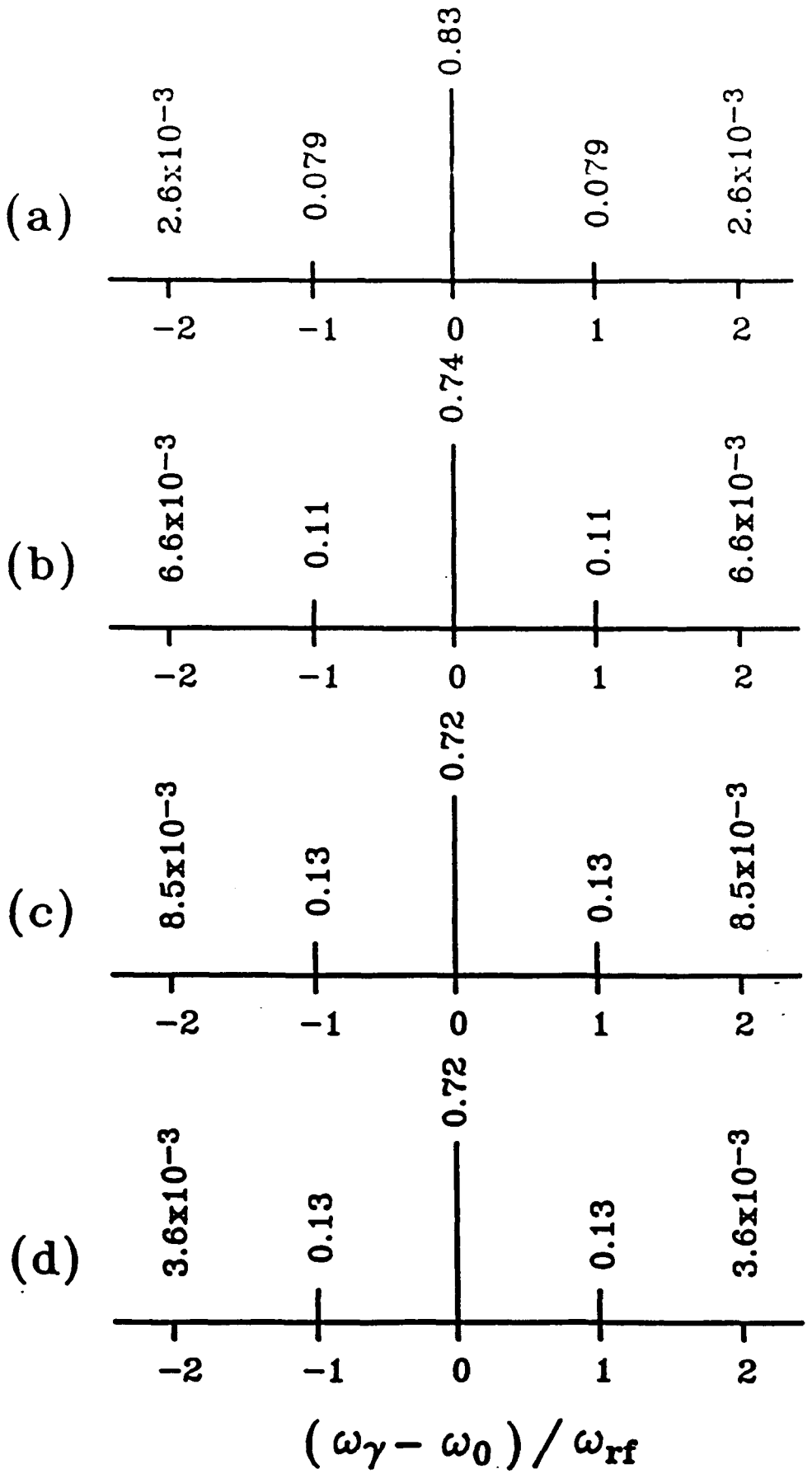
(a)
2.6x10⁻³
0.079
0.83
0.079
2.6x10⁻³
(b)
6.6x10⁻³
0.11
0.74
0.11
6.6x10⁻³
(c)
8.5x10⁻³
0.13
0.72
0.13
8.5x10⁻³
(d)
3.6x10⁻³
0.13
0.72
0.13
3.6x10⁻³
-2
-1
0
1
2
(ωγ − ω0) / ωrf

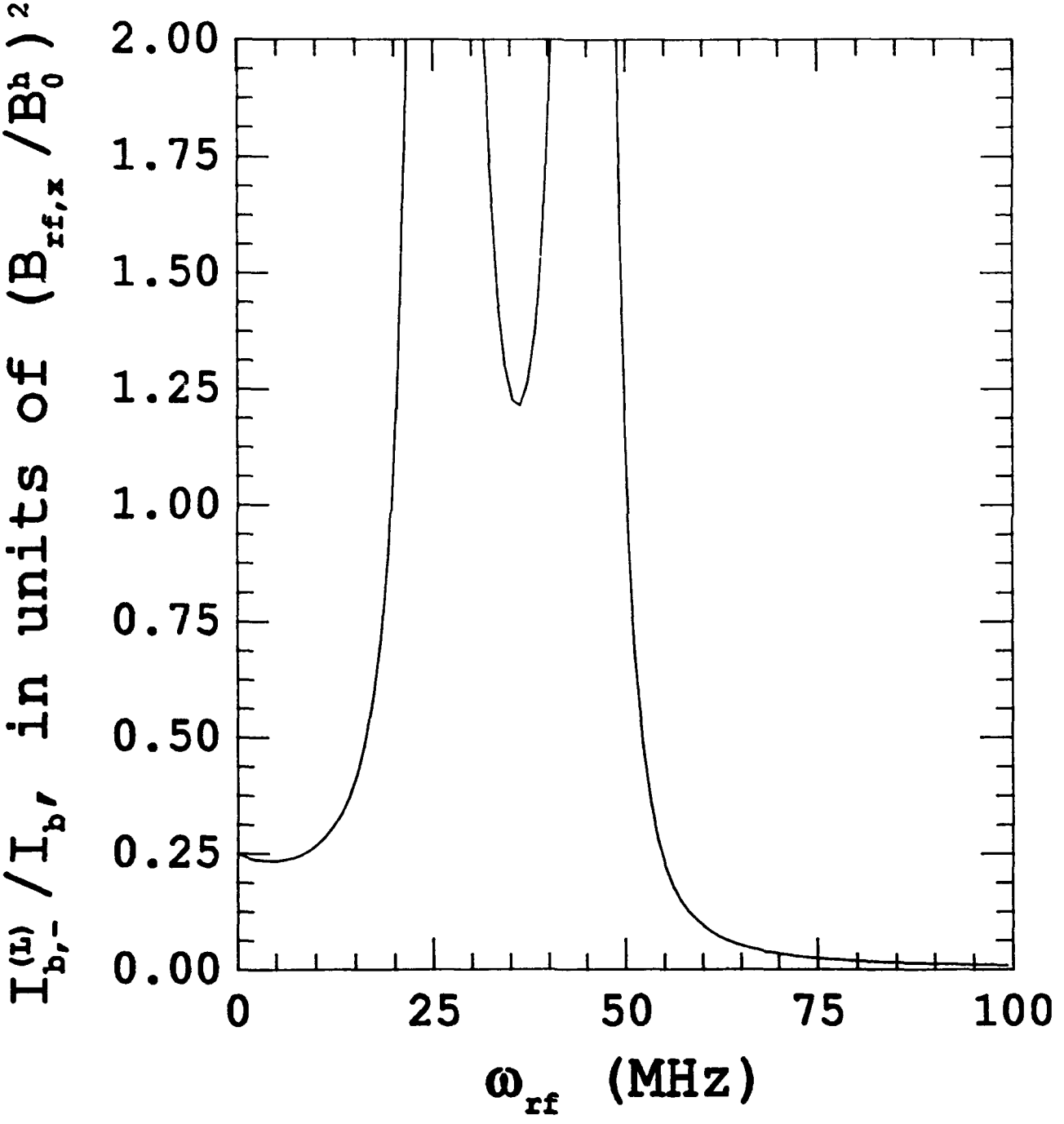
$I_{b,-}^{(1)} / I_{b,}$ in units of $(B_{rf,x} / B_0^b)^2$
2.00
1.75
1.50
1.25
1.00
0.75
0.50
0.25
0.00
0
25
50
75
100
ω_{rf} (MHz)

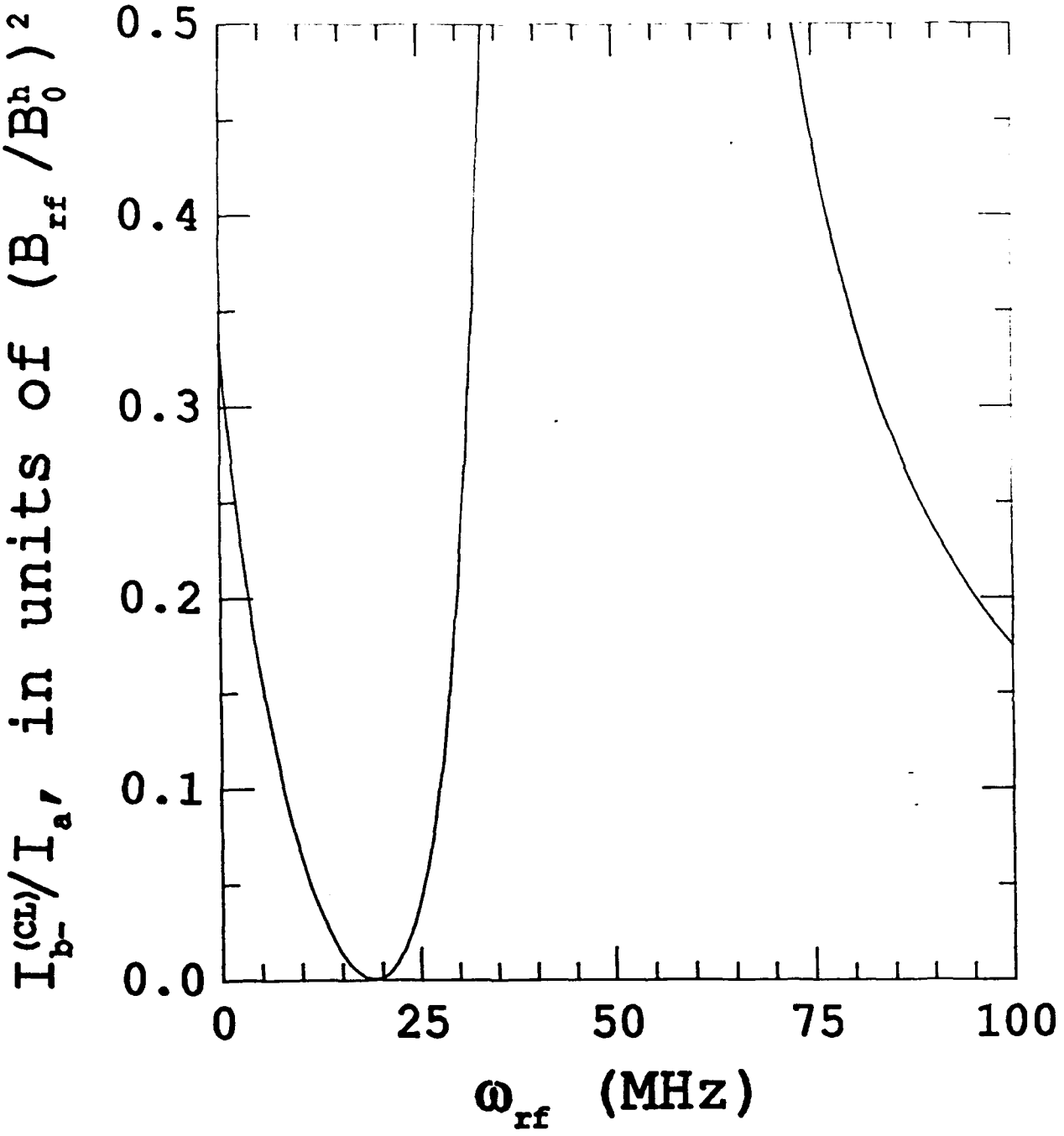
0.5
0.4
0.3
0.2
0.1
0.0
0
25
50
75
100
$I_{b-}^{(CL)}/I_{a'}$ in units of $(B_{rf}/B_0^h)^2$
ω_{rf} (MHz)

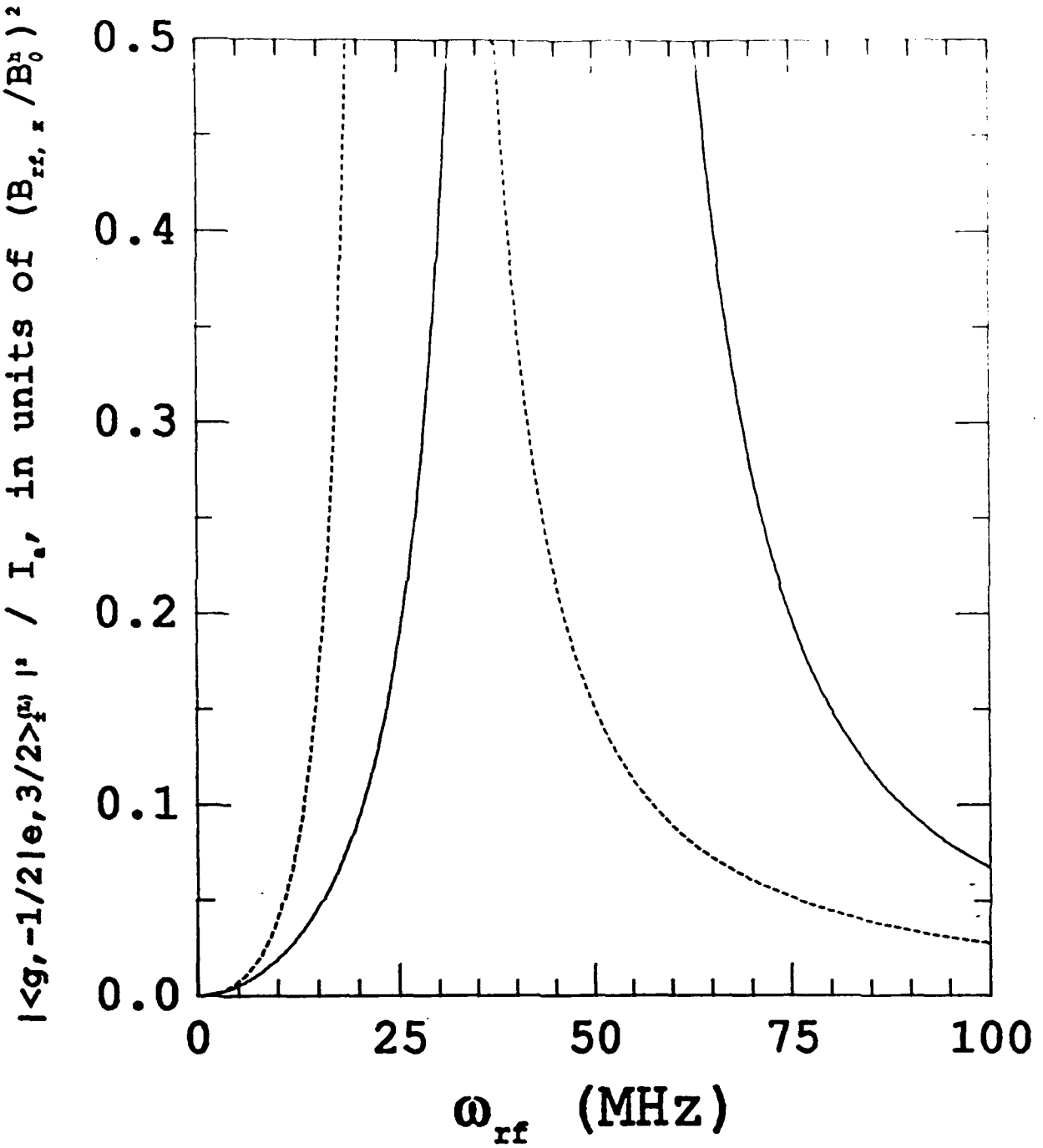
0.5
0.4
0.3
0.2
0.1
0.0
0
25
50
75
100
ω_{rf} (MHz)
$|\langle g,-1/2|e,3/2\rangle^{(1)}|^2 / I_s$, in units of $(B_{rf,x}/B_0^2)^2$

INDUCED GAMMA-RAY EMISSION AND RELATED TOPICS: RECENT STUDIES IN RUSSIA

Lev A. Rivlin
Moscow Institute of Radioengineering,
Electronics, and Automation
78 Vernadsky Prospect, Moscow 117454, Russia
Telephone and FAX: (095) 434 9317

ABSTRACT

The analysis of overall self-consistent scenarios for the process of stimulated gamma-emission is now required because of the nuclear pumping experiments demonstrated at The University of Texas at Dallas. Two separate schemes will be discussed here: (1) The stimulation of radiative transitions in beams of free isomeric nuclei without overall population inversion. The central concept is the "cooling" down of particles in the beams to the submicroKelvin range. (2) The stimulated annihilation of electrons and positrons in colliding particle and photon beams by external low-frequency radiation. Numerical estimates for both schemes are presented.

1. INTRODUCTION

The study of the problems inherent in achieving induced emission of gamma-rays began more than three decades ago and interest has frequently peaked in the intervening years. The very first maximum of effort arose in the early sixties when preliminary treatments were made independently in the USA [1,2] and in Russia [3-5].

The second peak arose in 1974. In Russia this peak was initiated by the efforts of a brilliant scientist, Professor Rem Khokhlov, the President of the Moscow State University. Unfortunately, this promising period ended in 1977, when Khokhlov, an enthusiastic mountain-climber, perished in the Pamirs range.

Today we can record a new peak of interest, perhaps the most significant in terms of experimental investigations. This period has been marked by the world's first experimental approach to one of the most important part of the problem, the pumping of populations of nuclear isomers. This has been undertaken by the group of Professor C. B. Collins from the Center for Quantum Electronics of The University of Texas at Dallas, and in collaboration with some other Institutes.[6]

Now, additional emphasis is needed upon other parts of the problem of induced gamma-ray emission that are worthy of examination. Of particular importance at this time are those which are aimed at -

* extending fundamental understanding of the stimulated boson emission, successfully applied in the optical laser physics, to a new class of quantum oscillators - nuclei and antiparticles;

* discovering ways of utilizing in modern science a new energy range of coherent photons - keV and perhaps even MeV;

* introducing into theoretical and experimental practice a new type of nuclear reactions - stimulated radiative transitions. In particular this would include stimulated radiative chain reactions, or in other words, gamma-ray lasing.

The realization of these ideas may also lead to important progress in theoretical work that could launch a new branch of science and technology, QUANTUM NUCLEONICS, as an analog and continuation of the development of Quantum Electronics.

The problems in achieving this challenging goal are very diverse and complex. The first successful experimental results mentioned above have motivated the analysis of different self-consistent scenarios for the pumping/stimulated emission process as a whole. In this context the discussion presented here will often take more the character of a task statement giving a direction for further investigations than that of a final solution for the whole problem. However, it seems that these efforts may be truly well-timed. Here two separate approaches to the problem will be discussed: stimulated radiative transitions in populations of isomeric nuclei without overall inversion, and stimulated annihilation of electrons and positrons by external low-frequency radiation.

2. CONCEPTS

2.1 Stimulated Gamma Transitions

Most proposals for a feasible system in which to observe stimulated gamma-ray emissions have as an essential condition the necessity for Mössbauer (recoilless) transitions for nuclei situated in a solid matrix. At this point it is best to review some well-known facts about such transitions. When the temperature of the crystal containing the active nuclei is high compared to the Debye temperature, the gamma-transition line is spectrally split into two lines. These are the emission line for excited nuclei and the absorption line for unexcited ones. Both lines are inhomogeneously broadened by thermal motion and other factors. If the line splitting, equal to twice the nuclear recoil energy, exceeds the inhomogeneous broadening a spectrally local nuclear population inversion may occur, even without the presence of an overall inversion of excited nuclei. Therefore, gamma-ray gain is positive but small because the ratio of the homogeneous (natural) radiative line width to the inhomogeneous width is very small. In the low temperature case the line splitting does not exist and recoilless Mössbauer emission and absorption can take place. Then the line width ratio is equal to unity but an overall inversion of excited nuclei must be present to achieve gain. Thus the gain is again small when the inversion is not sufficiently large or even negative when an inversion is absent.

Unfortunately, the fault of the solid state approach is the formation of some kind of vicious circle. In order to achieve an inversion the lifetime of the excited nuclei must be long to reduce the requirements for intense pumping. However, an unbroadened Mössbauer line of natural width can not be realized for isomers with too long lifetimes (i. e., for a lifetime exceeding one

microsecond) because of crystal structure inhomogeneity. Because of additional damage to the lattice this problem grows catastrophically under the influence of intense pumping as well as in other circumstances.

The result has been that all known attempts to use the solid state approach have so far proven unsuccessful. At this time there are wide disagreements about the further benefits of this approach. The question remains whether it is possible make use of the advantages of the physical picture mentioned above while avoiding its negative features?

A very simple alternative approach involves a departure from the necessity for a solid matrix. What will happen when an ensemble of free excited nuclei is cooled? The recoil effects together with the line splitting remain and so it is again possible to obtain a local inversion over parts of the spectral line without an overall inversion. Simultaneously the line width decreases drawing nearer to the natural homogeneous value and the gain grows.

Thus one can imagine a possible scenario based on the use of deeply cooled atomic or ion beams[7,8]. The realization of this scenario will require the following sequence of operations:

1) pumping of nuclei (i.e., by (γ,γ') reactions or by radiative neutron capture) and preparing the preliminary cooled ion or atom ensemble;

2) forming a nuclear beam and rapid supplying them from a "hot" pumping zone;

3) deep "cooling," that is to say, longitudinal monokinetization of the nuclear beam;

4) beam compression (if needed);

5) stimulated gamma-ray emission in the prepared "cold and dense" nuclear beam.

In addition all the steps must be achieved consistently with each other.

On the final step the threshold condition for amplification for gamma transitions is reached when the rate of stimulated emission exceeds that for losses due to the photoeffect and Compton scattering. The temperature dependence of this threshold value shows that deep "cooling" or monokinetization down to the submicroKelvin range is needed. In addition the maximum value of the total gain over the optimum length of a beam of spontaneously relaxing nuclei is inversely proportional to the Doppler width. For this reason deep "cooling" is also needed to increase the total gain. Therefore the beam "cooling" is the central point of this whole scenario.

To achieve this may mean the use of known and promising methods of laser light pressure that can provide an effective temperature in the nanoKelvin range, but these need to be improved in order to accommodate an enormous rise in the particle concentration. In further studies new methods to increase

the density of deeply cooled beams should be proposed and the limiting factors should be analyzed.

It may be useful to also consider some combined methods of particle monokinetization involving an electrical acceleration of ions accompanied by optical laser velocity selection. Optical pressure is not used here, but the laser light plays the role of a Maxwell's demon by accurately determining the properties of particles, whereas the electric field executes the task set by the demon. The idea is as follows[9].

Negative ions are accelerated up to some threshold velocity which considering the Doppler effect is sufficient for photodetachment of electron by a collinear optical laser beam. The resultant monokinetized neutral atoms continue to move without acceleration at the same constant velocities equal to a threshold value.

A reversed variant of this method[10] involves the compensation of the initial random spread of the particle velocities by controlling the duration of the positive ion acceleration in a static electric field. Doppler velocity discrimination is performed by frequency scanning of a laser ionizing the parent atom beam.

Another group of very simple methods[7,8] is derived from the wide experience available for radiofrequency amplifiers with low-noise electron beams. When ions are simultaneously accelerated by an electrical field, their longitudinal random velocity spread drops drastically due to the quadratic dependence of the ion kinetic energy on the velocity. For instance, a voltage of 100 kV reduces the effective longitudinal temperature from 80 Kelvin down to 1 microKelvin. Consequently the Doppler line width also decreases as considered from the longitudinal direction. Obviously the degree of beam "cooling" as a result of acceleration is not unlimited. The limitations should be studied further in the light of known theories of plasma instabilities and noise in electron beams.

The gain in induced gamma photons is proportional to the concentration of excited nuclei. So the problem of the density enhancement arises in parallel to the "cooling" problem. Leaving aside the known and useful methods of electron optics and laser assisted density enhancement let us discuss another method, the ballistic focusing of neutral particles.[8] To some extent this combines both the other approaches. A technique of electron optics is used for setting the initial conditions for the parent negative ions. Then laser photodetachment forms the ensemble of neutral atoms with almost the same unperturbed initial conditions and leads to further focusing unhindered by Coulomb repulsion.

A simple example, but by no means the best, of a way of implementing this method may involve focusing a fragment of a negative ion beam having an annular cross section within coaxial electrodes of circular cylinder geometry[8]. A pulsed radial electric field imparts to all the ions an axial velocity component. A laser beam then performs photodetachment and motion of the neutral atoms toward the axis takes place without any influence from Coulomb repulsion. This ballistic motion is accompanied by an increase in the beam density. The highest degree of density enhancement is achieved in the region of the beam

waist and depends on a small transverse random velocity components. Estimates show an expected density enhancement of 1000.

To sum up this analysis let us consider a numerical example for a hypothetical isomer with a nuclear charge of 20, a transition energy of 2.5 keV, and a lifetime of 1 microsecond. Longitudinal monokinetization by electrical acceleration up to the ion energy of 100 keV reduces the effective temperature from 4 Kelvin down to 2.5 nanoKelvin and the Doppler velocities down to 1 mm/s. Positive gain over an optimum beam length of 180 cm arises when the parent ion beam current density exceeds 1 A/cm^2 (taking into account a density enhancement factor of 1500).

This result is promising, but the concepts need further development along lines including:

* searches for possible isomers with suitable nuclear and atomic properties;

* development of efficient pumping schemes and efficient sources of metastable nuclei;

* improvement of methods of particle monokinetization and density enhancement relevant to the present problem and critical analysis of physical and technological limitations.

2.2 Stimulated Annihilation Radiation

Antimatter is the perfect source of states with negative temperature[11]. Nevertheless there are grounds for skepticism as to the feasibility of a simple, self-maintaining photon chain reaction, in other words direct annihilation lasing. It is more realistic to consider a method for initiating electron-positron annihilation in which the emission (or absorption) of one of the photons in a multiquantum event was produced from an external electromagnetic field, in particular an intense optical laser field[12,13]. This concept in the three-photon case is based on a continuous redistribution of the energy of the antiparticles between the emitted quanta, so that there is a finite probability for the emission of photons of any specific low frequency[12]. However, soft-photon stimulation of two-photon annihilation is possible only when the corresponding motions of particles and stimulating photons are such that the energy of Doppler shifted photons becomes equal to the particle rest mass energy[13]. In the case of optical stimulation this requires an inadmissibly high particle energy (approximately equal to 50 GeV).

The new scenario for inducing the annihilation of parapositronium in colliding photon and particle beams (namely, two positronium beams and two infrared photon beams moving in opposite directions) consists of three steps:

1) exciting 1s-2p transitions of moving positronium atoms by an infrared beam propagating in the opposite direction;

2) lasing in the beam of these excited atoms (2p-1s transition), the inversion being achieved as a result of a reduction of lower-state population due to spontaneous annihilation;[14] and

3) stimulating the annihilation in the opposite positronium beam by Doppler shifted photons from the moving atomic laser realized in the previous step.

The Lorentz transformations on each step leads to the resonant condition, determining the particle energy of 80 MeV and the wavelength of the external radiation source of 80 micrometers. The resulting stimulated annihilation radiation produces characteristic photon energies of 160 MeV in the forward direction and 1.6 keV in the backward direction in the laboratory frame. It should be noted that in this process the population inversion of the antiparticles is not necessary and the competitive processes of pair creation are absent, but to achieve a good experimental contrast of stimulated radiation against a spontaneous background a very high density of the positronium beams is needed (an equivalent current density of more than 10 kA/cm^2).

This work was supported in part by the Russian Foundation of Fundamental Research under grant # 93-02-3768.

REFERENCES

1. G. C. Baldwin, J. P. Neissel, J. P. Terhune and L. Tonks, Proc. IEEE, Vol. 51, 1247 (1963).
2. V. Vali and W. Vali, Proc. IEEE, Vol. 51, 182 (1963).
3. L. A. Rivlin, USSR Patent # 621265., Appl. January 10, 1961.
4. L. A. Rivlin, Vopr. Radioelectron. Ser 1, Vol. 6, 43 (1963).
5. B. V. Chirikov, Sov. Phys. JETP, Vol.17, 1355 (1963).
6. C. B. Collins, J. J. Carroll, K. N. Taylor, T. W. Sinor, C. Hong, J. D. Standifird and D. G. Richmond, *Proc. Japan-US Seminar on Physics of High Power Laser Matter Interaction,* Kyoto, Japan, 43 (1993).
7. L. Cohen, J. Quant. Spectr. Radiat. Transfer, Vol. 40, 735 (1988).
8. L. A. Rivlin, Sov. J. Quant. Electron., Vol. 22, 471 (1992).
9. L. A. Rivlin, Sov. J. Quant. Electron., Vol. 20, 564 (1990).
10. L. A. Rivlin, Sov. J. Quant. Electron., Vol. 21, 593 (1991).
11. L. A. Rivlin, Sov. J. Quant. Electron., Vol. 4 (1974).
12. L. A. Rivlin, Sov. J. Quant. Electron., Vol. 6, 1313 (1976).
13. L. A. Rivlin, Sov. J. Quant. Electron., Vol. 8, 1412 (1978).
14. M. Ya. Amusia and M. L. Shmatov, J. Phys. B, Vol. 25, L313 (1992).

THE GAMMA-RAY LASER: ISSUES AND PROGRESS IN 1993

J. J Carroll and C. B Collins
The University of Texas at Dallas, Center for Quantum Electronics
P. O. Box 830688, Richardson, Texas 75083-0688

Abstract

A gamma-ray laser would provide stimulated emission at the shortest possible wavelengths (< 1 Å) from transitions between excited nuclear states. The unique advantages provided by those transitions promise the integration of pump energy over nanosecond to microsecond times and thus to larger values than are possible with x-ray lasers which must be pumped on the order of picoseconds. However, at the end of the first cycle of study (1963 - 1981) it was concluded that a gamma-ray laser was impossible using the traditional approach to pumping nuclei with particle fluxes. Since then research has taken an entirely new character with the introduction of concepts for "optical" pumping of a gamma-ray laser, in its most straightforward form as a nuclear analog to the ruby laser. Over the past seven years the United States' main-line project at the Center for Quantum Electronics has experimentally demonstrated the components of those concepts. Computations based on the new data have shown that a gamma-ray laser is feasible if some isotope has its properties sufficiently close to the ideal. Now breakthroughs realized in the study of the systematics for the optical pumping of nuclei have permitted the identification of the first-ranked candidate nuclide for a gamma-ray laser. Problems currently being addressed are the acquisition of macroscopic samples for testing and the demonstration of appropriate instrumentation.

Introduction

Studies of the feasibility of a gamma-ray laser have been motivated by the promise of achieving stimulated emission of photons with wavelengths below 1 Å using the unique advantages presented by nuclear systems. Among these is the appearance in many nuclei of extremely long-lived excited states called isomers with energies above the ground state of keV to MeV. Populations of these metastable levels can store teraJoules per liter at solid densities for lifetimes up to thousands of years. This makes upconversion possible since it would not be necessary to provide all the energy for a gamma-ray laser in situ. Even more important, electromagnetic transitions in nuclei provide a variety of transition moments, the most common being the magnetic dipole, in contrast to electric dipole transitions which dominate our usual experience with lasing transitions. Thus the matrix element linking spontaneous lifetime with the usual ν^3 factor is orders-of-magnitude more favorable for output transitions of a gamma-ray laser than might otherwise be expected at such short wavelengths. Populations can be transferred from isomeric storage states to lasing levels having lifetimes ranging from nanoseconds to microseconds, integrating the energy in a pump pulse for much longer times than for x-ray lasers. Also, gamma-ray transitions routinely have natural line widths, as in the Mössbauer effect, insuring large cross sections for stimulated emission. Without broadening, values for 1 Å nuclear transitions typically exceed the cross section for the stimulation of Nd in YAG.

Despite this impetus, there was little real progress towards a gamma-ray laser prior to 1982 as a result of a concentration of research on the traditional approach to pumping nuclei with intense particle fluxes. As discussed in the encyclopedic review of Baldwin, et al.,[1] the general impossibility of those schemes was concluded since particle fluxes would deposit unmanageable amounts of heat in the host matrix, destroying the Mössbauer effect. That review effectively signaled the end to the traditional approach to a gamma-ray laser and emphasized that the critical test for any new approach must be the efficacy of pumping to release the energy stored in isomers while maintaining a natural line width for the lasing transition.

A new interdisciplinary approach[2] to a gamma-ray laser emerged in 1982 following precursive work[3-9] that appeared near the end of the first cycle of research but which were largely ignored. The basic concepts called for the "optical" pumping of nuclei by the absorption of photons from intense coherent or incoherent fields. Coherent optical pumping would use multiphoton processes to release the energy stored in nuclear isomers into freely-radiating levels located nearby in energy. Incoherent pumping would employ intense pulses of x rays to pump nuclei as in a direct analog to the ruby laser. In either case, the use of photons as the pump entity would allow the preservation of the Mössbauer effect for nuclei within a thin film host of low-Z material like carbon or beryllium.

The blueprint for a gamma-ray laser now appears in the textbooks,[10] and research following this approach at the Center for Quantum Electronics has been rich with achievement. The fundamental concepts of coherent pumping have been demonstrated[11-13] but not surprisingly the greatest rate of progress has been realized in the direction of incoherent pumping.[14-25] Major breakthroughs have been experimentally demonstrated in the pumping and dumping of populations of nuclear isomers with x rays.

The greatest impediment to a gamma-ray laser has remained the lack of materials. Of the 1886 distinguishable[26,27] isotopes, 29 had been identified as first-class candidates but only the two poorest, ^{180}Ta and ^{123}Te were available in sufficient amounts for testing. Still the discovery of resonances with giant cross sections for optically pumping those nuclides[18-20] strengthened the feasibility of a gamma-ray laser by orders-of-magnitude. Without further materials for study, research has concentrated on the systematics for pumping simulation isomers from their ground states[21-25] to aid in ranking the candidates and to motivate production of the best nuclides. The findings have now made it possible to identify the 31-year isomer of the nuclide ^{178}Hf as the first-ranked candidate for a gamma-ray laser.

Background

Pump Model

The critical key to the development of the ruby laser was the identification and exploitation of a bandwidth funnel in which a broad absorption band was linked through efficient cascading to a narrow laser level. Likewise this is an essential element in the nuclear analog to the ruby laser depicted in Fig. 1. The principal figure of merit for populating an upper-laser (or fluorescence) level is the integrated cross section, $(\sigma\Gamma) = \pi b_a b_o \sigma_0 \Gamma/2$, whether the initial state is the ground state or an isomer. The figure shows only one pump band, sometimes called a gateway or intermediate state, but there could be more at higher excitation energies. The probabilities that the gateway will decay in one step back to the initial level and in any cascade to the laser level are b_a and b_o, respectively. These quantities together with the natural width of the absorption band, Γ give the useful, partial width $b_a b_o \Gamma$ for the transfer of population from initial to fluorescence states. The cross section for the absorption step, σ_0 is given by the Breit-Wigner formula

$$\sigma_0 = \frac{\lambda^2}{2\pi} \frac{2I_j + 1}{2I_g + 1} \frac{1}{\alpha_p + 1} \quad , \tag{1}$$

where λ is the wavelength of the pump photon, I_j and I_g are the angular momenta of the intermediate and ground states, respectively, and α_p is the internal conversion coefficient corresponding to the pump transition. The cross section for useful absorption of pump energy by nuclei is much larger for photons than for particles of the same energy.

In the context of nuclear physics, optical pumping processes like that of Fig. 1 have been known for more than 50 years.[28] They are commonly designated as (γ,γ') reactions with γ and γ' referring to the incident and scattered photons, respectively. Typical values of integrated cross section for these reactions have been known to range[14-17,29] from 1's to 10's in the "usual units" adopted here, uu. $\equiv 10^{-29}$ cm^2 keV. However, until the past decade studies of these processes never reached the level of precision seen in research using particle reactions due to the difficulty in accurately calibrating the output spectra of the intense photon sources required. In particular the most difficult to characterize sources of x rays proved to be radionuclides for which all intensity away from the spectral lines resulted from environmentally sensitive Compton scattering. Little quantitative agreement could be found in the literature between integrated cross sections obtained in different experiments and as late as 1987 there were serious contentions[30] over the mechanism by which these reactions occurred. However, in recent years extensive experiments based on new technology and computer codes for the simulation of x-ray spectra have resolved this controversy and the basic model for the optical pumping reaction shown in Fig. 1 is now on a firm quantitative basis. This was one of the earliest challenges to the gamma-ray laser project.

When a population of nuclei, N_i in some initial state is irradiated with a continuum of photons extending up to a maximum "endpoint" energy, E_0, the time-integrated yield of final-state nuclei, N_f is given by

$$N_f = N_i \Phi_0 \int_0^{E_0} \sigma(E)\, F(E,E_0)\, dE \quad , \tag{2}$$

where Φ_0 is the total incident fluence and $F(E,E_0)$ is the distribution of energies within the continuum for the given endpoint. The initial-to-final state transfer is represented by the energy-dependent cross section, $\sigma(E)$. It is well-known that (γ,γ') reactions for incident photon energies below the threshold for photoneutron production resonantly excite discrete states like that shown in Fig. 1. Each resonance is described by a Lorentzian line shape with a width which may be large on the nuclear scale, but is narrow compared to the structure of most incident photon continua. Furthermore, if gateways are well-spaced compared to their widths, Eq. 2 becomes

$$A_f(E_0) \equiv \frac{N_f}{N_i \Phi_0} = \sum_j (\sigma\Gamma)_j F(E_j,E_0) \quad , \tag{3}$$

in which the amount of final-state population has been expressed as a fractional yield, or activation, per unit photon fluence, $A_f(E_0)$. The $(\sigma\Gamma)_j$ is the cross section for population of the final state through the j^{th} gateway, integrated over the Lorentzian line shape, and the summation includes all pump bands with excitation energies $E_j < E_0$.

Experimental Confirmation

The model of Eq. 3 was validated by experiments using bremsstrahlung from six different accelerators. These devices included two nuclear simulators, DNA/PITHON and DNA/Aurora, two medical linacs and two research linacs, the injector to the superconducting Darmstadt linear accelerator (S-DALINAC) and the Texas X at the Center for Quantum Electronics. Gram-sized samples containing the few calibration isomers whose gateways were well-known from the literature were exposed for times ranging from seconds to hours for the cw machines and to single flashes from the pulsed-power devices. The yields of isomers produced by each irradiation were obtained from the fluorescence detected after transferring the samples to a quieter environment. Standard corrections were made for the isotopic abundance, isomer lifetime, detection and emission efficiencies, and transparency of the samples to the fluorescence. Photon spectra were calculated with

the EGS4 electron/photon transport code[31] which was adapted for each experiment to give both Φ_0 and $F(E,E_0)$. In some cases Φ_0 was verified by in-line dosimetry

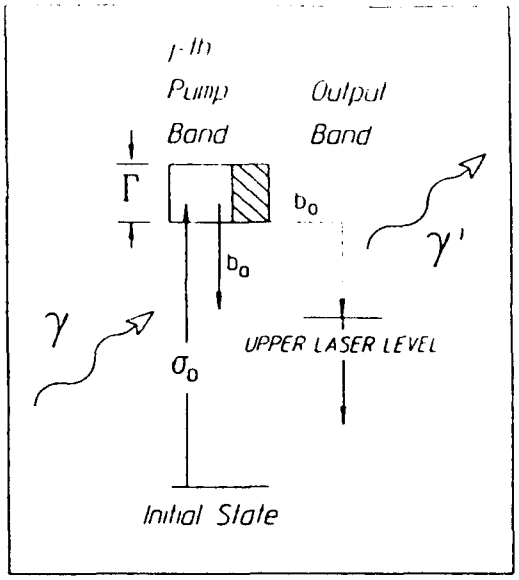

Figure 1: Schematic representation of the bandwidth funneling of population to a laser level through a gateway state with natural width, Γ. The incident photon γ is absorbed with a cross section σ_0 from the initial level which may be either the ground state or an isomer. The cascade from gateway to laser level is shown by the dotted line with promptly emitted photons being the γ'. Only one gateway is shown but there could be more.

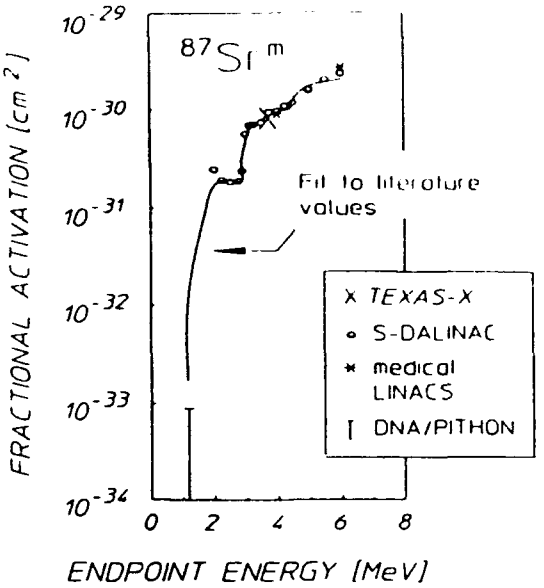

Figure 2: Fractional activation, A_f for the reaction $^{87}Sr(\gamma,\gamma')^{87}Sr^m$ as a function of bremsstrahlung endpoint, E_0 obtained with 5 different accelerators. The solid curve plots values computed from Eq. 3 using gateway parameters found in the literature and calculated photon spectra. The agreement of these values with the measurements was excellent, validating the procedures.

The results of those experiments[14-17,19] were in excellent agreement with the predictions of Eq. 3 using literature values[26,27,29] for gateway energies and integrated cross sections. A typical example is given in Fig. 2 which shows a composite excitation function obtained for the calibration isomer $^{87}Sr^m$ using five of the accelerators.[19,21] It is important to note that at an endpoint of 4 MeV, the yield of the $^{87}Sr^m$ isomer was enhanced 16 orders-of-magnitude by the process shown in Fig. 1 over that which could have been produced by direct excitation of the metastable level from the ground state. This is bandwidth funneling at the nuclear level.

Those experiments established that there could no longer be any reasonable doubt of the model or the procedures for quantitatively measuring nuclear fluorescence efficiencies using bremsstrahlung. In addition they led to the development of a new method[32] for providing absolute characterizations of intense x-ray fields using isomeric photoexcitation reactions. The model was then used to examine candidate nuclei for a gamma-ray laser.

Candidates and Simulations

Candidate Structure

Many of the candidate isotopes for a gamma-ray laser are deformed nuclei whose energy levels are built upon rotational bands like those of diatomic molecules. For a spheroidal nucleus an additional quantum, K must be conserved which is the projection of the total angular momentum, J on the major axis of nuclear symmetry. Within each band the resulting system of energy levels follows

$$E_n(K,J) = E_n(K) + B_n J(J+1) \quad , \tag{4}$$

where $J \geq K \geq 0$, and $J = K, K+1, K+2, \ldots$ for $K \neq 0$ and $J = K, K+2, K+4, \ldots$ for $K = 0$. The B_n is a constant and $E_n(K)$ is the energy of the lowest-lying level in the band, the "bandhead." Other quantum numbers are identified by n. The selection rules for electromagnetic transitions require $|\Delta J| < M$ and $|\Delta K| < M$ where M is the multipolarity of the radiation.

Deformed nuclei possess the longest-lived isomeric levels because those states lie in bands whose K differs greatly from that of freely-radiating states to which they could energetically decay. Such isomers would be ideal as storage levels in an upconversion scheme since most of the energy is already in the nucleus, reducing trigger requirements. Of the 1886 distinguishable nuclear isotopes, 29 first-class candidate nuclides were identified by a search of the nuclear data base in 1986, but an exact ranking could not be determined due to the paucity of nuclear fluorescence data.

Giant Pumping Resonances

Although attractive from the perspective of shelf life and availability, the nuclide ^{180}Ta was nevertheless ranked among the poorest candidates since its isomer stores only 75 keV and requires $\Delta K = 8$ for transitions to the ground-state band.[26,27] A bandwidth funnel would also have to span a similar ΔK and theoretical estimates of the integrated cross section for the pumping were expected to be small, perhaps 10^{15} uu. Still, this isotope exists naturally in 100 % inversion since its isomer has a lifetime in excess of 10^{12} years while its ground state has a halflife against transmutation of only 8.1 hours. A macroscopic sample was readily available so ^{180}Ta^{m} was the first candidate tested.

An experiment was conducted[18] in 1987 in which 1.2 mg of ^{180}Ta^{m} was irradiated with bremsstrahlung from a 6 MeV medical linac and a large fluorescence yield was observed following the exposure. That was the first experimental demonstration that the energy stored in a nuclear isomer could be dumped to freely-radiating states as needed for a gamma-ray laser. Simply the observation of any fluorescence from a milligram-sized target when grams of material were needed for the calibration isotopes showed an unexpected efficiency for the process. Analysis of the data indicated that the partial width for the dumping of the ^{180}Ta^{m} population was about 0.5 eV with an integrated cross section on the order of 42,000 uu.

The energies of the pump levels were determined from the excitation function of Fig. 3 measured by a series of irradiations[19] using the variable-energy S-DALINAC. As was the case for the calibration isomer ^{87}Sr^{m}, sharp increases in the normalized yield, called activation edges, indicated those energies. Computed photon spectra were used with Eq. 3 to iteratively fit the measurements by using trial values for the integrated cross sections. The lowest-lying pump band was located at 2.8 MeV and with an integrated cross section of 12,000 uu. It was classified as a "giant pumping resonance" compared to usual (γ,γ') reactions. The demonstration that populations of nuclear isomers can be dumped by x rays with much larger integrated cross sections than could have been expected stood as the first major breakthrough towards a gamma-ray laser, enhancing its feasibility by at least four orders-of-magnitude.

Systematics

Giant pumping resonances were also observed[20] for the second poorest candidate, ^{123}Te. However, better candidates were not available in sufficient amounts for testing so research focused on the pumping of simulation isomers to study the systematics of their gateways. A preliminary survey[21] of 19 isomeric nuclei was conducted over a coarse mesh of bremsstrahlung endpoints using the nuclear simulators and the medical linacs. As shown in Fig. 4, giant pumping resonances were indicated for nuclei in a region of masses near A = 180, where the most deformed candidates lie. A refined survey[22] performed with the S-DALINAC found the gateway locations and integrated cross sections for four isotopes neighboring ^{180}Ta that had various degrees of ground-state deformation. The results are also given in Fig. 4 and indicate that both the excitation energies and integrated cross sections for the pump levels vary slowly amongst neighboring nuclides within each mass island, despite dissimilar single-particle structures. The strengths of those giant pumping resonances were correlated[22] with the ground-state deformation, a nuclear core property.

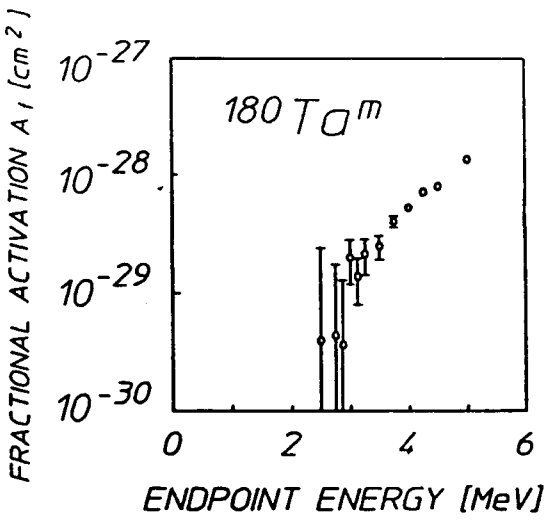

Figure 3: Fractional activation, A_f for the reaction ^{180}Ta$^{m}(\gamma,\gamma')^{180}$Ta as a function of bremsstrahlung endpoint, E_0 obtained with the S-DALINAC. Gateway parameters were determined by fitting the measured excitation function using Eq. 3 with trial values for the $(\sigma\Gamma)_j$. The integrated cross sections were found to be 10^4 larger than those usually measured for (γ,γ') reactions. These data demonstrate the dumping of an isomeric population with x rays.

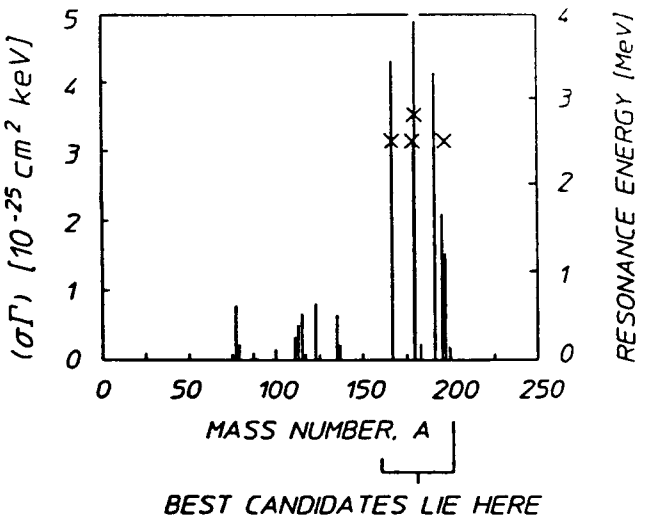

Figure 4: Systematics for excitation energies and integrated cross sections of gateway states providing optical pumping of nuclear isomers. The groupings correspond to mass islands between magic numbers for neutrons and protons. The best candidates for a gamma-ray laser lie in the mass-180 island where the largest values of $(\sigma\Gamma)_j$ are found. Within each island the integrated cross sections and excitation energies, plotted by the right-hand ordinate and the X symbols, vary slowly with changing mass number, A. This is a sign of the core nature of the giant pumping resonances.

The systematics for optically pumping nuclear states were further investigated for the excitation of laser-like levels with lifetimes on the order of tens of μs. To accomplish this an experimental technique was developed[33] which employed a gated CsF scintillator to detect fluorescence from samples irradiated with the pulsed Texas X linac. The PMT was gated off during the x-ray pulses to prevent the system from being blinded by real-time Compton scattering from the sample and the environment. A total of four additional nuclei were studied using that technique, ^{81}Br, ^{176}Hf, ^{181}Ta and ^{201}Hg. Figure 5 shows a typical decay spectrum for ^{181}Ta obtained with a time-to-amplitude converter (TAC) and was collected over 7 x 10^5 cycles (linac pulses). Fluorescence was detected at energies of 133, 345, 476 and 482 keV from the decay of a level at 615 keV and the agreement between the measured halflife and the literature value[26] of 18 μs was excellent. The data analysis[33] for all four nuclides indicated that the integrated cross sections for optically pumping laser-like levels were comparable to those previously found for the population of long-lived isomers, as shown in Fig. 6.

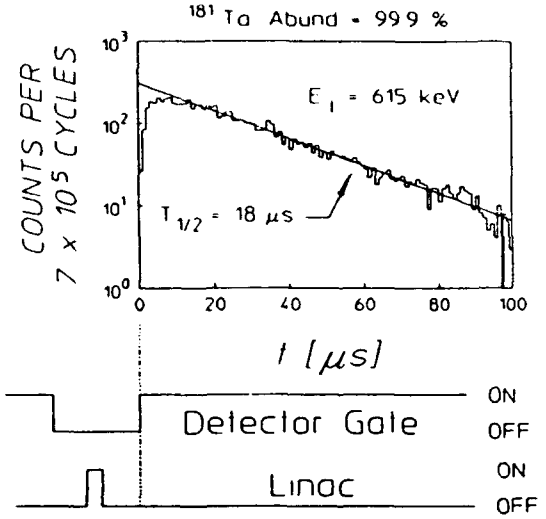

Figure 5: Fluorescence detected from the 18 μs, 615 keV level in ^{181}Ta following its excitation by bremsstrahlung from the Texas X. These data were collected for nearly 10^6 cycles (linac pulses) using a recently developed gated CsF detector system. The PMT was gated off during each x-ray pulse and then returned rapidly to a stable gain to observe fluorescence from the sample.

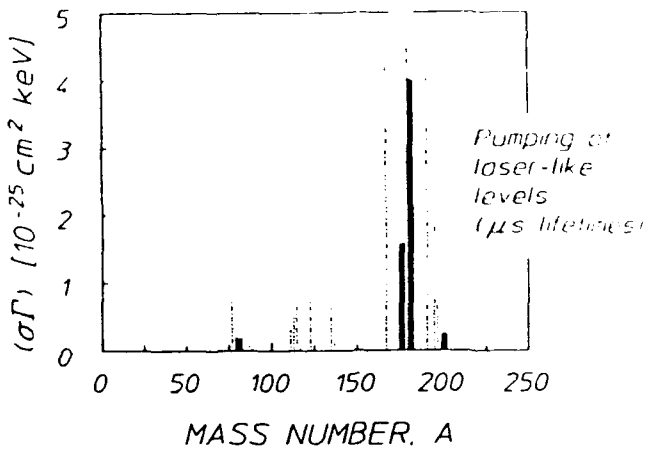

Figure 6: Integrated cross sections for pumping laser-like levels along with those of Fig. 4 for the pumping of long-lived isomers (shown by the dotted lines). Again, the groupings correspond to mass islands between magic numbers and the best candidates are identified as neighbors of the nuclide ^{180}Ta.

NRF Measurements

The discovery of giant optical pumping resonances significantly improved the feasibility of a gamma-ray laser by lowering pump requirements. However, the resolution of those experiments only permitted gateways to be located within ± 0.1 MeV. This left open the possibility that the reaction strength might not be concentrated in a few transitions, but might be spread over a great number of closely spaced levels. If this were the case the cross section for each participating state could be small, seriously degrading the ratio of useful, resonant absorption to that absorbed nonresonantly and contributing to heating of the sample. This was of particular concern for the nuclei favored in Figs. 4 and 6 which have large excited-state densities, and even more so for ^{180}Ta which is a rare odd-odd nucleus. A series of experiments was performed to explore this possibility.

Isomeric excitation functions like that shown in Figs. 2 and 3 reflect only one specific exit channel for the pumping process depicted in Fig. 1. That channel consists of a decay cascade leading to the metastable level following an absorption event in a transition from the ground state to a gateway. However, a complimentary exit channel corresponds to direct decay of the gateway back to the ground state, with the prompt emission of "elastic" photons of the same energy as those absorbed. It can be seen from Fig. 1 that in the event of a large $(\sigma\Gamma)_j$ for the population of an isomer, there must also be a large integrated cross section for the elastic channel, $(\sigma\Gamma)_{el} = \pi b_a^2 \sigma_0 \Gamma/2$. The square of the branching ratio from gateway to ground state occurs because the entrance and exit channels are the same. This integrated cross section can be determined by measuring the energies and numbers of photons scattered in real time during an irradiation. The observation of those photons in the presence of Compton background forms the basis of nuclear resonance fluorescence (NRF) experiments.

An experimental arrangement designed for NRF was used to investigate[23,24] the pumping of two isomers, ^{89}Y^m and ^{115}In^m which have large natural isotopic abundances. Gram-sized samples were sandwiched between aluminum and boron calibration targets and were irradiated with well-collimated bremsstrahlung from the S-DALINAC. Photons elastically scattered by strong transitions were detected with carefully shielded germanium detectors placed off-axis and appeared in pulse-height spectra as peaks superimposed on a large Compton continuum. Isomeric excitation functions were also measured for these nuclides. Detailed spectra are available in the literature[23,24] but the relevant point is that only a few strong elastic transitions were detected in the NRF measurements over the energy range from 1.5 to 4.5 MeV and these were only found within the experimental resolution of their pumping resonances. In the case of ^{115}In, these were located at 2.8 ± 0.1 MeV and 3.3 ± 0.1 MeV, as shown in Fig. 7. Thus a subset of those few transitions corresponded to the gateways responsible for the

optical pumping of the isomer. That conclusion was confirmed qualitatively by unified-model calculations which showed that the absorption strength was concentrated into a small number of E1 or E2 transitions with excitation energies near those found experimentally.

K Mixing - A Speculation

The surprising magnitudes of integrated cross sections for getaways in the mass-180 region indicate an ease in pumping and dumping isomers through large ΔK that is difficult to interpret in terms of a single-particle model. Levels capable of strong "K breaking" or "K mixing" have also been recently observed for other nuclei[34] in which electric dipole transitions to levels near 2.5 MeV were found to be enhanced despite substantial change in K. Most striking was the measurement[35] of a level at 2.65 MeV which provides ΔK = 14 in the spontaneous decay of the 3.312 MeV, 3.7 μs isomer of ^{174}Hf. That K-mixing state is remarkably close to the gateway at 2.8 ± 0.1 MeV discovered for the dumping of ^{180}Ta^{m}. A full understanding of this pervasive behavior is not yet available, but there is a suggestive speculation.

Calculations[36] have confirmed that some nuclides develop multiple minima in nuclear potential as a function of core deformation. Second minima can contain fission isomers for higher masses, but for lighter nuclei the Coulomb barrier prevents fission. Shape isomers result when states bound within a second well cannot easily decay to freely-radiating states of significantly different nuclear shape corresponding to the primary well. If instead of a second minimum a plateau occurs in the potential energy, as depicted in Fig. 8, shape isomers could not occur. However, within the narrow band of energies shown excited states would not correspond to a fixed core deformation. Thus K would not be a good quantum number for such levels and unhindered, low-multipolarity transitions could connect them to states with widely differing K values. This would provide the large degree of K-mixing observed experimentally. It is interesting to note that shape isomers, and therefore second minima, are predicted to lie at excitation energies of 2 to 3 MeV.

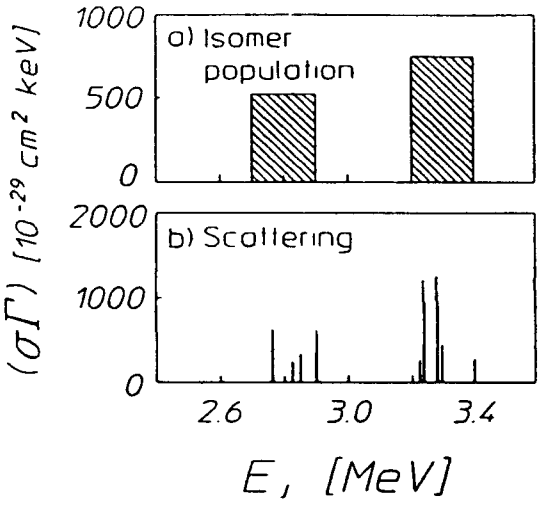

Figure 7: Schematic representing integrated cross sections for a) population of the isomer ^{115}In^{m} obtained from a measured excitation function and for b) elastic scattering by absorption transitions obtained from NRF measurements. Gateway locations of a) were determined within ± 0.1 MeV and strong elastic scattering levels were only observed within those bands. Thus a subset of the transitions of b) are responsible for the population of the isomer as confirmed by unified model calculations.

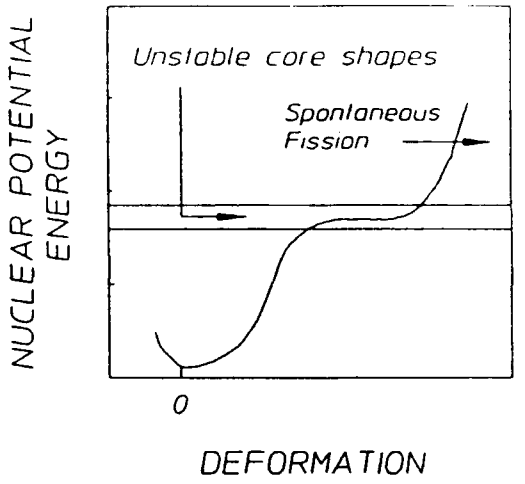

Figure 8: Schematic representation of a dependence of potential energy upon nuclear deformation that would tend to produce a second local minimum. Shape isomers have been predicted to lie in auxiliary minima and for large enough mass numbers spontaneous fission can occur when populations tunnel out of a secondary well. Here a plateau rather than a well-developed local minimum is shown.

The First-Ranked Candidate

The studies of the systematics for optically pumping isomers conducted over the past six years have yielded the following conclusions:

1) Nuclear populations trapped in long-lived storage isomers can be optically pumped to freely-radiating states with x rays,
2) Optical pumping reactions for the deexcitation or excitation of nuclear isomers (and laser-like levels) occur resonantly by bandwidth funneling through a small number of gateway states,
3) Gateways lying in the mass-180 island are giant pumping resonances and can break K with integrated cross sections on the order of 10,000 um. compared with 1 to 10 um. as is usually found for (γ,γ') reactions, and
4) Within the mass-180 island, the magnitudes of the integrated cross sections vary slowly among neighboring nuclides; the excitation energy for the first giant pumping resonance is between 2.6 and 2.8 MeV.

On this basis the 31-year isomer ^{178}Hf^{m2} has been identified as the first-ranked candidate for a gamma-ray laser from the perspective of triggering. As can be seen in the energy-level diagram of Fig. 9, the metastable level stores 2.45 MeV, one of the highest-lying isomers known[26] that does not exceed the energy of a K-breaking gateway. The 31-year halflife of the isomer results from its being the head of a band

with K = 16. It must first decay by a severely hindered E3 transition to the J = 13⁺ member of the K = 8 band. This ΔK = 8 transition is followed by a cascade that ends on the J = 8⁻ isomer ($^{178}Hf^{m1}$) which decays with a halflife of 4.0 s to the ground-state band.

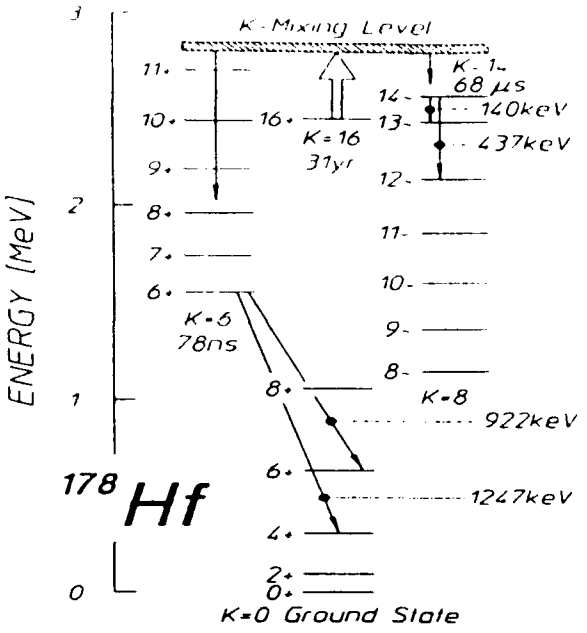

Figure 9: Energy level diagram of the nuclide ^{178}Hf. The 31-year isomer stores 2.45 MeV and forms the head of a band with K = 16. The natural decay occurs through the K = 8 and K = 0 bands and cannot excite either the higher-lying K = 14 bandhead with a lifetime of 68 μs or members of the K = 6 band on the left-hand side whose bandhead has a halflife of 78 ns. A K-mixing gateway level inferred from systematics is shown near 2.8 MeV and could populate those laser-like states.

The hatched level in the figure indicates a giant pumping resonance whose position is inferred from systematics. This assignment is also supported by recent Coulomb scattering measurements[37] which identified a level at an excitation energy of 353 keV above the isomer and which could not exclude other levels lying even closer. The gateway could be reached by the absorption of a pump photon of less than 500 keV, shown by the large upward arrow in the figure. Due to the λ^2 dependence for the pump step shown in Eq. 1, this reduced photon energy may enhance the integrated cross section by a factor of nearly 50 over that observed in ^{180}Ta. The presence of two possible output channels, one through the K = 14 band and the other through the K = 6 band, greatly increases the probability of success. Pragmatically, the lifetimes of both laser-like levels are well-suited to the typical output durations of nanoseconds to microseconds of pulsed-power devices likely for use in optically pumping a gamma-ray laser.

Decay from the gateway to the K = 14 band would require only ΔK = 2 and would populate the bandhead having a halflife of 68 μs. Observation of this event following the irradiation of a sample would require the detection of 140 keV photons, as shown in the figure. This energy, as well as the 68 μs halflife, is already well within the present capabilities of the CsF scintillator system.

In the event of a stronger degree of K mixing, the K = 6 bandhead with a halflife of 78 ns could be reached. Requiring ΔK = 8, this is no larger than that transferred through the gateway in the dumping of $^{180}Ta^{m}$ and less than that observed in the decay of $^{174}Hf^{m}$. It is expected that the next generation gated detection system will allow measurements on a time scale approaching the 78 ns halflife. In addition, the fluorescence signatures are at the relatively high energies of 922 keV and 1247 keV. Those are particularly convenient energies for detection if bremsstrahlung with a lower endpoint is used to pump the sample.

Unfortunately, from the viewpoint of availability $^{178}Hf^{m2}$ is far inferior to $^{180}Ta^{m}$. While $^{180}Ta^{m}$ exists at 0.012 % of all tantalum and can be prepared simply by mass separation, the 31-year isomer of ^{178}Hf must be prepared by nuclear reactions such as spallation or α bombardment. At present the entire world inventory of $^{178}Hf^{m2}$ appears to be about 10^{15} nuclei. Procurement of a sample sufficient for testing remains a problem being addressed.

Conclusions

The discovery of giant K-breaking resonances for pumping and dumping nuclear populations and the development of new technology have enhanced the feasibility of a gamma-ray laser by orders-of-magnitude over that projected in the blueprint of 1982. All of the component concepts have now been demonstrated experimentally, and a recent model[38,39] supported by the new data indicated that there is a significant region in parameter space for which a nuclear system can be optically pumped to threshold without the need to melt a low-Z host lattice. In addition simulation hosts have been created by implanting isotopically pure nuclei of ^{57}Fe into a thin diamond film produced using well-established technology.[40] ***At this time here are no a priori obstacles to the realization of a gamma-ray laser.*** However, exact pump requirements depend sensitively on the structure of the actual isotope and the feasibility of a gamma-ray laser cannot yet be determined. Research by the United States' main-line project has now identified the 31-year isomer of ^{178}Hf as the first-ranked candidate and procurement is currently being pursued. Testing is planned for the coming year.

Acknowledgments

The authors wish to acknowledge the contributions of Dr. C. Hong, Dr. T. W. Sinor and Dr. K. N. Taylor of the Center for Quantum Electronics, N. Huxel, Prof. Dr. A. Richter and Dr. P. von Neumann-Cosel of the Institut für Kernphysik, Technische Hochschule Darmstadt, and Prof. S. A. Karamian and Prof. Yu. Ts. Oganessian of the Flerov Laboratory of Nuclear Reactions, Joint Institute for Nuclear Research, Dubna. This work was supported by SDIO/TNI through NRL.

References

1. G. C. Baldwin, J. C. Solem and V. I. Goldanskii, Rev. Mod. Phys. 53, 687 (1981).
2. C. B. Collins, F. W. Lee, D. M. Shemwell, B. D. DePaola, S. Olariu and I. Popescu, J. Appl. Phys. 53, 4645 (1982).
3. V. S. Letokhov, Sov. J. Quant. Electron. 3, 360 (1974).
4. B. Arad, S. Eleizer and Y. Paiss, Phys. Lett. 74A, 395 (1979).
5. C. B. Collins, S. Olariu, M. Petrascu and I. Popescu, Phys. Rev. Lett. 42, 1397 (1979).
6. C. B. Collins, S. Olariu, M. Petrascu and I. Popescu, Phys. Rev. C 20, 1942 (1979).
7. S. Olariu, I. Popescu and C. B. Collins, Phys. Rev. C 23, 50 (1981).
8. S. Olariu, I. Popescu and C. B. Collins, Phys. Rev. C 23, 1007 (1981).
9. C. B. Collins, in Proceedings of the International Conference on Lasers '80, ed. C. B. Collins (STS Press, McLean, VA, 1981) 524.
10. C. B. Collins, in *CRC Handbook of Laser Science and Technology, Supplement 1: Lasers*, ed. by M. J. Weber (CRC Press, Boca Raton, Fl., 1991) 561.
11. B. D. DePaola and C. B. Collins, J. Opt. Soc. Am. B 1, 812 (1984).
12. C. B. Collins and B. D. DePaola, Optics Lett. 10, 25 (1985).
13. T. W. Sinor, P. W. Reittinger and C. B. Collins, Phys. Rev. Lett. 62, 2547 (1989).
14. J. A. Anderson and C. B. Collins, Rev. Sci. Instrum. 58, 2157 (1987).
15. J. A. Anderson and C. B. Collins, Rev. Sci. Instrum. 59, 313 (1988).
16. C. B. Collins, J. A. Anderson, Y. Paiss, C.D. Eberhard, R. J. Peterson and W. L. Hodge, Phys. Rev. C 38, 1852 (1988).
17. J. A. Anderson, M. J. Byrd and C. B. Collins, Phys. Rev. C 38, 2833 (1988).
18. C. B. Collins, C. D. Eberhard, J. W. Glesener and J. A. Anderson, Phys. Rev. C 37, 2267 (1988).
19. C. B. Collins, J. J. Carroll, T. W. Sinor, M. J. Byrd, D. G. Richmond, K. N. Taylor, M. Huber, N. Huxel, P. von Neumann-Cosel, A. Richter, C. Spieler and W. Ziegler, Phys. Rev. C 42, R1813 (1988).
20. J. J. Carroll, T. W. Sinor, D. G. Richmond, K. N. Taylor, C. B. Collins, M. Huber, N. Huxel, P. von Neumann-Cosel, A. Richter, C. Spieler and W. Ziegler, Phys. Rev. C 43, 1238 (1991).
21. J. J. Carroll, M. J. Byrd, D. G. Richmond, T. W. Sinor, K. N. Taylor, W. L. Hodge, Y. Paiss, C. D. Eberhard, J. A. Anderson, C. B. Collins, E. C. Scarbrough, P. P. Antich, F. J. Agee, D. Davis, G. A. Huttlin, K. G. Kerris, M. S. Litz and D. A. Whittaker, Phys. Rev. C 43, 1238 (1991).
22. C. B. Collins, J. J. Carroll, K. N. Taylor, D. G. Richmond, T. W. Sinor, M. Huber, P. von Neumann-Cosel, A. Richter and W. Ziegler, Phys. Rev. C 46, 952 (1992).
23. P. von Neumann-Cosel, A. Richter, C. Spieler, W. Ziegler, J. J. Carroll, T. W. Sinor, D. G. Richmond, K. N. Taylor, C. B. Collins and K. Heyde, Phys. Lett. B266, 9 (1991).
24. M. Huber, P. von Neumann-Cosel, A. Richter, C. Schlegel, R. Schultz, J. J. Carroll, K. N. Taylor, D. G. Richmond, T. W. Sinor, C. B. Collins and V. Y. Ponomarev, Nucl. Phys. A559, 253 (1993).
25. J. J. Carroll, C. B. Collins, K. Heyde, M. Huber, P. von Neumann-Cosel, V. Yu. Ponomarev, D. G. Richmond, A. Richter, C. Schlegel, T. W. Sinor and K. N. Taylor, Phys. Rev. C 48, 2238 (1993).
26. National Nuclear Data Center Online Evaluated Nuclear Structure Data File, Brookhaven National Laboratory, 1993.
27. E. Browne and R. B. Firestone, *Table of Radioactive Isotopes*, ed. by V. S. Shirley (Wiley, New York, 1986).
28. B. Pontecorvo and A. Lazard, C. R. Acad. Sci. 208, 99 (1939).
29. E. C. Booth and J. Brownson, Nucl. Phys. A98, 529 (1967).
30. I. Bikit, J. Slivka, I. V. Anicin, L. Marinkov, A. Ruydic and W. D. Hamilton, Phys. Rev. C 35, 1943 (1987).
31. W. R. Nelson, H. Hirayama and D. W. O. Rogers, *The EGS4 Code System*, Stanford Linear Accelerator Center Report No. SLAC 265, 1985 (unpublished).
32. J. J. Carroll, D. G. Richmond, T. W. Sinor, K. N. Taylor, C. Hong, J. D. Standifird, C. B. Collins, N. Huxel, P. von Neumann-Cosel and A. Richter, Rev. Sci Instrum. 64, 2298 (1993).
33. C. Hong, Ph.D. Dissertation, University of Texas at Dallas, 1993.
34. H. Friedrichs, B. Schlitt, J. Margraf, S. Lindenstruth, C. Wesselborg, R. D. Heil, H. H. Pitz, A.Zilges, D. Häger, G. Müller and M. Schumacher, Phys. Rev. C 45, 892 (1992).
35. P. M. Walker, F. Sletten, N. L. Gjørup, M. A. Bentley, J. Borggreen, B. Fabricius, A. Holm, D. Howe, J. Pedersen, J. W. Roberts and J. F. Sharpey-Schafer, Phys. Rev. Lett. 65, 416 (1990).
36. M. Girod, J. P. Delaroche, D. Gogny and J. F. Berger, Phys. Rev. Lett. 65, 416 (1990).
37. Th. Happ, H. Folger, J. Gerl, R. Kulessa, H. J. Wollersheim, J. de Boer, T. Faestermann, A. Gollwitzer, N. Gollwitzer, G. Graw, D. Hofer, A. Lösch, W. Oelmeier, F. Rieß, M. Springier, B. D. Valnion, E. Vogt, M. Würkner, E. Müller-Zanotti, M. Hussonnois, O. Constantinescu, S. Fortier, L. Rosier, G. Rotbart, Ch. Briançon, Yu. Ts. Oganessian, S. A. Karamian and Z. Szeglowski, Gesellschaft für Schwerionenforschung GSI Scientific Report 1992 (unpublished).
38. C. B. Collins, J. J. Carroll, K. N. Taylor, T. W. Sinor, C. Hong, J. D. Standifird and D. G. Richmond, Laser Int. Rel. Plasma Phenom. 10, 151 (1992).
39. C. B. Collins, J. J. Carroll, K. N. Taylor, T. W. Sinor, C. Hong, J. D. Standifird and D. G. Richmond, Laser Part. Beams 11, 43 (1993).
40. C. B. Collins, F. Davanloo, T. J. Lee, J. H. You and H. Park, Am. Ceram. Soc. Bull. 10, 1535 (1992).